Probing Nanomechanics of Aggrecan and the Aggrecan-Rich Pericellular Matrix of Chondrocytes in Cartilage

by

Laurel Jean Ng

B.S., Bioengineering, University of California, San Diego, 2000

Submitted to the Division of Biological Engineering
in partial fulfillment of the requirements for the degree of

Doctor of Philosophy in Biological Engineering

at the

MASSACHUSETTS INSTITUTE OF TECHNOLOGY

August 2005
[September 2005]

Author .....
Division of Biological Engineering
August 19, 2005

Certified by .....
Alan J. Grodzinsky
Professor of Electrical, Mechanical, and Biological Engineering
Thesis Supervisor

Certified by .....
Christine Ortiz
Associate Professor of Materials Science and Engineering
Thesis Supervisor

Accepted by .....
Alan J. Grodzinsky
Chairman, Department Committee of Graduate Students

Thesis Committee Members

Thesis Committee Chairperson: Bruce Tidor
Title: Professor of Biological Engineering and Computer Science

Thesis Supervisor: Alan J. Grodzinsky
Title: Professor of Electrical, Mechanical, and Biological Engineering

Thesis Supervisor: Christine Ortiz
Title: Associate Professor of Material Science and Engineering

Probing Nanomechanics of Aggrecan and the Aggrecan-Rich Pericellular Matrix of Chondrocytes in Cartilage

by

Laurel Jean Ng

Submitted to the Division of Biological Engineering
on August 19, 2005, in partial fulfillment of the
requirements for the degree of
Doctor of Philosophy in Biological Engineering

Abstract

The mechanical properties of articular cartilage are associated with the extracellular matrix network of type II collagen and the proteoglycan, aggrecan, which in combination provide the tensile, shear, and compressive stiffness of the tissue. While the collagen network mainly provides resistance to tensile and shear deformation, aggrecan enmeshed within this network contributes significantly to the tissue's compressive and shear properties under equilibrium as well as dynamic loading conditions. Aggrecan has a "bottle-brush" structure that includes ~100 negatively charged chondroitin sulfate glycosaminoglycan (CS-GAG) chains attached covalently to a core protein. Electrostatic interactions between these GAGs contribute to the compressive and shear stiffness of the tissue. Variations in the structure of aggrecan and its GAG constituents are known to exist as a function of tissue age, disease, and species.

Using atomic force microscopy (AFM), we directly visualized the nanometer scale structure of aggrecan deposited on a 2-D substrate, including the first high resolution imaging of individual GAG chains along the core protein. We also visualized and quantified the differences in structure between aggrecan obtained from fetal epiphyseal and mature nasal bovine cartilages. A combination of AFM, biochemical, and polymer statistical methodologies was used to better understand the dependence of aggrecan structure and stiffness on the properties of its constituent GAG chains. The fetal epiphyseal aggrecan had a denser GAG brush region and longer GAG chains, which correlated with a higher effective persistence length of fetal core protein compared to that of mature nasal aggrecan. The effect of increasing the concentration of aggrecan on the substrate resulted in a decrease in molecular extension, suggesting a flexible protein core backbone, which allowed aggrecan to entangle and interact with neighboring molecules. AFM imaging of the conformation of aggrecan that had been deposited on substrates from solutions of varying ionic strength (IS), from DI water to the physiological IS of 0.1 M NaCl, allowed for direct visualization of the collapse of the molecule on the substrate at the highest IS, due to charge shielding of the CS-GAGs by by Na+ counter-ions.

Lastly, the nanomechanical properties of cartilage cells (chondrocytes) and their

aggrecan-collagen-rich pericellular matrix (PCM) were probed via AFM nanoindentation using both a sharp nano tip and a larger micro-colloidal tip to better understand the deformation of cells in cartilage. The properties of cells freshly isolated from cartilage tissue, devoid of PCM, were compared to that of cells isolated and then cultured for selected times in 3-D alginate gel to obtain cells surrounded by their newly developed PCM. Using Hertzian contact mechanics as well as finite element analyses, material properties were estimated from the AFM force-indentation curves measured with these cell preparations. We also studied the effects of culture conditions on the resulting PCM properties, comparing 10% fetal bovine serum vs. medium containing a combination of insulin growth factor-1 (IGF-1) + osteogenic protein-1 (OP-1). While both systems showed increases in matrix stiffness with time in culture between days 7 to 28, the IGF-1 + OP-1 combination resulted in a higher effective modulus for the cell-PCM composite. These AFM cell indentation studies were enabled by the use of microfabricated chips containing wells designed to immobilize the spherical chondrocytes during testing. Due to the nonconventional but known geometry of the microfabricated wells, finite element analysis was used to include the effects of the cell-well boundary conditions and tip geometries on the calculated cell-PCM material properties. Taken together, these studies examining cartilage mechanics at the molecular and cellular levels give insight into the intricate roles that proteoglycans and collagen play in governing tissue-level mechanical properties.

Thesis Supervisor: Alan J. Grodzinsky
Title: Professor of Electrical, Mechanical, and Biological Engineering

Thesis Supervisor: Christine Ortiz
Title: Associate Professor of Materials Science and Engineering

Acknowledgments

Five years in Boston and so many people to thank! Each one has had an impact on my life to make my Ph.D. experience memorable. I would first like to thank my terrific advisors, Alan Grodzinsky and Christine Ortiz. Their constant support, guidance, and enthusiasm is greatly appreciated and is what really kept me movtivated over these five years. I have learned so much not just in terms of how do to research but more importantly how to be a good scientist, teaching me how think critically about experiments and papers. Alan has also showed me that hard work can be balanced with a good TGIF. Christine has taught me the importance of detail and thoroughness.

I would also like to thank Bruce Tidor for being a great committee chair. From down South, I would like to thank my invaluable collaborators, Anna Plaas and John Sandy.

I am so lucky to be surrounded by and interact with some of the smartest and nicest people I have ever met. It's been fun sharing the title of Nano group with Joonil, Delphine, Lin, and Bo Bae. Joonil was the pioneer of the group. Delphine put up with all of my questions about everything from discussion of my aggrecan results to the never ending questions about Matlab. She also kept me in shape by dragging me with her to Taekwondo practices. Lin helped me out a ton with AFM bugs and peculiarities. He is also one heck of karaoke singer. Bo Bae will continue the AFM indentation tradition and will do a great job! My UROP, Jacqueline, was extremely helpful with all of the tedious AFM imaging and calculations on aggrecan surfaces.

My officemates have listened to my complaints, kept me entertained, and helped lessen my fear of swimming. Shuodan, so patient and encouraging throughout my last few months, inspires me to be a more rounded out person with her dozen extracurricular activities. Diana with her positive attitude has helped me to see the optimistic side even when experiments don't work. Diana and Shuodan, I am sure you will keep up the swimming. Anna with her vast knowledge of everything has been a great resource. The competition in the thesis race against Jon F. has been fun. I've enjoyed all of our lunch chats. Mike was always willing to help me out on experiments, find references, and do statistics. Bernd was very nice and patient through the multitudes of agarose compressions. Jon S. was the man to turn to for sports trivia and for running columns. John K. seemed to know everything on all cell culture related topics. Jenny continued the lab tradition of participating in a marathon. Parth and Moonsoo, who graduated early in my time here, with their quick wit always kept me on my toes. Nora's driven personality helped to motivate me when I first joined the lab. Carlos was always helpful with using the CBE microscope. Cameron, Yi, Paul, Laura, and Yael have been great additions and will continue the fun and friendly lab environment. I know they will bring their projects to new levels over the next few years.

I will always appreciate all the help that Han-Hwa has been to my project. She was a trooper and braved freezing temperatures, rain, and humidity to make the

trips to MGH to spin the cells onto slides, taught me a variety of assays, and always made sure the lab was stocked. I will miss her delicious homemade treats. I really appreciated the thesis defense carrot cake. Without Eliot, many of the instruments in lab would be in disarray. I will never forget his quote after my defense, "The data tells the story. And the data is f*ing amazing." Linda has always brought fun and hijinks into even ordinary days. Thanks for lightening things up! What would the lab do without them?

While I didn't spend as much time with Christine's group, I cherish all of the relationships I have made. I still turn to Monica for advice about work and life after grad school. Kuangshin and Cathal have put up with my multitudes of ABAQUS questions. They had the ability to bring humor to any situation. Thanks to Ben for assisting me with AFM sign-ups in the ISN lab. I will always remember the delicious bubble tea drink outings with Jen. Thanks to Jae for capturing lab moments with his amazing photography. Miao is the first person I would ask if I had questions about polymer synthesis.

I would like to thank all of my new and old friendships in Boston. Melissa and Ping are the best friends and roommates you could ever ask for. I've enjoyed the late night chats into the wee hours with Melissa. She's also taught me now to properly ice a cake. Ping's humorous outlook has helped me keep perspective on life. She and Ben never fail to make me laugh. Leigh, one of my closest friends, showed me the fun nightlife of Boston, dragged me to multiple parties, and made me realize how important it is to relax sometimes. Twiggy was always willing to go on crazy adventures such as white water rafting. Ann, my oldest and dearest friend who has shared memories dating all the way from third grade, continues to listen to and partake in all of life's big events and never fails to bake delicious snacks. Eugene continues to impress me with his culinary skills. My friends (Tami, Quyen, Toyoko, Kristy, Daisy, Amparo, Naoko, Mayumi, Hung, Aram, so many more) scattered all over the world have kept me sane all of these years from elementary, high school, college to grad school.

I would especially like to thank Alex for putting up with my complaints about Boston weather, for cooking me dinner when I didn't have time to do it myself, and for converting this entire thesis to Latex. Now that is dedication. He has always been there when I needed someone to talk to and has supported me through my ups and downs over the past few years.

I wouldn't be here today without my family. My parents, Dean and Shirley, have always provided me with anything I needed and supported me throughout my education. My brother, Russell, helped out in small ways whenever he could. My aunt, Susan, could always be counted on to listen and offer encouraging words. My aunts, uncles, and cousins always put a smile on my face with their never-ending supply of positive thoughts and funny stories. My grandmother and rest of the family in New York helped to make me feel more at home in the Northeast.

Thanks to the Whitaker Foundation for supporting my graduate career through my fellowship.

Contents

List of Figures

List of Tables

Nomenclature

α	AFM tip angle (degrees)
δ	Indentation distance (μm)
ϵ	Strain
ν	Poisson's ratio
σ	Stress (kPa)
θ	angle formed between consecutive l's (degrees)
A	Area
E	Young's modulus (kPa)
F	Indentation force (nN)
l	vector segment length (nm)
L_c	contour trace length (nm)
L_p	persistence length (nm)
R_1	Micron-sized tip radius (μm)
R_2	Cell radius (μm)
R_{ee}	end-to-end distance (nm)
z	indicator variable

Chapter 1

Introduction

1.1 Motivation

Articular cartilage is the white connective tissue that covers the ends of articulating bones. It acts to absorb loads and shocks as well as protect bones from rubbing against each other. This tissue is unique in that it is avascular and aneural. Because little blood supply is available, damaged cartilage is slow to heal if at all. Cartilage mechanical properties come from the delicate balance between the tensile collagen network as well as the compressive resistance of the proteoglycans (PGs). Any alteration to this balance can lead to osteoarthritis (OA), the degeneration of cartilage. Over 20 million in the US are affected with OA [96], and incidences will only increase as the average lifespan is extended by new medical technologies. Little can be done to reverse OA, and those with severe OA must undergo total joint replacement. Understanding the molecular origins responsible for tissue-level properties may help to elucidate the role of each component to overall structural behavior, and may provide clues into molecular changes that OA tissue may undergo.

1.2 Objectives

Aggrecan, the major PG in cartilage, is responsible for >50% of the compressive modulus [14]. The structure and dense packing of the negatively charged glycosamino-

glycans (GAGs) along the core protein impart this molecule with the ability to resist compression. Aggrecan structure has been deduced through a series of biochemical analyses. However, the molecular details of individual molecules are lost in biochemical assays which give measurements of ensembles of molecules. Larger aggregates of aggrecan self-assembled along a hyaluronan backbone have been visualized via transmission electron microscopy (TEM). However, the fine structure of the GAG chains and their attachment to the core protein could not be not clearly resolved. With the advent of atomic force microscopy (AFM), nano- and micro- scale measurements could be obtained accurately of single molecules in their native state. Therefore, the first goal of this thesis was to use AFM to directly visualize individual aggrecan from two different populations with nanometer resolution and then relate its structure to its resultant equilibrium conformation.

Collapse of end-grafted GAG chains [119] and end-grafted aggrecan [24] surfaces have been measured through changes in height from ellipsometry measurements and AFM imaging. With compression of cartilage during loading or changes in the local environment, the interaction of aggrecan with neighboring molecules may be altered, leading to mechanical changes to the tissue level. Extending upon the first goal to look at aggrecan-aggrecan interactions, three surface densities were prepared to give insight into the resultant conformation as the molecule density increased to a point where aggrecan interacted with neighboring aggrecan. In addition, the dependence of individual aggrecan conformation in varying ionic strengths from low to physiologic conditions was visualized via AFM and its conformation quantified with changes in contour length.

Third, the mechanical properties of newly synthesized of aggrecan and collagen from chondrocytes were assessed via nanoindentation of developing pericellular matrix (PCM). The mechanical properties of chondrons, adult chondrocytes with a fully developed PCM, have been found to be an order of magnitude stiffer than the cell itself. However, enzymatically isolated chondrocytes seeded into scaffolds developed a PCM with a more diffuse appearance than native chondrons [73] and may have significantly different mechanical properties, which may have implications in tissue

engineering near-native cartilage constructs. Finite element analysis was employed to extract a modulus from AFM indentation curves on individual cells plus PCM. To obtain AFM measurements on non-adherent spherical cells, a surface was microfabricated to immobilize the cells during indentation.

1.3 Overview

This thesis starts with a general overview to give the reader a basic background on the topics pertinent to the series of experiments and models used in this project. A short description of AFM, cartilage components such as aggrecan and chondrocytes, as well as culture conditions are described. In Chapter 2, molecular resolution of two populations of individual aggrecan, fetal epiphyseal and mature nasal, was obtained via AFM. Structural differences in GAG length and density were correlated to conformational differences. The effects of aggrecan density and ionic strength on aggrecan conformation were further explored in Chapter 3. In Chapter 4, the combination of aggrecan, collagen, and other matrix molecules that were newly synthesized into the pericellular matrix were probed with a nano-size AFM tip and a micro-size colloidal tip. A surface was microfabricated to immobilize individual cells during indentation. Finite element analysis was implemented to more precisely analyze the force vs. indentation curves obtained via AFM.

1.4 Background

1.4.1 Atomic Force Microscopy

The design of atomic force microscopy was first described by Binnig et al. in 1986 [8]. As seen in Figure 1-1, a laser aligned at the tip of a low spring constant cantilever is deflected into a photodetector. The spring constant must be matched with the surface being probed. Biological samples in particular are generally delicate and require a low spring constant (e.g. $k \sim 0.06\,\frac{\mathrm{N}}{\mathrm{m}}$) to minimize damage to the surface. As the stylus ($R_c < 50\,\mathrm{nm}$) located at the tip of the cantilever traces the topology,

the soft cantilever deflects causing movement of the laser across the quadrants of the photodetector. This "error" signal is part of the feedback loop being sent to the computer which then tells the piezo to correct for the error. The piezo sits below the sample of interest and adjusts the sample height in order to minimize the amount of force from the tip. Thus, there are two types of signals in the end. One signal (height data) comes from the piezo tracking the features. The other signal (deflection data) comes from the error recorded from the photodiode segment differences.

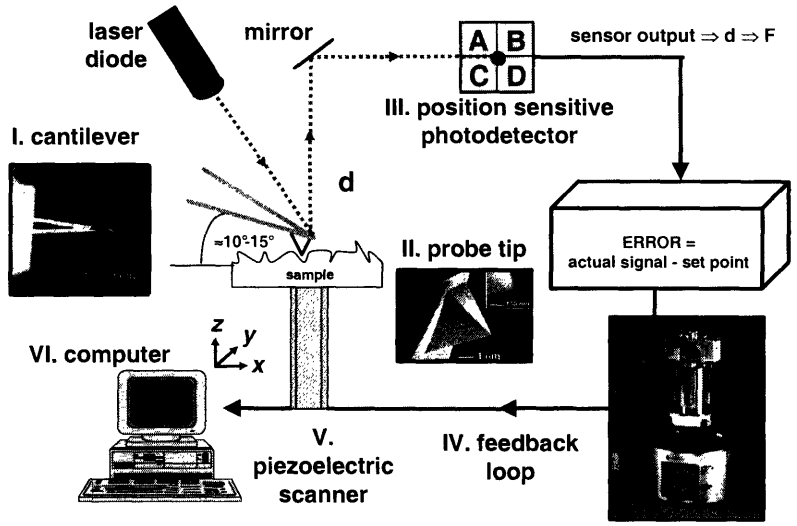

Figure 1-1: Schematic of AFM details from deflection of a cantilever tracking the topology of a sample to the recording of height and deflection data. Courtesy of C. Ortiz.

AFM has the ability to resolve angstrom and nano-level forces and features of molecules, proteins, or cells in their native state since no fixation or special coating is required [120, 123]. Simultaneous mechanical testing of viscoelasticity, adhesion, and friction measurements can be carried out on the same sample being imaged [52, 47]. Sample preparation is extremely important and varies depending on the sample type. If nanometer-sized objects are being measured, special care must be taken to ensure the cleanliness of the sample. At this length scale, small pieces of dust or oil from fingerprints can be seen and introduce artifacts into the image or force measurement. AFM can yield direct proof of biochemical findings and can inspire new directions for biochemical investigation.

1.4.2 Cartilage

Articular cartilage is the white connective wear resistant tissue that covers the ends of articulating bones. It is designed to transmit and distribute loads during joint motion. Healthy articular cartilage has a smooth, shiny appearance whereas osteoarthritic cartilage has a rough, calcified appearance (Figure 1-2). The dense cartilage matrix is composed mainly of a network of collagen fibrils and charged macromolecules known as proteoglycans (Figure 1-3). Collagen is responsible for the tensile component [81] while aggrecan, the main PG, is responsible for $> 50\%$ of the compressive modulus of cartilage [14]. Normal hydrated cartilage weight is mostly water at 70-85%, with 10-20% collagen, and 5-10% proteoglycan [89].

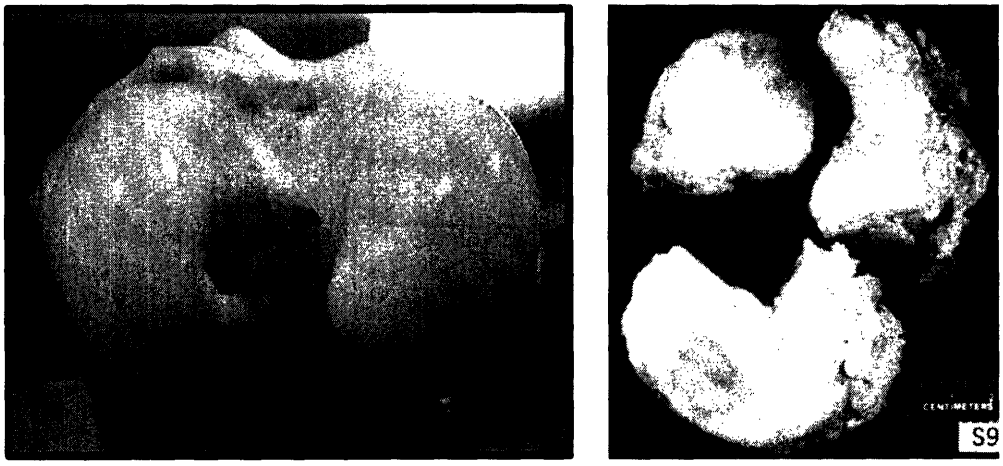

(a) Healthy articular cartilage (from young bovine condyles) has a smooth, shiny white appearance. Courtesy S. Chen.

(b) End-stage osteoarthritic cartilage shows calcification and appears rough.

Figure 1-2: Comparison of healthy articular and end-stage osteoarthritic cartilage.

Variation of structure and composition of cartilage is seen with depth [81, 4, 46, 89]. The top ~10-20%, known as the superficial layer, is characterized by the parallel arrangement of collagen to the surface and the highest collagen content. The next ~40-60%, known as the middle layer, is characterized by the random arrangement of collagen. The last ~30%, the deep layer, is characterized by perpendicular arrangement of collagen to the growth plate (Figure 1-4) [125]. PG content has been found to increase with depth from superficial to deep cartilage [62]. Chondrocyte matrix

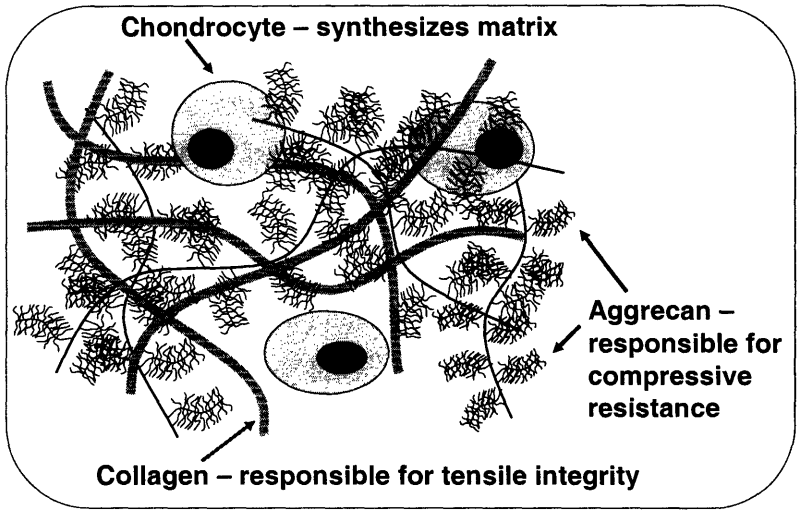

Figure 1-3: Cartilage is composed mainly of collagen, responsible for the tensile integrity, and aggrecan, responsible for the compressive resistance. Chondrocytes occupy <10% volume but are responsible for the catabolism and anabolism of all matrix molecules.

synthesis has also been found to vary in a zonal fashion [4].

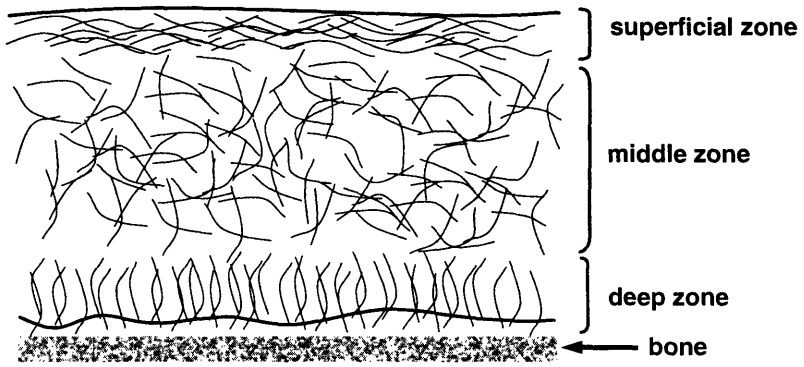

Figure 1-4: Diagram of collagen structure in cartilage. In the superficial zone, collagen is parallel to the surface whereas it is randomly oriented in the middle zone. In the deep zone, collagen is perpendicularly oriented to the bone.

1.4.3 Aggrecan

Aggrecan, the main proteoglycan in cartilage, self assembles non-covalently, stabilized by link protein [10], along a larger hyaluronan chain into a larger aggregate (Fig 1-5(a)). Aggrecan is composed of a core protein of ~2300 amino acids [28, 55] with a

dense brush region of ~100 covalently attached GAG chains, giving it a molecular weight of 2-3·10^6 Da (Figure 1-5(b)). The core protein has three globular domains (G1, G2, and G3.) G1, at the N-terminus, interacts with link protein, through their immunoglobulin folds [49]. G2 has a similar structure to G1 but does not participate in binding. The GAG brush lies between G2 and G3. The function of G2 and G3, the latter located at the C-terminus, is unknown.

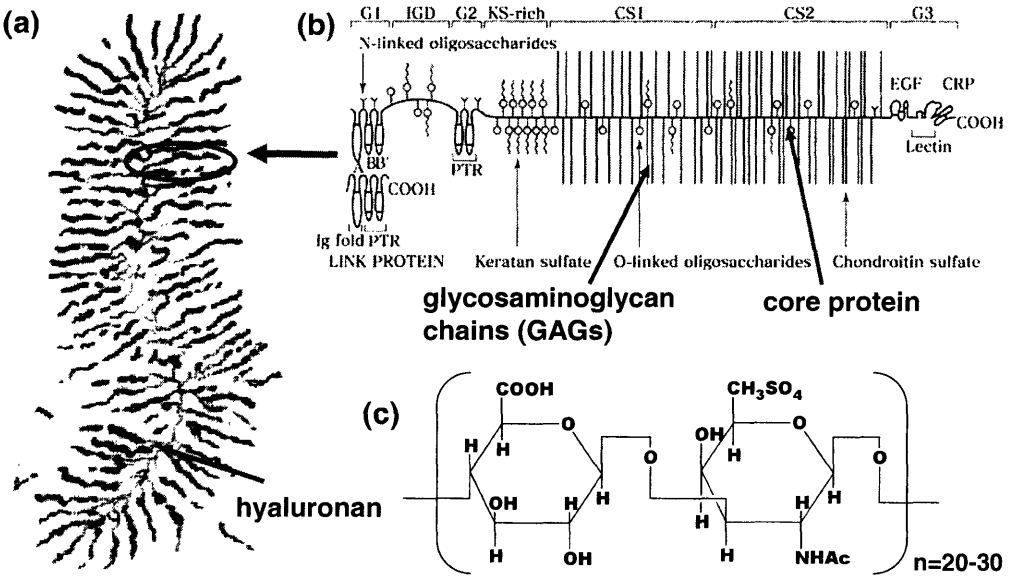

Figure 1-5: (a) Transmission electron micrograph of aggrecan self-assembled along a hyaluronan backbone, forming a large aggregate [13]. (b) Diagram of aggrecan with ~30 kDa GAGs attached every 2-3 nm along the ~250 kDa core protein. (c) Disaccharide repeats, D-glucuronic acid (GlcUA) and N-acetyl-D-galactosamine (GalNAc) lfated at C-6, that form GAG chains of chondroitin sulfate.

The GAGs are composed of linear chains of chondroitin sulfate (CS) that are made of repeat disaccharides D-glucuronic acid (GlcA), containing a carboxyl group, and N-acetyl-D-galactosamine (GalNAc), which can be sulfated at the C-4 or C-6 positions (Figure 1-5(c)), giving each disaccharide 1-3 negative charges when fully ionized. CS-GAGs are usually 20-30 disaccharides in length and the chains are attached at the serine-glycine residues, every 2-4 nm along the core protein. Therefore, each aggrecan can have as many as 3 charges/disaccharide x 30 disaccharides/chain x 100 chains = 9000 negative charges. This high aggrecan charge density along with aggrecan

concentration (20-80 mg/ml) is responsible for >50% of the compressive modulus of articular cartilage [14]. With age, structural changes such as increase in keratan sulfate content [7] and C-6 sulfation [26] occurs.

1.4.4 Chondrocytes and their Pericellular Matrix

While chondrocytes make up <10% of cartilage volume, they are responsible for the anabolism, catabolism, and assembly of the extracellular matrix (ECM) molecules. Studies at the cell and tissue level have helped to elucidate the composition of the pericellular, territorial, and interterritorial matrix surrounding the cells. The pericellular matrix (Figure 1-6), located immediately around the cell, differs from extracellular matrix composition in that it contains a higher concentration of proteoglycans and hyaluranon as well as collagen type VI, a key marker of the PCM [106, 104, 17]. Small amounts of fibronectin [39] and its colocalisation with col VI, and other smaller molecules of decorin, col IX, and col XI have been visualized with immunohistochemistry [17]. Adult cartilage contains a well defined chondrocyte plus PCM, termed a chondron. While the microstructure of the chondron is not well understood, scanning electron microscopy has revealed collagen fibers organized to form a woven, dense capsule around the PCM [106]. In immature tissue and enzymatically isolated chondrocytes seeded and cultured in a 3D scaffold, there is no well-defined chondron morphology. The newly developing PCM appears as a diffuse halo in immunohistochemistry images [73].

The PCM pays an important role though biomechanical modulation of the stresses and strains and by biochemical regulation of signals being sent to the cell. Static compression has been shown to decrease biosynthesis [44] and transcription [133, 32]. However, dynamic compression of cartilage explants have been shown to increase biosynthesis [65] and transcription levels [31, 33]. The hierarchical structure in articular cartilage has been shown to modulate the stresses and strains felt by chondrocytes during loading as shown in previous finite element models as the elastic modulus varies by two orders of magnitude from bulk cartilage to the PCM to the cell [45].

The chondrocyte modulus ranges from 0.65 to 4 kPa [63, 74, 38] while the chondron

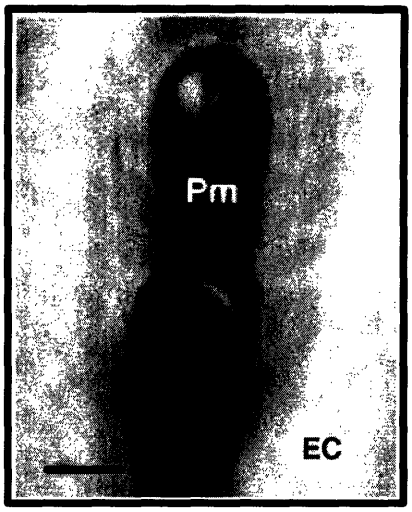

Figure 1-6: Histology articular cartilage: A chondrocyte with surround pericellular matrix (Pm) and the extracellular matrix (EC). Scale bar = 10 μm. [103]

modulus is an order of magnitude higher at ~40 kPa [2]. Cartilage tissue modulus is yet another order of magnitude higher at ~1 MPa. The biomechanical properties of individual chondrocytes and adult chondrocytes plus their pericellular matrix (PCM) have been studied by micropipette aspiration [43, 132, 1] and confocal microscopy [46, 67]. Enzymatically isolated chondrocytes attached to substrates have been measured via cytoindentation [68, 74]. A decrease in PCM modulus of osteoarthritic cartilage has been measured via micropipette aspiration [73, 1] and volume [63, 56].

1.4.5 Growth Factors as Culture Supplements

Fetal bovine serum (FBS) has been the traditional supplement used in cartilage explant and tissue culture systems to maintain chondrocytes and stimulate production of proteoglycans [51, 66]. While FBS contains a number of proteins, growth factors, amino acids, sugars, and lipids, it has been found that insulin-like growth factor-I (IGF-1) is the main stimulating component in FBS [84, 79]. In an effort to further enhance the metabolic and anabolic activities of chondrocytes in culture, the addition of other growth factors to culture medium has been investigated by a few groups. The addition of of osteogenic protein-1 (OP-1), a bone morphogenetic protein that

induces new bone formation, has been found to stimulate both proteoglycan and collagen synthesis in cartilage explants and chondrocyte cultures [35, 97]. In an effort to enhance growth over that of FBS, the combination of IGF-1 + OP-1 was used for culture supplement and found to induce proteoglycan synthesis over two times medium supplemented with only IGF-1 and only OP-1 [77]. Therefore in our chondrocyte studies, two culture conditions (FBS vs. IGF-1+OP-1) were tested for influence on mechanical properties of PCM.

1.4.6 Alginate

Chondrocytes plated onto Petri dishes dedifferentiate into fibroblastic-like cells and decrease aggrecan and col II synthesis [9, 75]. Therefore, chondrocytes require a 3D environment to retain their spherical phenotype. Alginate has been successfully used as a scaffold to culture chondrocytes [53, 54, 19]. The novelty of this scaffold over other scaffolds in that it can be depolymerized easily with a calcium chelator such as sodium citrate, releasing the cells undamaged. The cells retain their cell-associated matrix, thus making it possible to identify matrix molecules in the newly developing pericellular matrix from molecules released into the inter-territorial space. More recently, Masuda et al. [82], released day 7 chondrocytes plus their PCM from alginate, reseeded them into a culture insert (polyethylene terephthalate membrane), and produced a cartilaginous tissue a week later, much faster than enzymatically isolated chondrocytes seeded into a scaffold, indicating that the newly developing matrix aided in synthesis and retention of ECM molecules.

1.5 Overall Goals

We hope to understand the complexities of molecular interaction that result in tissue level properties by studying structure and mechanics at the molecular and cellular levels. The overall hypothesis is that structure at the nanoscale is important for tissue-level mechanical properties. The first goal was to investigate the effect of nanostructure of aggrecan on its molecular conformation through visualization with AFM.

The second goal was to quantify the effect of aggrecan density and ionic strength on aggrecan conformation. Lastly, the mechanical properties of and the effect of growth factors on single chondrocytes and their newly synthesized matrix, which is rich in aggrecan, were studied on the nano- and micro-length scales via AFM.

Chapter 2

Individual Cartilage Aggrecan and Their Constituent Glycosaminoglycans Visualized via Atomic Force Microscopy

This chapter was published as a paper in Journal of Structural Biology in 2003 [95].

Authors: Laurel J. Ng, Alan J. Grodzinsky, Parth Patwari, John Sandy, Anna Plaas, Christine Ortiz

2.1 Introduction

Aggrecan, the major load-bearing proteoglycan in the extracellular matrix of all cartilaginous tissues, is composed of a ~300 kDa core protein substituted with ~100 chondroitin sulfate (CS) and, in some species, keratan sulfate (KS) glycosaminoglycan (GAG) chains (Figure 2-1). Aggrecan is a member of the hyaluronan (HA)-binding proteoglycan family (which also includes brevican, neurocan and versican) and associates noncovalently with HA and the ~45 kDa link glycoprotein to form high molecular weight aggregates (> 200 MDa). In cartilage, these aggregates form a densely packed, hydrated gel that is enmeshed within a network of reinforcing col-

lagen fibrils. Electrostatic repulsion forces between the highly negatively charged GAGs of aggrecan are known to provide > 50% of the equilibrium compressive modulus of cartilage [14, 81]. Structural variations are known to exist as a function of age, disease, and species, including differences in GAG chain length, sulfate ester substitution, and KS and CS substitution [101, 102]. It is also known that progressive C-terminal truncation of the core protein by proteolytic enzymes takes place with increasing maturation [10, 13, 29, 34, 98, 118].

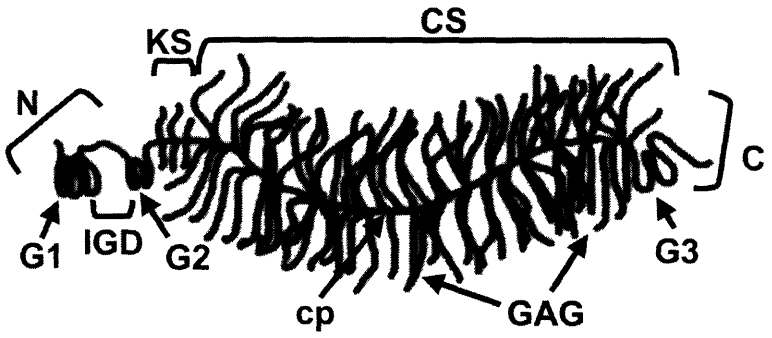

Figure 2-1: Structure of aggrecan. N=amine-terminal; G1, G2, G3=globular domains; IGD=interglobular domain between G1 and G2; cp=core protein; KS=keratan sulfate region; CS=chondroitin sulfate brush region; GAG=glycosaminoglycan chains; C=carboxyl-terminal.

Aggrecan, HA, and CS have been studied in solution by biophysical techniques such as small angle neutron scattering (SANS), quasielastic light scattering (QELS), X-ray Diffraction (XRD), nuclear magnetic resonance (NMR), sedimentation, and viscosity [20, 21, 50, 83, 99], as well as biochemical techniques such as electrophoresis and chromatography. This extensive body of literature is largely based on polydisperse populations of molecules, so the fine details of molecular heterogeneity, conformation, and structure at the level of the individual aggrecan molecule have not yet been obtained. Such molecular-level information is often crucial for theoretical models that are used to predict molecular interactions and macroscopic tissue behavior [25, 119]. Electron microscopy (EM) imaging has been used successfully to visualize fixed, dried, and metal-coated samples of cartilage proteoglycan aggregates as well as individual aggrecan monomers and reveal the presence of a thick CS-brush region and a thinner

segment attached to HA [11, 87, 113]. While individual CS-GAG chains were occasionally resolved, they often appeared as collapsed bundles, making determination of their number, spacing, dimensions, and conformation difficult.

With the advent of high resolution atomic force microscopy (AFM), chemically and positionally sensitive force spectroscopy, nanoindentation, and the direct visualization and probing of numerous biological macromolecules (including DNA, proteins, and polysaccharides) in fluid and ambient conditions, nm-scale resolution has been achieved. Measurements have been made of the dimensions and conformation (e.g. persistence length and entanglements), supramolecular association, and nanomechanical properties of individual macromolecular chains in physiological and near-physiological conditions [111, 120, 121, 138]. Researchers have recently begun to use these new nanotechnological tools in the study of cartilage and its constituent extracellular matrix (ECM) macromolecules. Fluid AFM and nanoindentation of articular cartilage sections, both native and after partial enzymatic digestion of the ECM proteoglycans, allowed for visualization and nanomechanical probing of the collagen fibril network [23, 59, 64]. Individual bovine articular cartilage aggrecan forms were observed by AFM [92, 93], and reconstruction techniques that take into account the finite size and shape of the probe tip were employed to infer further structural information [130]. Recently, we reported the distinct resolution of the non-GAGylated N-terminal region from the CS/KS-substituted "brush" region, as well as visualization of the individual CS-GAG chains of bovine cartilage aggrecan via AFM [94]. Here, we expand these initial studies and give a detailed quantitative comparison between bovine fetal epiphyseal and mature nasal cartilage aggrecan using a combination of biochemical, AFM, and polymer statistical methodologies. Our long term goal is to use these sample preparation, imaging, and data analysis techniques in conjunction with nanomechanical testing to gain insights into the function of cartilage ECM constituents.

2.2 Materials and Methods

2.2.1 Purification of Cartilage Aggrecan

Mature nasal cartilage from 18 month old bovines was removed, washed in ice-cold 50 mM sodium acetate, pH 7.0, containing a mixture of protease inhibitors, and stored on ice until further processing. The tissue was cut into 3x3 mm^2 pieces and extracted in 4 M guanidium hydrochloride, 100 mM sodium acetate, pH 7.0, with protease inhibitors for 48 hours. Unextracted tissue residues were separated by centrifugation, and the clarified supernatant dialyzed against two changes of 100 volumes of 0.1 M sodium acetate, pH 7.0, with protease inhibitors [11, 50]. Fetal bovine cartilage was obtained from the epiphyseal growth plate region, processed, and stored as described above. Purified aggrecan fractions (A1A1D1D1) were dialyzed consecutively against 500 volumes of 1 M NaCl and deionized water to remove excess salts. Aggrecan yield was determined by the dimethyl methylene blue (DMMB) dye binding assay [30].

2.2.2 Biochemical Characterization of Aggrecan and GAGs

Aggrecan preparations were analyzed for core protein heterogeneities by SDS-Page and Western Blot analyses. Briefly, about 200 μg of fetal and 200 μg of mature aggrecan were digested at 37°C in Chase buffer containing 30 mU chondroitinase ABC (ChABC), 0.5 mU keratanase II, and 0.5 mU endobetagalactosidase. For Western analysis, 10% of each sample was lyophilized and then resuspended in a sample buffer of DTT (dithiothreitol), urea, and Tris-Gly SDS 2x sample buffer (BioRad Laemmli #161-0737). The sample was heat inactivated, loaded onto a 4-12% Tris-Gly gel, and the gel was run at 200 V for 40 min. in an ice bath. Transfer to the blotting membrane was run at 100 V for 1 hr, and the membrane was blocked with TBS-T (Tris-buffered saline with Tween 20) with 1% dry nonfat milk for 10 minutes. The blots were probed with affinity-purified antibodies [118] to either the aggrecan G1 domain (JSCATEG) or to the G3 domain (JSCTYK).

To determine the hydrodynamic radius of the CS-GAG chains, aggrecan prepa-

rations (200 μg as sulfated (S)-GAG) were first digested with 1.5 units/ml of papain in 0.1 M sodium acetate, pH 6.5. Desalting and separation of the CS from KS chains were done on a G50 sizing column. CS chains were liberated from the core protein by b-elimination in 100 mM sodium borohydride and 100 μM NaOH [26]. Excess borohydride was reduced by addition of 50% acetic acid and samples rinsed with methanol. The dried samples were suspended in 0.5 M ammonium acetate, pH 7.3, assayed for CS content using DMMB, and eluted on Superose 6 FPLC column (Amersham Pharmacia Biotech) chromatography. Fractions (0.5 ml) were collected at 0.5 ml/min and assayed for S-GAG contents by DMMB, and the average chain lengths of CS (number average disaccharides per chain) were computed from the K_{av} of the peak elution [26]. GAG compositional analyses were performed by fluorophore assisted carbohydrate gel electrophoresis (FACE) using methods described in detail previously [15, 101].

2.2.3 Sample Preparation for AFM

Muscovite mica surfaces (SPI Supplies, West Chester, PA, #1804 V-5) were treated with 0.01% 3-aminopropyltriethoxysilane (APTES; Sigma Aldrich Co., St. Louis, MO) v/v MilliQ water (18 MΩ-cm resistivity, Purelab Plus UV/UF, US Filter, Lowell, MA). 60 μl of APTES solution was deposited onto freshly cleaved mica, incubated for 20-30 minutes at room temperature in a humidity controlled environment, rinsed gently with MilliQ water, and air dried. The silanol groups on the muscovite mica [$KAl_2[AlSi_3]O_{10}(OH)_2$] were covalently bound to APTES via aminosilane chemistry to leave an amine group exposed on the mica surface (Figure 2-2). The rms roughness of the APTES-mica was measured to be 9.9 Å by tapping mode AFM in air. X-Ray Photoelectron Spectroscopy (XPS) was used to verify the amine-functionalization of the surface by comparison of the fluorine-to-nitrogen ratio after the surface amines were reacted with trifluoroacetic acid anhydride (Figure 2-3). The aggrecan surface monolayer density was controlled via the solution concentration and incubation time. Dense monolayers were obtained by placing ~30 μl aliquots of aggrecan solution containing of 500 μg/ml GAG (measured from DMMB) on the surface for 30-40 minutes, while sparse monolayers of well-separated aggrecan monomers were

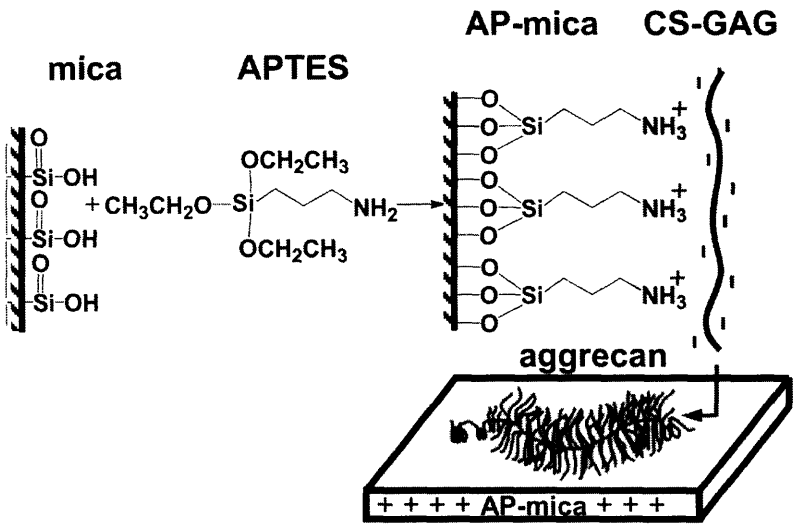

Figure 2-2: AFM sample preparation. Silanol groups on the mica surface were functionalized with 3-aminopropyltriethoxysilane (APTES) producing surface amine groups (pKa=10.5) which were protonated in the neutral buffered solution used for adsorption. This positively-charged AP-mica surface facilitated electrostatic binding with the negatively-charged COO- and SO_3- groups on the GAG chains to hold the aggrecan noncovalently on the surface.

obtain using ~60 μl aliquots of 250 μg/ml GAG incubated for only 20-30 minutes. After incubation, the samples were gently rinsed in a stream of MilliQ water and air dried. Electrostatic interaction between the APTES-mica and the aggrecan GAG chains enabled retention of a population of aggrecan despite rinsing. Samples were imaged within a day of preparation.

2.2.4 AFM Imaging

The Nanoscope IIIa Multimode AFM (Digital Instruments (DI), Santa Barbara, CA) was used to image all samples via the EV or JV scanners. Tapping mode (TMAFM) was employed in ambient temperature and humidity using Olympus AC240TS-2 rectangular Si cantilevers (k = 2 N/m). Scanning electron microscopy (SEM, JOEL 6320FV) was employed to characterize the probe tip (Figure 2-4) and typical end-radii were found to be <10 nm. The cantilever was driven just below resonance frequency, ω_o, and a slow scan rate of 1-3 Hz was used to minimize sample disturbances giv-

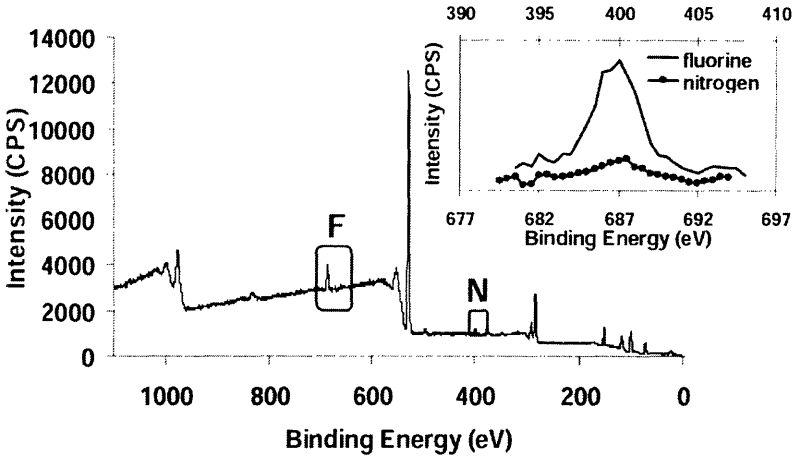

Figure 2-3: Characterization of AP-mica. XPS data of the AP-mica surface show the presence of fluorine and nitrogen. The inset is a higher magnification of the nitrogen and fluorine peaks, which shows a 3:1 ratio of N:F confirming the presence of amine groups on the mica surface.

ing a scan rate that was much slower (<25,000x) than the tap rate. The maximum sample size of 512 x 512 pixels was used. The system was allowed to pre-equilibrate for at least 30 minutes prior to imaging to minimize drift. The drive amplitude and amplitude set-point were maximized to get the fullest peak upon tuning. Gains were chosen to maximize either the height image (gains ~0.65) or the amplitude image (gains ~0.1). The RMS amplitude (~27 nm) of the cantilever oscillation at resonance frequency was determined by increasing the Z scan start and plotting the amplitude vs. z-position on the force calibration plot in tapping mode. At these z-amplitudes, attractive forces due to any water meniscus capillarity are overcome [128]. The x- and y- scan directions were calibrated with a 10x10 μm^2 grid. The z-direction was calibrated with 5 nm diameter beads on a cleaved mica surface. The scans were tested for typical AFM imaging artifacts by varying scan direction, scan size, and rotating the sample.

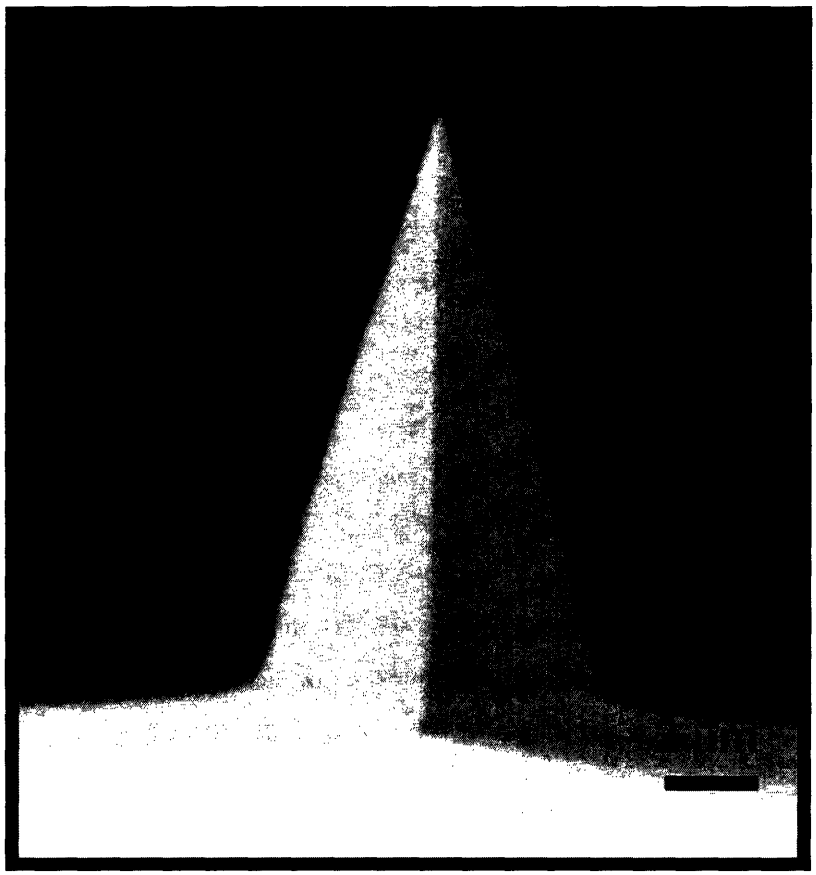

Figure 2-4: SEM of tapping mode probe tip for AFM imaging

2.2.5 Calculation of Trace, End-to-End, and Effective Persistence Lengths from AFM Images

Using SigmaScan Pro image analysis software (SPSS Science, Chicago, IL), the core protein and GAG contour lines in the AFM images were digitized into pixels yielding the spatial coordinates of each position along the polymer chain. The trace lengths, L_c, and end-to-end lengths, R_{ee}, were measured directly from these images. An effective persistence length, L_p, a parameter related to the local chain stiffness of the core protein as well as the individual GAGs, was also calculated assuming the validity of the Kratky-Porod Worm-Like Chain (WLC) model [70]) which describes a polymer chain that is intermediate between a rigid-rod and a flexible coil and takes into account both local stiffness as well as long-range flexibility. The WLC model represents an isolated polymer chain as an isotropic, homogeneous elastic rod whose trajectory varies continuously and smoothly through space. The chain consists of n rotating unit vectors (statistical segments) of length l joined in succession, where each vector is oriented at an angle θ with respect to the previous vector (shown below in Results). For 2D conformations obtained after surface equilibration (as opposed to "kinetic trapping") [112], the probability density $P(\theta(l))$ of the bend angle $\theta(l)$ is theoretically expected to be normally distributed with mean zero and variance, $\langle\theta^2(l)\rangle$, as shown below:

$$P(\theta(l))_{2D} = \sqrt{\frac{L_p}{2\pi l}} e^{-\frac{L_p\theta^2(l)}{2l}} \tag{2.1}$$

$$\langle\theta^2(l)\rangle \geq \left(\frac{1}{L_p}\right) \tag{2.2}$$

To verify that the observed values of $\theta(l)$ were consistent with the behavior predicted by the WLC model and that the 2D images were equilibrated on the surface (i.e. representative of the 3D conformation), the normality of θ was assessed at different levels of l by examination of the distribution of θ on histograms and by calculation

of kurtosis.

$$\text{kurtosis} = \frac{\langle \theta^4(l) \rangle}{\langle \theta^2(l) \rangle^2} - 3 \tag{2.3}$$

Kurtosis, defined by Equation 2.3, is an indication of the peakedness of the distribution (i.e. whether the shape of the distribution is more or less peaked compared to the normal distribution), and equals zero for a normally distributed variable. It has previously been interpreted as an assessment of the observed 2D conformations [112, 116].

To obtain θ as a function of l from the images, a series of equal length vectors was iteratively projected onto the digitized trace of the core protein and GAG contours from $5l$ (l$\sim$1.2 nm) to nl (n=35, $nl\sim$42 nm) in increments of l. The angle θ between consecutive vectors was calculated over the length of the molecule. The linear relationship of the variance of θ as a function of l was then used to estimate an effective persistence length L_p for aggrecan molecules and for GAG chains. For each image of a molecule, the variance of θ was estimated at multiple values of l. These resulting estimates of variance are thus not independent but correlated with the molecule image from which they were obtained. A linear mixed-effects analysis [27] was performed (SPlus, MathSoft Inc.; now Insightful Corp., Seattle WA). Molecule-to-molecule variation was included as a random effect in the model and l was included as a fixed effect. In addition, an indicator variable, z, was used to identify whether the aggrecan was from mature (z=1) or fetal (z=0) cartilage. To test for differences between L_p from mature and fetal aggrecan, the statistical significance of the interaction term between z and l was assessed, since this term represents the difference in the slopes of the lines relating the variance of θ to l. The full model for the fixed effects was thus:

$$s^2(\theta) = \beta_0 + \beta_1 \cdot l + \beta_2 \cdot z + \beta_3 \cdot lz \tag{2.4}$$

where s^2 = sample variance, and β_i = estimated coefficients. L_p was calculated as the inverse of β_1, since this coefficient is equal to $1/L_p$ for the WLC, as described

		# disacch	μg	0S sulfation	6S sulfation	4S sulfation	% monoS	% diS
Fetal	**CS**	50	13.1	10.5	38.3	51.2	–	–
	KS	–	0.33	–	–	–	38	62
Mature	**CS**	42	12.1	5.5	65.6	28.9	–	–
	KS	–	0.95	–	–	–	42	58

Table 2.1: Results from biochemical analysis of GAG chains

above. An equivalent model was used to estimate L_p for GAG chains and to test for differences between L_p of fetal and mature GAG.

2.3 Results

2.3.1 Biochemical Characterization of Aggrecan and GAGs

Western analysis with antibody JSCATEG specific to the G1 domain (Figure 2-5) suggested that the majority of aggrecan core protein species (>90%) in these samples were high molecular weight (~350 kDa) full-length molecules for both the fetal and mature preparations. Identification of the single major band in each preparation as the full-length species was confirmed by showing immunoreactivity of this band with antibody JSCTYK which reacts with an epitope at the extreme C-terminus of the G3 domain (data not shown). While the predominant aggrecan core species detected (>90%) was full length, there was evidence of C-terminally truncated species of very low abundance (Figure 2-5). The average chain length of GAGs from fetal epiphyseal aggrecan was calculated from Superose 6 chromatograms (Figure 2-6(a)) to be ~50 disaccharides (corresponding to ~48 nm), while that from nasal aggrecan was ~42 disaccharides (corresponding to ~40 nm). FACE gel analyses of aggrecan GAG chains (Figure 2-6(b)) revealed that the fetal epiphyseal GAG had a CS:KS ratio three times higher than that of the mature nasal GAG. The chondroitin-4-sulfate disaccharide (C4S) amount was higher than the chondroitin-6-sulfate (C6S) for the mature aggrecan, whereas the C4S and C6S contents were essentially equal in the fetal aggrecan (Figure 2-6(b) Table 2.1).

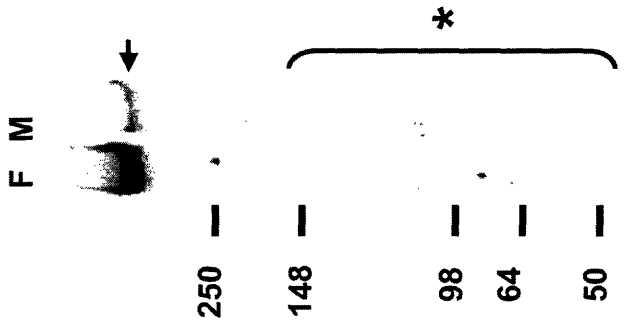

Figure 2-5: Western Blot analysis with anti-G1 peptide (JSCATEG) shows a high majority (>90%) of full-length core protein (arrow) with some evidence of a very small amount of C-terminally truncated core species (*) in the mature sample

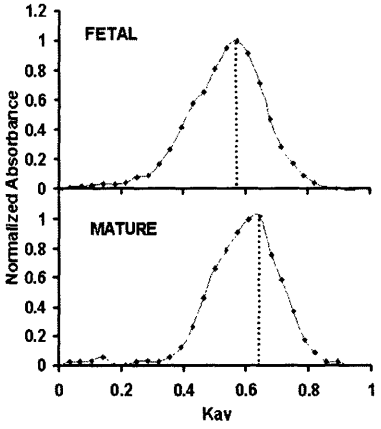

(a) Superose 6 chromatograms show the fetal epiphyseal GAGs are longer than mature nasal GAGs with K_{av}=0.60 and 0.64, respectively

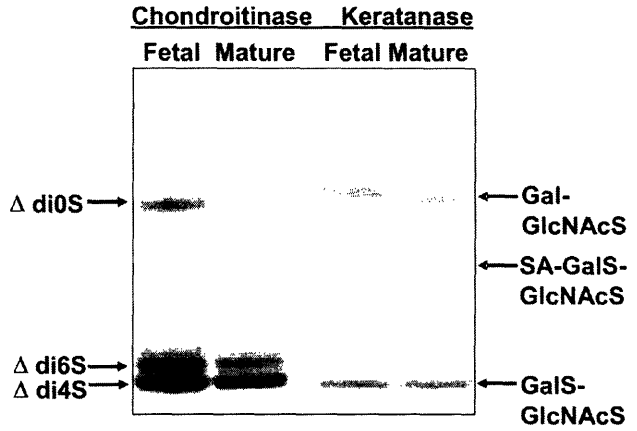

(b) FACE gel of the fetal epiphyseal and mature nasal cartilage aggrecan GAG chains.

Figure 2-6: Biochemical characterization of GAG chains

2.3.2 Visualization of Dense and Sparse Aggrecan Monolayers

Tapping mode AFM images of dense monolayers of fetal epiphyseal aggrecan showed that individual aggrecan monomers (Figure 2-7(a)) and their constituent GAG chains (Figure 2-7(b)) are clearly resolved. The monomers exhibited varying degrees of extension and did not appear to be aligned in any preferred direction. Rather, they conformed to each other to create a dense packing on the 2D surface suggesting that the core protein backbone had some degree of flexibility. At higher magnification (Figure 2-7(b)-boxed regions), interdigitation between GAG chains of adjacent aggrecan molecules could sometimes be observed. More structural details of individual aggrecan molecules became apparent on lower density monolayers (representative images, Figure 2-8) where the thicker GAG brush region can be clearly distinguished from the thinner N-terminal region. As observed in dense monolayers, the monomers in sparse monolayers exhibited varying degrees of extension and, again, were not aligned in any preferred direction. The heights of the aggrecan monomers were found to be approximately equal to the diameter of one GAG chain ($\sim$1 nm, [129]) suggesting that the aggrecan molecules appeared fully flattened on the surface, possibly due to surface attractive interactions and/or compression by the tip during imaging. "Thinner" aggrecan monomers (marked ** in Figure 2-8(a)) were occasionally apparent and were found to have heights of $\sim$2 GAG chains; hence, the GAG chains of such monomers were likely collapsed or folded over, and were not necessarily shorter than those of the much more numerous fully flattened aggrecan. The widths of the CS-GAG brush region, a reflection of GAG extension, were found to exhibit a continuous distribution with 57$\pm$11 nm for the fetal and 47$\pm$12 nm for the mature. Compared to fetal aggrecan (Figure 2-8(a)), the size and structure of mature aggrecan (Figure 2-8(b)) appeared more dimensionally heterogeneous, as manifest in the distributions of the aggrecan and GAG contour and end-to-end lengths (quantified below).

A side-by-side comparison of higher resolution images of individual (fully flattened) fetal epiphyseal versus mature nasal aggrecan (Figure 2-9(a)) revealed the

(a) A dense monolayer.

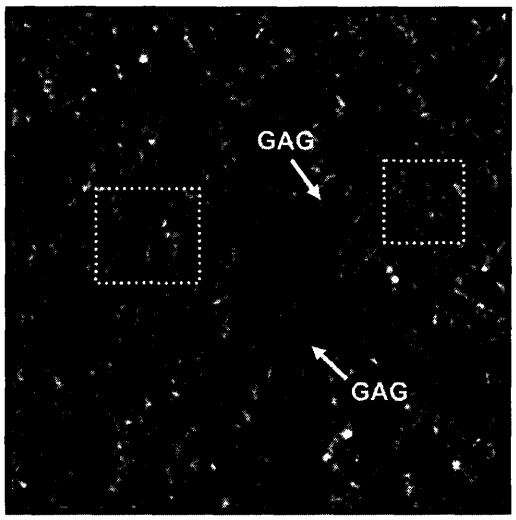

(b) Center region of Figure 2-7(a) magnified.

Figure 2-7: Amplitude AFM images of fetal epiphyseal aggrecan monomers. Boxed regions indicate interdigitation of GAG chains.

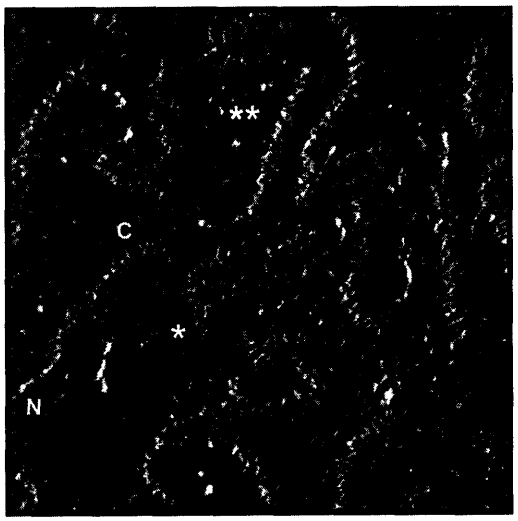

(a) fetal epiphyseal aggrecan

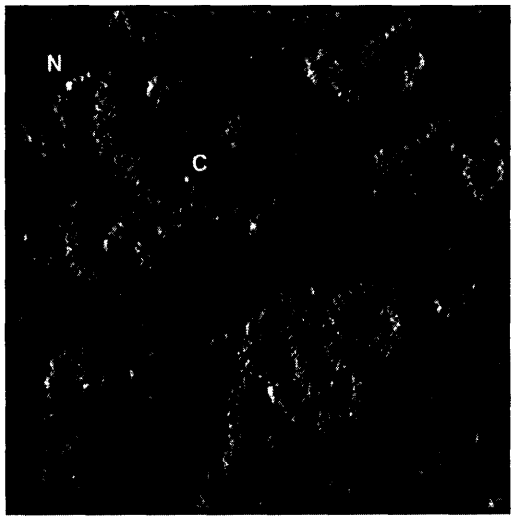

(b) mature nasal aggrecan

Figure 2-8: Amplitude AFM images of lower density monolayers. The height scale is read with the darkest color as the base line to white as the maximum height. N- and C- terminal regions of the aggrecan are denoted on the images. GAG chains take on an extended (*) form, or occasionally a collapsed (**) form.

detailed nanoscale differences between these two populations with marked clarity. Close examination of the N-terminal region showed no distinct GAG attachment in this part of the core protein (Figure 2-9(b)). The globular domains, G1 and G2, could not be easily resolved as these domains may have collapsed since the 135 amino acid sequence joining them forms a flexible chain [55]. The contour length of the core protein components of the two aggrecan molecules of Figure 2-9(a), measured from the trace of each molecule, were 470 nm (fetal) and 396 nm (mature), and the widths of the brush-like GAG region were 96 nm (fetal) and 65 nm (mature). In addition, the GAG chains on the fetal monomer appeared longer and more extended. It was more difficult to distinguish individual CS-GAG chains in the brush region of mature aggrecan (e.g. Figure 2-9(c)). This may be attributed to the higher density of keratan sulfate relative to chondroitin sulfate chains along the core protein of mature aggrecan and/or other structural differences. To measure the distance between GAG chains in the brush region, cross-sections of the images were taken near the point of GAG attachment to the core protein (Figure 2-10). The distribution of GAG spacing for the fetal and mature monomers of Figure 2-10(a) is shown in the frequency histograms of Figure 2-10(c) and the mean distance between GAG chains was found to be 3.2±0.8 nm for the fetal aggrecan and 4.4±1.2 nm for the mature aggrecan monomers.

2.3.3 Statistical Analysis of Trace and End-to-End Lengths of Core Protein and CS-GAG Chains

The trace of the core protein of individual aggrecan monomers from multiple images was digitized into pixels yielding the spatial coordinates of each position along the polymer chain. The trace lengths, L_c, and end-to-end lengths, R_{ee}, shown in Figure 2-11(a), were measured directly from these images and the probability distribution histograms calculated (Figures 2-11(b) and 2-11(c), Table 2.2). L_c was found to be 398±57 nm for fetal compared to 352±88 nm for mature, and R_ee was 257±87 nm for fetal compared to 226±81 nm for mature aggrecan. The average extension of the core

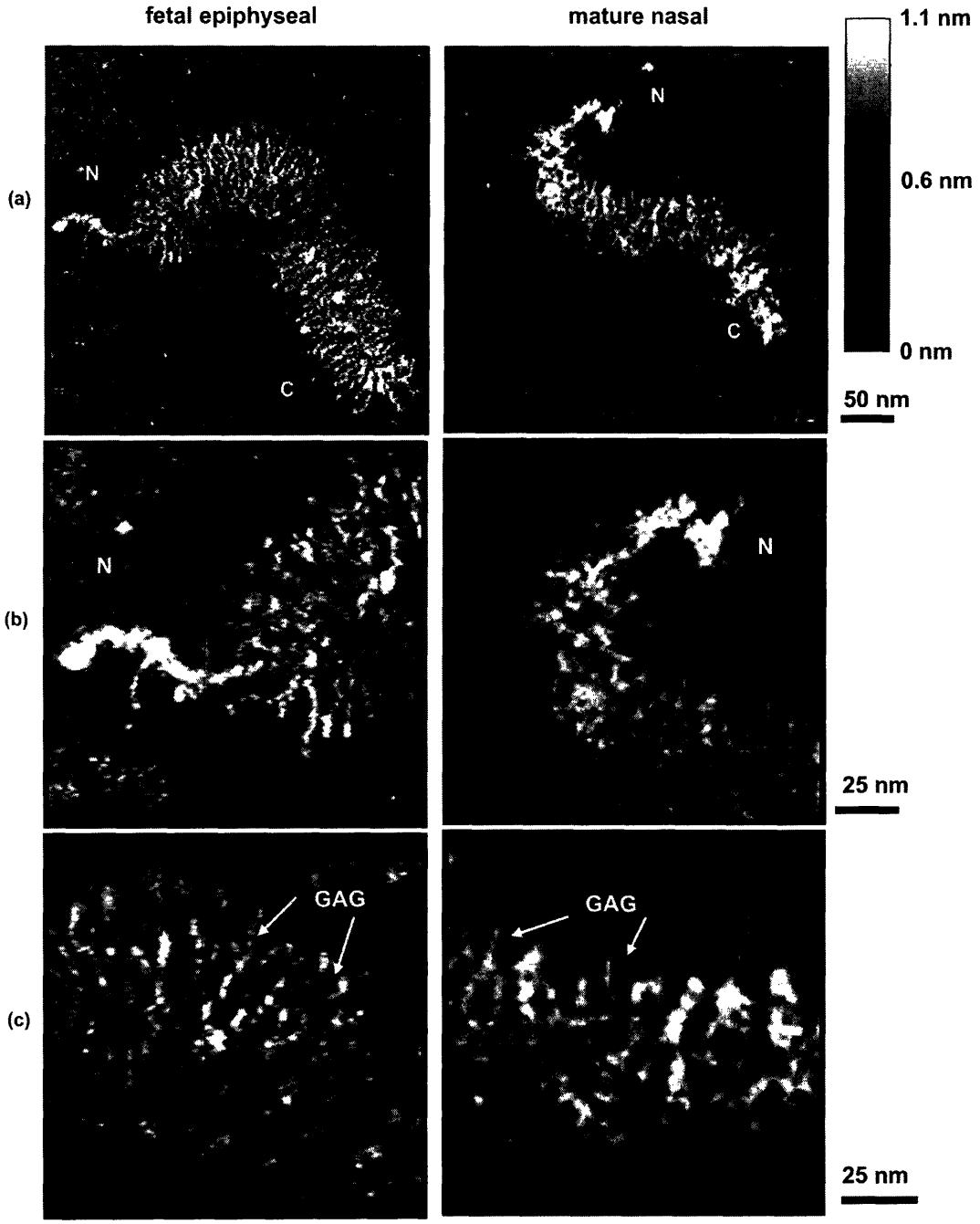

Figure 2-9: Higher resolution comparison of AFM height images of an individual isolated (a) fetal epiphyseal and mature nasal bovine aggrecan monomer. (b) Core protein visible in the N-terminal region on both monomers. (c) GAG chains, clearly visible in the CS brush region, on both the mature and fetal monomers appear shorter on the mature nasal vs. fetal epiphyseal.

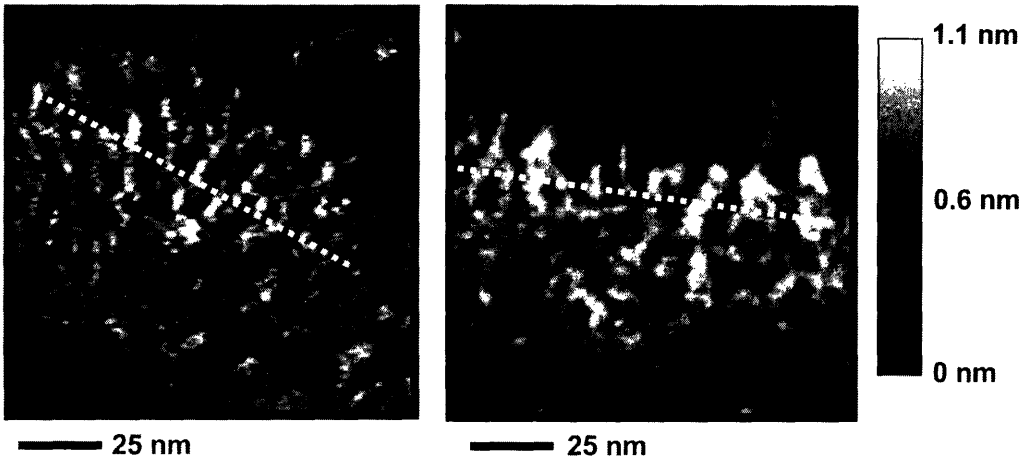

(a) Higher resolution comparison of AFM height images of the fetal epiphyseal (left) and the mature nasal (right) aggrecan CS-brush region.

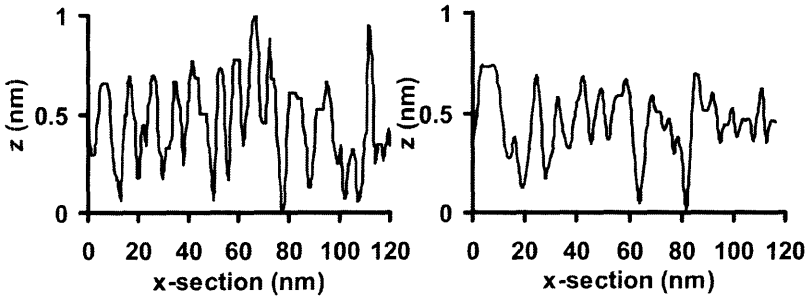

(b) Cross-sectional profiles of the GAG spacing along one side of the core protein, corresponding to the white dotted lines of Figure 2-10(a).

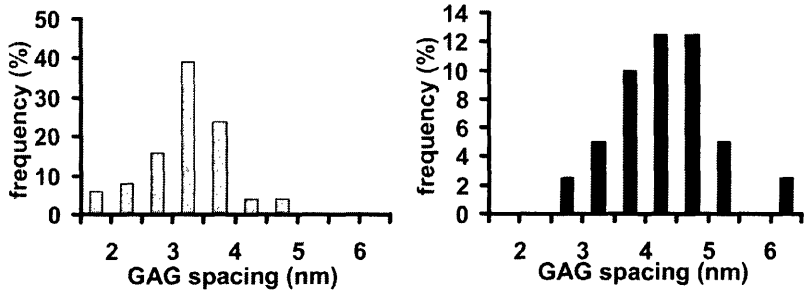

(c) Histograms of GAG spacing between chains of fetal epiphyseal (μ = 3.2 ± 0.8 nm; $n = 102$) and mature nasal ($\mu = 4.4 \pm 1.2$,nm; $n = 40$)

Figure 2-10: Measurements of GAG brush region from AFM images.

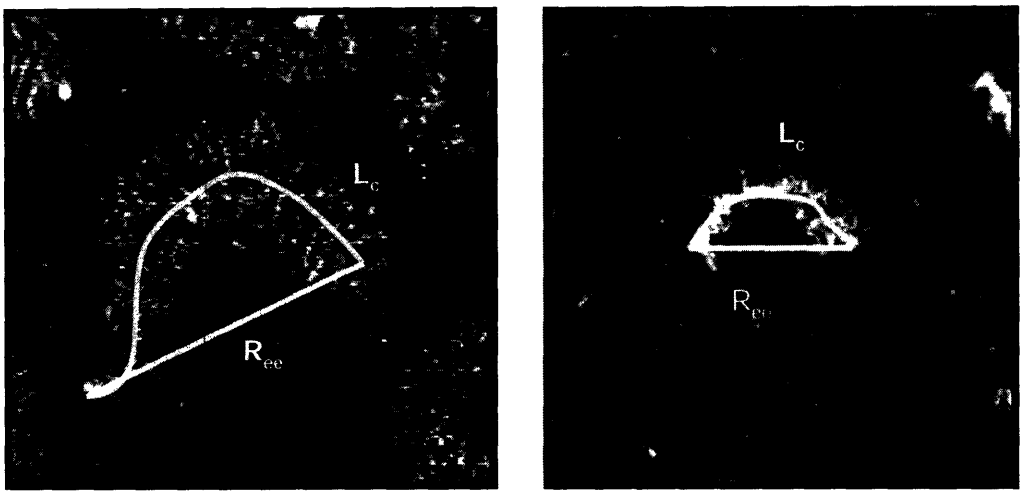

(a) AFM height image in air of an individual isolated fetal epiphyseal aggrecan monomer (left) and a mature nasal aggrecan monomer (right). A trace of the aggrecan contour core protein is indicated by L_c and the end-to-end distance measurement is indicated by R_{ee}.

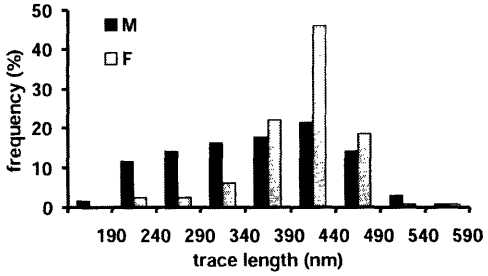

(b) The histogram of aggrecan L_c shows that mature nasal aggrecan (M) ($L_c = 352 \pm 88$ nm; $n = 141$) is slightly shorter and has a broader distribution than the fetal epiphyseal aggrecan (F) ($L_c = 398 \pm 57$ nm; $n = 113$).

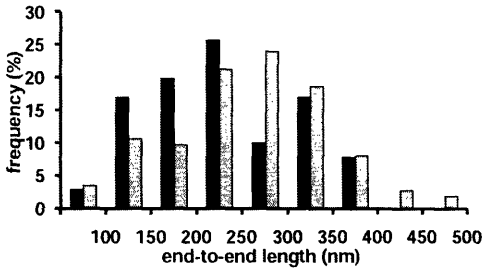

(c) The histogram of R_{ee} for mature nasal aggrecan ($R_{ee} = 226 \pm 81$ nm) and fetal epiphyseal aggrecan ($R_{ee} = 257 \pm 87$) follow the same trend.

Figure 2-11: Measurements of aggrecan core protein from AFM images.

protein, defined as (R_{ee}/L_c), was 65% and 64% for fetal and mature, respectively. More than 75% of the extension distribution was clustered between 50% and 95% for nasal and 50% and 90% for epiphyseal (data not shown).

L_c and $R_e e$ for the GAG chains (Figure 2-12) were found to be 32 ± 5 nm and 27 ± 7 nm for the mature nasal versus 41 ± 7 nm and 32 ± 8 nm for the fetal epiphyseal, yielding an average GAG chain extension of 80% and 78% for mature nasal and fetal epiphyseal, respectively. More than 75% of the extension distribution was clustered between 70% and 95% for both mature nasal and fetal epiphyseal GAGs, respectively (data not shown). For the molecules in which the CS-brush region was well defined

	$L_{c,total}$ (nm)	R_{ee} (nm)	GAG Spacing (nm)	$L_{c,bare\ core\ protein}$ (nm)	$L_{c,CS-brush}$ (nm)
mature nasal aggrecan	353±88 (n=141)	226±81 (n=141)	–	81±17 (n=29)	268±73 (n=29)
fetal epiphyseal aggrecan	398±57 (n=113)	257±87 (n=113)	–	93±14 (n=29)	327±43 (n=29)
mature nasal GAG	32±5 (n=49)	26±7 (n=49)	4.4±1.2 (n=40)	–	–
fetal epiphyseal GAG	41±7 (n=102)	32±8 (n=102)	3.2±0.8 (n=102)	–	–

Table 2.2: Summary of measured dimensions from AFM images of aggrecan

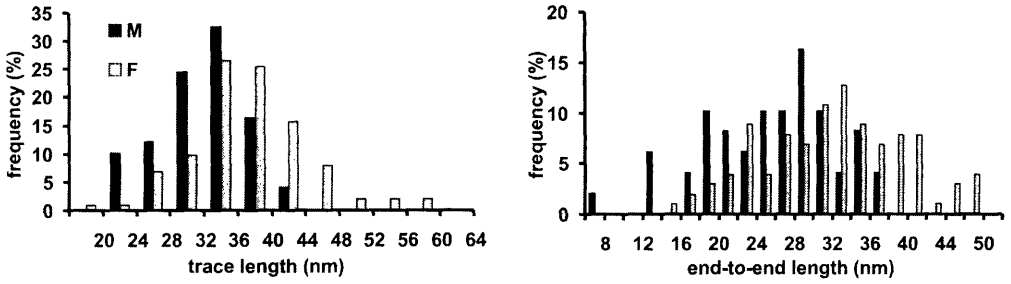

(a) Histogram of contour trace length, L_c (b) Histogram of end to end length, R_{ee}

Figure 2-12: Histograms show that the contour trace length L_c (a) of mature nasal GAG (M) ($\mu = 32 \pm 5\,\text{nm}$; $n = 49$) was shorter than L_c of fetal epiphyseal GAG (F) ($\mu = 41 \pm 7\,\text{nm}$; $n = 102$). The R_{ee} (b) of mature nasal GAG ($\mu = 26 \pm 7\,\text{nm}$) was shorter than that of fetal epiphyseal GAG ($\mu = 32 \pm 8\,\text{nm}$).

and distinguishable from the N-terminal bare core protein region, the contour length of each of these regions was measured separately. L_c of the bare N-terminal region was found to be 93±14 nm and 81±17 nm for fetal and mature aggrecan, respectively. A greater difference in L_c was found for the CS-brush region, 327±43 nm and 268±73 nm, for the fetal and mature, respectively (Table 2.2).

	mature nasal aggrecan	fetal epiphyseal aggrecan	mature nasal GAG	fetal epiphyseal GAG
L_p (nm), mean	82	110	14	21
95% confidence interval (nm)	73-94	102-120	10-21	17-25

Table 2.3: Persistence length calculated from the mixed-effects model

2.3.4 Persistence Length Measurements of Core Protein and GAG Chain

In the calculation of the aggrecan core protein persistence length, the values for the vector segment lengths l were limited on the lower bound by pixelation of the trace and limited on the upper bound at $l < L_c$ (Figure 2-13(a)). Statistical analysis of the linear relationship between $\langle\theta^2\rangle$ and l resulted in an effective mean core protein L_p of 110 nm for whole fetal epiphyseal aggrecan and 82 nm for whole mature nasal aggrecan (Figure 2-13(b), Table 2.3). This difference was found to be statistically significant based on the confidence intervals. The mean effective L_p values for fetal epiphyseal and mature nasal GAG were 21 nm and 14 nm, respectively, but were not significantly different. The degree to which the observed 2D angles reflected the behavior predicted by the WLC model was assessed by calculation of the kurtosis of θ vs. l (Figure 2-13(c)). At larger values of l, the kurtosis was nearly zero for both aggrecan and GAG chains, as predicted for a normally distributed variable. A distribution plot of θ showed deviation from the Gaussian distribution at $\theta = \frac{\pi}{4}$ and $\frac{\pi}{2}$ for the lower values of l, suggesting that this deviation is probably due in part to the effects of pixelation.

2.4 Discussion

In this study, we first presented methodologies for the direct high resolution visualization of individual aggrecan monomers using the technique of tapping mode AFM. We then quantitatively assessed the contour, end-to-end, and persistence lengths of

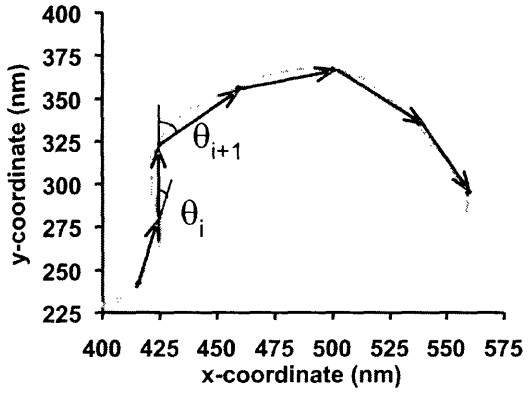

(a) Trace for a single fetal epiphyseal aggrecan monomer (see Figure 2-11(a)) from an AFM image. Vectors of length, l, were projected onto the trace. An angle was calculated from consecutive vectors and used in the calculation of persistence length.

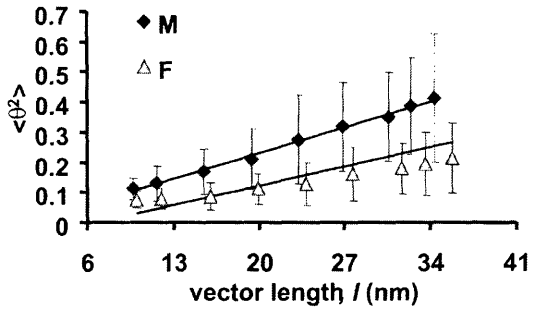

(b) $\langle\theta^2\rangle$ vs. vector length l (nm) comparing mature nasal (n = 15) and fetal epiphyseal (n = 15) aggrecan monomers measured from AFM images. L_p,mature=82 nm; L_p,fetal=110 nm (see 95% confidence intervals in Table 2.3).

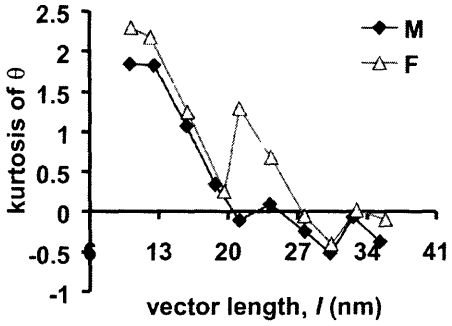

(c) Kurtosis of θ vs. l (nm) was plotted for the same population of monomers examined in Figure 2-13(b), to determine if the Gaussian distribution of angles was maintained from the 3D to the 2D state.

Figure 2-13: Calculation of persistence length.

fetal epiphyseal aggrecan monomers and contrasted these parameters with those of mature nasal monomers.

2.4.1 General Methodology for High Resolution AFM Imaging of Aggrecan

High purity aggrecan (A1A1D1D1) was used to minimize nonspecific adsorption of other biomolecules onto the APTES-mica surface which could obscure the resolution of the target macromolecule (aggrecan) during imaging. Minimal sample preparation was employed (no fixation, coating, or other chemical treatments). The negatively charged GAGs facilitated electrostatic binding of aggrecan to the APTES-mica amine groups (pKa$\sim$10.5). Since a thin layer of water ($\sim$2-10Åthick) exists on the mica surface [123] even in ambient conditions, electrostatic binding interactions are maintained and minimize lateral displacements of the aggrecan during imaging. This adsorbed water layer partially binds to and hydrates the hydrophilic aggrecan and its GAGs, helping to preserve near physiological conditions. Tapping mode in air was found to produce the highest resolution using relatively soft cantilevers and low set points to minimize sample deformation, damage, and displacement due to the forces exerted by the probe tip during imaging. Even though the probe tip end-radii were up to 10 nm or greater, resolutions down to or below 1 nm were achieved presumably due to an individual asperity or smaller region of the probe tip forming the actual contact during imaging [120]. In many cases, however, "tip broadening" artifacts are frequently reported in the literature [130] where the biomolecular dimensions at high resolutions are overestimated due to the finite size and shape of the probe tip.

2.4.2 Comparison of Aggrecan Core Protein Dimensions and Conformation Assessed by AFM, EM, and Biochemical Methods

One major result of these AFM studies was the fact that the mature nasal aggrecan showed a slightly broader distribution of L_c shifted to lower values compared to the fetal epiphyseal aggrecan. Previous EM studies [113, 11, 12, 13] on bovine mature nasal and fetal epiphyseal aggrecan and their self-assembled aggregates (aggrecan non-covalently bound to HA) have reported dimensions such as trace length L_c of core protein, GAG chains, and HA, as well as the number of attached aggrecan to HA. While the differences in EM versus AFM sample preparation techniques make it difficult to compare absolute values of L_c obtained by these two techniques, the same trend of relative reduction in L_c of the core protein with age was observed by EM, though higher values of L_c were found by AFM (by as as much as 10-40%). The L_c of the G1-IGD-G2 core protein regions measured by AFM was slightly shorter than EM measurements.

Western analysis (Figure 2-5) suggested that the large majority of the high buoyant density preparations from both fetal and mature cartilages used in this study were full-length aggrecan, and since C-terminal truncation of the core protein by proteases appears to occur in distinct regions to generate discrete products of defined size ranges [118], it is unlikely that there is an abundance of such high molecular weight truncated species present in these samples. If the distribution of surface adsorbed aggrecan measured by AFM is similar to the distribution of aggrecan in the starting solution (i.e. containing predominantly full-length core protein), then the distribution of core protein trace lengths measured by AFM (Figure 2-11(b)) can be interpreted as that associated with full-length core protein extended to various degrees. Conformational and secondary structure variations of the core protein in the CS-brush region will most likely be affected by repulsive intra- and intermolecular GAG-GAG electrostatic double layer interactions, the range of which is determined by the GAG length, spacing, and heterogeneity. The observed reduction in the trace length for the

mature sample compared to the fetal could arise from a number of different sources including: 1) entropic collapse to a more random coil like configuration, 2) formation of additional intramolecular noncovalent bonds (e.g. "protein folding"), or 3) enthalpic changes due to a reduction in the individual amino acid bond angles. This interpretation is consistent with EM studies [88] which reported aggrecan core protein trace lengths that were significantly shorter in the deglycosylated form (263±27 nm) compared to the glycosylated form (405±37 nm).

It should be noted that the distribution of surface adsorbed aggrecan does not necessarily have to be equivalent to the distribution of aggrecan in the starting solution and, hence, there does exist the possibility that the shorter length monomers observed by AFM could in part be C-terminally truncated aggrecan monomers [118] that preferentially adsorbed to the surface. However, in the absence of transport limitations, preferential adsorption of smaller molecules is unlikely since larger molecules have a greater number of attractive contacts holding them down as well as a greater attractive interaction force on approach to the surface.

Even though statistically significant differences in the trace contour lengths and end-to-end lengths were observed for the two aggrecan populations, it is interesting to note that the average larger length scale extension ratios (R_{ee}/L_c) (Figure 2-11) were essentially the same. If the molecules have conformations that have equilibrated in 2D on the surface, the fact that $\frac{R_{ee}}{L_c}$ (Figure 2-11) for both the mature and fetal aggrecan populations were found to be essentially the same suggests that the molecular origin of these parameters, presumably GAG-GAG electrostatic double repulsion, is the same. R_{ee} clearly represents straightening or bending of the whole aggrecan molecule as directly visualized by the AFM images and we have suggested that the trace length, L_c, reflects the extension or compression along the main core protein backbone. Both of these parameters reflect an equilibrium balance between repulsive (e.g. electrostatic double layer forces imparted by CS-GAGs and determined by CS-GAG length, spacing, etc.) and attractive (e.g. entropic, noncovalent bonding) intra- and intermolecular interactions.

2.4.3 Comparison of CS-GAG Dimensions and Conformation Assessed by AFM and Biochemical Methods

Another major result of this AFM study was the fact that for the first time, unmodified, individual GAG chains attached to the aggrecan core protein were clearly visualized. Physical evidence of two different densities of the CS-GAG brush regions was observed for the fetal epiphyseal and mature nasal aggrecan (Figure 2-10). GAG spacing along the mature aggrecan of Figure 2-10 was 72% greater than that of the fetal epiphyseal monomer. The measured spacing of 3.2 nm and 4.4 nm for fetal epiphyseal and mature nasal, respectively, correlates well with the predicted attachment of GAGs at the Ser-Gly residues based on the amino acid sequence of the core protein [55]. The difference may be attributed to the number increase in shorter KS chains in the CS-GAG brush-region in the mature aggrecan compared to the fetal aggrecan as demonstrated by the FACE compositional analyses (Figure 2-6). KS content has been shown to increase with age [7]. The distinguishing of individual CS chains (~25 kDa) from the shorter KS chains (~5-15 kDa) in this region was not possible due to similarity in size and location of the chains. However, the substitution of KS for CS may help to explain the decreased GAG spacing as measured from AFM images. Analysis of GAG composition and sulfation was done to differentiate the aggrecan populations, and to obtain biochemical structural information that could not be obtained through AFM.

The trace length measurements of the CS-GAG chains showed that L_c of fetal aggrecan was longer than that of mature aggrecan, and those values compared well with the hydrodynamic radius determined via chromatography. The resolution of the Superose 6 column is 0.4 Kav (~5 disaccharides≈6 nm), and the resolution of the AFM at this level is less than a few nm. The difference between chromatography and AFM measurements may reflect inherent differences in the parameters being measured by those two techniques, as well as the slightly collapsed state of the GAG chains when moved from a fluid to an ambient 2D environment. Small sub-nm bend angles at the disaccharide level cannot be resolved in the AFM images. However, L_c

as well as the extension and conformation of the GAG chains could be extracted from the AFM images. The average extension of the CS-GAG chains was ~78% for both fetal and mature populations (as compared to ~65% for the core protein), indicating that typically, monomers and GAG chains preferred an extended arrangement.

2.4.4 Aggrecan and GAG Persistence Length

Persistence length calculations from AFM images have been performed on linear biological polysaccharides such as mucins [116], succinoglycan [5], and xanthan [16]. Complications arise in comparing the use of a WLC model for a simple polymer chain to that of the complex structure of aggrecan. Due to the close proximity of the charged GAG chains in a physiologic fluid environment, the GAGs as well as the core protein will take on a brush-like conformation. Charge repulsion and excluded volume play a role in creating this shape. However, a slight collapse of the structure may have occurred when moving from a fluid environment to an ambient environment. As described previously [112], the number of macromolecular conformations may be dramatically reduced by the constraining transition from three to two dimensions after physisorption from solution onto a surface. For weak intermolecular-surface interactions the macromolecules can rearrange and equilibrate on the surface as they would in a 2D solution, while for stronger interactions, the molecules are quickly fixed to the surface in a conformation that is close to a 2D mathematical projection of the 3D solution conformation onto the surface. For the first case (weak binding), the lowest energy conformation of the macromolecules existing in a 2D space are achieved and thus, meaningful structural information can be extracted from the 2D images [112]. For the second case (strong binding), "kinetic trapping" of the molecules on the surface takes place and conformations are determined by the details of the approach to the surface (e.g. diffusion processes) and the nature of the intermolecular surface forces (e.g. adsorption and solvent evaporation). In addition, the 2D conformation can be modified and biased by the lateral force exerted by the probe tip during imaging, which for tapping mode in air with capillary forces can be up to 9 nN for a tip radius of 10 nm [120].

The non-zero kurtosis for lower values of l suggest that the assumptions inherent to the WLC approach may not apply as well in this range of l for complex glycosylated molecules like aggrecan, whose contour trace length is not an order of magnitude longer than L_p. Nevertheless, the distributions of θ for aggrecan and GAGs were reasonably consistent with the distribution of θ predicted by the WLC model for larger l (Figure 2-13(c)). We therefore, used the WLC model to calculate an effective persistence length L_p and found that the fetal aggrecan was significantly stiffer ($L_p = 110\,\text{nm}$) than the mature aggrecan ($L_p = 82\,\text{nm}$). The shorter persistence length of the mature aggrecan is consistent with several other nanostructural measurements obtained from these images, since the increased CS-GAG spacing and shorter chain lengths of the mature aggrecan would be expected to result in reduced stiffness, which is reflected in both the shorter persistence length and the shorter end-to-end length. CS-GAGs may individually satisfy the assumptions of the WLC model; however, the influence of inter- and intramolecular repulsion of chains through polyelectrolyte effects due to intramolecular electrostatic double layer repulsion, as well as excluded volume, which is amplified by close proximity of the chains is manifested in an increased effective L_p to an extended rigid-rod type conformation. Although we observed a higher mean stiffness for the fetal GAG, the difference in effective L_p was not statistically significant. It is important to note that conformation into a 2D state brings the CS-GAG chains closer in proximity to each other compared to a 3D state in which the CS chains are allowed to extend without constriction in a certain direction. This and excluded volume may lead to a slightly increased calculated L_p for both whole aggrecan as well as single CS chains. Further study is needed to verify that assumptions in the WLC model are valid for these molecules under the conditions of our experiments.

2.4.5 Comments on the Relation of AFM Experiments to Native Physiological Conditions

From the appearance of the aggrecan monolayer in Figure 2-7, we can estimate a corresponding 3D aggrecan density and compare with the known concentration of aggrecan in native cartilage (20-80 mg/ml). When modeled as 2D and flat, the thickness of aggrecan would be on the order of 1-10 nm based on GAG dimensions; thus, a compacted monolayer thickness of 1-10 nm would give an aggrecan concentration of 15-150 mg/ml, which brackets the physiological range. This calculation suggests that the GAG density pictured in Figure 2-7 is likely to be on the order of that found in fully hydrated (3D) native cartilage. Alternatively, if we fix the positions of the core protein in Figure 2-7 and assume that the fully hydrated thickness of each aggrecan would be approximately twice the length of the CS-GAG chain (i.e. $\sim$ 100 nm), the aggrecan density pictured in Figure 2-7 would correspond to $\sim$1.5 mg/ml, about 40 times less than physiological concentration. This suggests that the aggrecan core density pictured in Figure 2-7 is likely to be far less than that in tissue when extrapolated to 3D. Even on this experimentally generated dense surface, flexibility and interdigitation are seen between the aggrecan molecules and in the CS-GAG region. It is expected that by scaling up the density 40x greater than this compact space will certainly lead to a significant amount of interdigitation and repulsive interaction between the aggrecan GAG chains. Moreover, with this high density of aggrecan at the tissue level, these nm-sized differences in aggrecan structure multiply quickly and can be translated into major differences in the compressive moduli of cartilage.

2.4.6 Conclusions

The fetal aggrecan was obtained from epiphyseal cartilage, which comes from the load bearing region of an articulating joint. The mature aggrecan was obtained from nasal cartilage, which provides a static shape but is not subjected to repeated mechanical loading. While the basic structure of aggrecan from these two cartilaginous tissues is similar, there are clear differences which may be associated with tissue mechanical

function. In confined compression, the equilibrium modulus of human articular cartilage was ~600 kPa [131] and that of human nasal cartilage was 233 kPa [114]. This data correlates nicely with the findings reported here that aggrecan from the load bearing epiphyseal cartilage has a denser CS-GAG brush region, longer CS chains, and a greater calculated stiffness which might be expected when compared to the non-load bearing nasal cartilage. Visualization of dense monolayers of these two aggrecan types gives important clues as to how neighboring aggrecan molecules may deform to accommodate each other under the highly compressed situations found in native cartilage.

Measurements on individual aggrecan molecules and constituent GAG chains were correlated to bulk measurements determined from standard biochemical techniques. In addition, the ability to measure single molecules in their near native state provides additional information on structure and conformation. Distinct differences between two aggrecan populations (e.g. mature nasal versus fetal epiphyseal) have been clearly observed and hence, it is clear that AFM studies of molecular constituents as a function of age, disease, and injury have great promise to yield new insights into for example, proteolytic degradation, and the molecular origins of cartilage dysfunction. Given the biochemical data confirming the presence of full-length aggrecan for both fetal and mature in conjunction with the measured dimensions of an overall shorter and a broader distribution of contour length of mature aggrecan core protein, it can be speculated that the increase in spacing between GAGs and decrease in GAG length results in a diminished repulsion between GAG chains, allowing the amino acid sequence of the protein core backbone to take on a lower energy state (i.e. from a strained linear shape to a relaxed coiled shape), thereby resulting in a shorter overall contour length. Decreased persistence length (i.e. stiffness) of the mature aggrecan may be a direct result of the reduced electrostatic repulsion in the CS-brush region.

AFM also has the potential to directly study the interaction between aggrecan and hyaluronan and the self-assembly process of the proteoglycan aggregate. Surfaces like this will allow for the measurement of intermolecular forces between a biomimetic surface such as a CS-coated tip or an aggrecan-coated tip versus an aggrecan coated

surface. Such nanoscale information is critical to the understanding and prediction of cartilage intermolecular forces (e.g. electrostatic double layer, steric, etc.) and unique nanoscale deformation mechanisms (e.g. interdigitation versus compression) responsible for macroscopic biomechanical function [25].

Chapter 3

Effect of Aggrecan Density and Bath Ionic Strength on Aggrecan Conformation

3.1 Introduction

Aggrecan, a brush-like macromolecule, is responsible for more than 50% of the compressive modulus in articular cartilage [14]. Glycosaminoglycans are spaced along the core protein at a very high density giving the molecule an overall extended conformation in a dilute, low salt solution. Individual aggrecan dimensions have been measured directly from atomic force microscopy (AFM) images [95]. Aggrecan and its aggregate structure have been studied by a number of techniques in an effort to elucidate the structure-function relationship [48, 11, 10].

In tissue, aggrecan is found at gel-like concentrations at 20-80 mg/ml and forms a dense mesh-like porous network [81]. The collagen fibers act to hold the matrix molecules in a small compact region, thus creating a very compressed matrix of proteoglycans, specifically of aggrecan. The carboxyl and sulfate groups on the disaccharides that make up the GAG chains are easily ionized at physiologic pH, and therefore cause electrostatic repulsion between GAG chains. This electrostatic repulsion is re-

sponsible for the compressive modulus. However, the interaction between aggregan or their GAG chains on neighboring molecules is still unknown. Compression of native cartilage can cause an increase in local aggrecan concentration leading to an anisotropic permeability [107, 108], whereas degradation of the collagen network can cause a decrease in local aggrecan concentration. For both cases, conformation may be altered leading to a change in molecular interaction.

In addition to local aggrecan density, conformation of the brush-like molecules may be dependent on a number of factors such as side chain length [90, 136, 123, 135], side chain spacing [36, 71], and side chain charge density [124, 115, 6]. Conformation of aggrecan may also be altered by counter-ions present in the bath solution which will act to decrease the Debye length, thereby reducing electrostatic repulsion leading to a conformational change [6].

Here we use the technique of AFM to elucidate the conformational changes of aggrecan, a highly charged brush-like macromolecule, in two types of environments. In the first condition, aggrecan conformation is studied as the local aggrecan density varies from a very sparse, dilute environment to a more concentrated environment. In the second condition, aggrecan conformation is studied in four low ionic bath conditions ranging from deionized water to physiologic ionic strength, 0.1 M.

3.2 Materials and Methods

3.2.1 Purification of Aggrecan

Thin slices of fetal bovine cartilage was obtained from the epiphyseal growth plate. The tissue was digested in 4 M guanidium hydrochloride, 100 mM sodium acetate, pH 7.0, with protease inhibitors for 48 hours. Undigested tissue was then removed through centrifugation. The supernatant containing digested tissue was dialyzed against two changes of 100 volumes of 0.1 M sodium acetate, pH 7.0, with protease inhibitors [50, 11]. Highly purified A1A1D1D1 fetal epiphyseal bovine aggrecan was extracted through a series of cesium gradient centrifugations. Biochemical charac-

terization was described previously [95]. SDS-PAGE and Western blot analyses were used to confirm that the aggrecan core protein was predominantly full-length. Superose 6 FPLC (Amersham-Pharmacia Biotech) column chromatography in combination with 1,9-dimethylmethylene blue (DMMB) was used to determine the number of disaccharides (~51) per GAG chain.

3.2.2 AFM Sample Preparation and Imaging

Muscovite mica surfaces (SPI Supplies, West Chester, PA) were chemically modified with 3-aminopropyltriethoxysilane (APTES; Pierce Chemical) to create a positively-charged surface. Amine groups were exposed on the mica surface after covalent linkage of the exposed silanol groups on freshly cleaved mica with the APTES molecule. Immediately after cleaving squares of mica (1x1 cm^2), forty microliters of 0.01% (v/v) APTES solution was deposited on the surface, given 20 minutes for the aminosilane reaction to occur, then rinsed thoroughly. One edge was blotted to remove excess moisture and then allowed to air dry for 5 minutes. Purified aggrecan was diluted with deionized water or varying salt solutions (0.001 M to 0.1 M NaCl) to a concentration of 500 μg/ml. 50 μl was deposited on the mica surface, allowed 20-30 minutes to equilibrate, rinsed gently, and blotted on one edge. Incubation time of the aggrecan solution on the surface was used to vary the 2-D surface density of aggrecan. The samples were allowed to air dry for at least 2 hours prior to imaging. Each sample was imaged the day of preparation. Tapping mode AFM (TMAFM) on the Nanoscope IIIa Multimode (Digital Instruments, Santa Barbara, CA) was employed for imaging of samples in ambient conditions using Olympus AC240TS-2 rectangular Si cantilevers ($k = 2$ N/m) with a typical tip radius <10 nm. The cantilever was driven just below resonant frequency (~70 kHz) and at a low scan rate of 1-3 Hz to minimize noise and sample perturbation. Data was collected on the maximum sample size of 512 x 512 pixels.

3.2.3 Analysis of AFM Images

AFM image files were flattened first order and converted to .jpeg, and analyzed using SigmaScan Pro image analysis software (SPSS Science, Chicago, IL). The core protein of each aggrecan was digitized into pixels yielding spatial coordinates of each position along the polymer chain. The trace length, L_c, and end-to-end length, R_{ee}, were measured directly from these images. An extension value,

$$Ext = \frac{R_{ee}}{L_c} 100, \tag{3.1}$$

for each molecule was calculated. Systat Software Inc. (Richmond, CA) was used to perform a one-way ANOVA to determine the significance of density or ionic strength on aggrecan conformation on a 2-D surface. If significance ($p<0.001$) was found, a Tukey post-hoc multiple comparisons test was performed to identify the significance between groups.

3.3 Results

3.3.1 Visualization of Varying Aggrecan Surface Densities

The brush-like chondroitin sulfate GAG region was clearly resolved, and the molecular details of the individual GAG on the fetal epiphyseal aggrecan monomers could be directly visualized via tapping mode AFM in ambient conditions. Three concentrations were achieved on the 2D modified-mica surface: 0.5, 1.4, and 2.3 mg/ml. The concentration was calculated by calculating a sphere of volume occupied by the average radius of gyration for an aggrecan monomer. Given the radius of gyration, the packing number of aggrecan per $1\,\mu m^3$ box was calculated. The volumes of the aggrecan spheres were converted to a weight using the molecular weight of full-length fetal aggrecan, $3{\cdot}10^6$ Da/aggrecan. Dividing this number by the $1\,\mu m^3$ box gave the concentration. This calculation assumes no interpenetration of neighboring aggrecan.

At the lowest concentration, 0.5 mg/ml, aggrecan were at a spacing greater than an aggrecan width apart and had room for movement without interaction with neigh-

boring molecules (Figure 3-1(a)). A thinner bare core protein in the N-terminal region was distinct from the brush-like GAG region. More structural details are described previously [95].

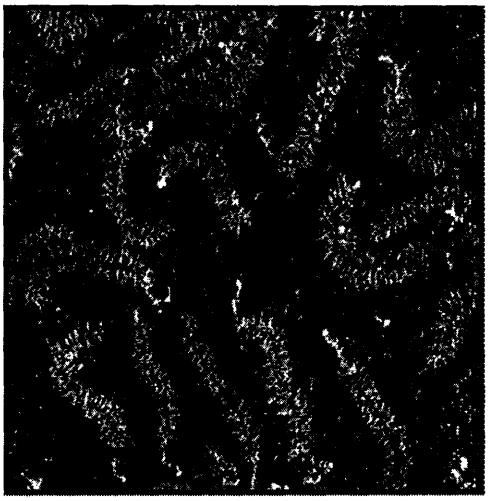

(a) 0.5 mg/ml height image

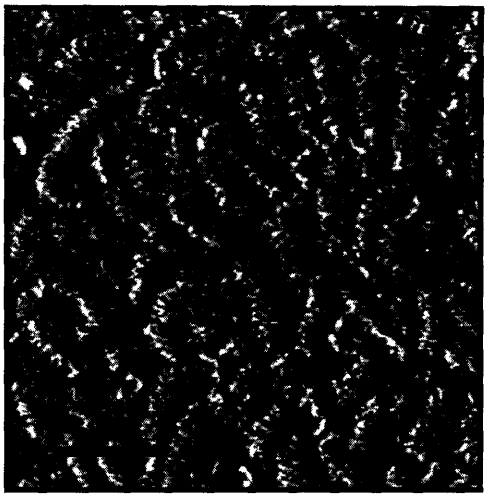

(b) 1.4 mg/ml amplitude image

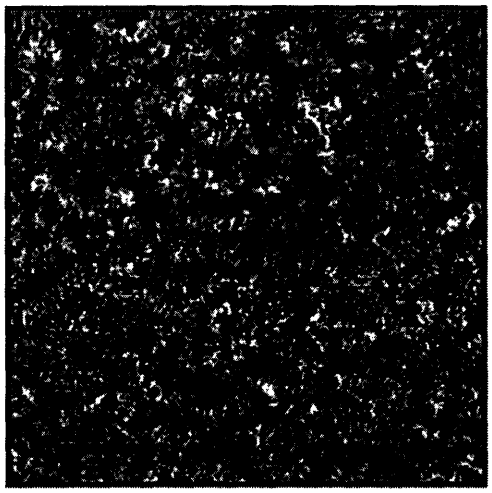

(c) 2.3 mg/ml height image.

Figure 3-1: Representative images taken with tapping mode AFM in air of fetal epiphyseal bovine aggrecan at three densities. The scale bars are 200 nm long.

At 1.4 mg/ml, aggrecan were $\sim$1/2 an aggrecan width apart, 23.7$\pm$1.3 nm, and more restricted in motion on the 2D surface although most had an extended conformation (Figure 3-1(b)). At 2.3 mg/ml, aggrecan were only nanometers apart from each other and thus conformed to surrounding molecules to fit into the given amount

space, and thus more collapsed in conformation (Figure 3-1(c)).

3.3.2 Statistical Analysis of End-to-End Length and Extension of Varying Aggrecan Surface Densities

Conformation was quantified through measurement of the end-to-end distance (Table 3.1), R_{ee}, of the aggrecan monomers. R_{ee} decreased with increasing concentration giving 267±9 nm (mean±SE), 253±10 nm, 185±5 nm, for lowest to highest concentration, respectively. The trend seen in Figure 3-2(a) showed a significant decrease between the 2.3 mg/ml aggrecan surface and the 0.5 mg/ml and 1.4 mg/ml surfaces confirmed by ANOVA ($p<0.001$) followed by a Tukey test. Extension of the molecule (Equation 3.1) was also found to decrease on the 2.3 mg/ml aggrecan concentration surface compared to the two lower concentration surfaces from 47±1 nm, 64±3 nm, to 60±3 nm, highest to lowest concentration, respectively. The histogram (Figure 3-2(b)) showed a peak in the distribution of extension between 75-90% for the two lower density surfaces, while the extension for the 2.3 mg/ml aggrecan surface shows a broader distribution between 30-75% extension.

Density (mg/ml)	$L_c \pm SE$	$R_{ee} \pm SE$	$Ext \pm SE$
0.5	442±9	267±9	60±2
1.4	395±10	253±10	64±3
2.3	389±5	183±5	47±1

Table 3.1: Summary of measurements from AFM images of aggrecan samples at various densities.

3.3.3 Statistical Analysis of End-to-End Length and Extension of Aggrecan in Varying Ionic Baths

Contact and tapping AFM images of aggrecan in varying ionic bath solutions on a mica surface were obtained but had poor resolution of the GAG chains due to thermal motion. For the higher ionic strengths, the electrostatic interaction between the negatively-charged GAG chains and positively-charged mica diminished, and the

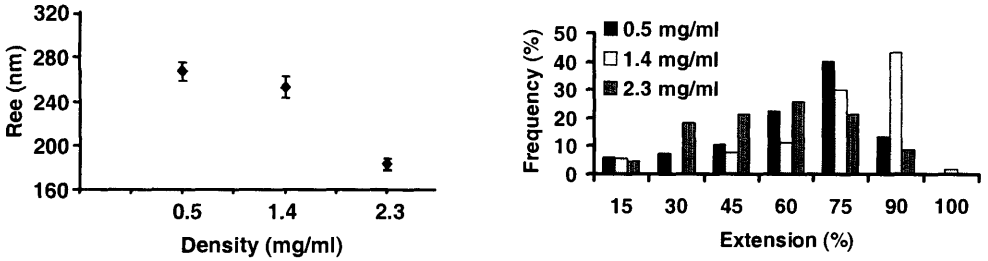

(a) Average $R_{ee} \pm SE$ of the 0.5 mg/ml (n=100), 1.4 mg/ml (n=53), and 2.3 mg/ml (n=170) aggrecan measured from AFM images.

(b) Histogram depicting distribution of extensions of aggrecan. The lower densities peak between 75-90% while the highest density shows a wider distribution between 30-75% extension.

Figure 3-2: Measurements of aggrecan conformation at three densities.

force applied by the tip tended to move the aggrecan off of the surface. Therefore, tapping mode AFM in ambient conditions (i.e. dry conditions) were used for imaging.

For all ionic strengths below 0.1 M, aggrecan overall had an extended conformation (Figure 3-3). At 0.1 M, aggrecan had a collapsed ball-like appearance (Figure 3-4(d)). The collapsed structure made it difficult to obtain a trace length of the core protein, so a trace along the center of curvature of the molecule was measured. As described before, the end-to-end measurement was taken by measuring the distance between the ends of the molecule. Ionic strength was found to have significant affect on whole aggrecan conformation R_{ee}, L_c, and Ext (ANOVA, $p<0.001$) (Table 3.2). A Tukey post-hoc test showed the 0.1 M L_c and R_{ee} were significantly different ($p<0.001$) from the other ionic strengths. A decrease in L_c (Figure 3-3(a)) of the core protein of the aggrecan sample prepared in DI water, 0.001 M, 0.01 M, and 0.1 M was measured at 441±9 nm, 451±9 nm, 367±13 nm, and 197±6 nm, respectively. A decrease in R_{ee} length (Figure 3-3(b)) of the core protein, L_c, of the aggrecan monomers was measured at 267±9 nm, 283±10 nm, 273±12 nm, and 116±12 nm for DI water, 0.001, 0.01, and 0.1 M, respectively. The extension varied with increasing ionic strength at 61±2 nm, 63±2 nm, 76±3 nm, and 59±6 nm for DI water, 0.001, 0.01, and 0.1 M, respectively. At 0.01 M, the extension varied significantly from the other ionic conditions (Tukey, $p<0.001$).

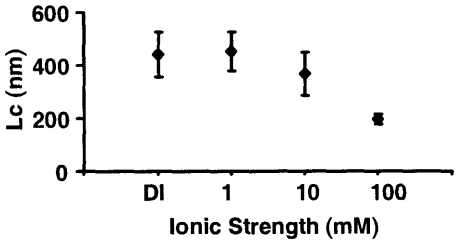

(a) A significant decrease in L_c is seen at 0.1 M compared to the lower ionic strengths.

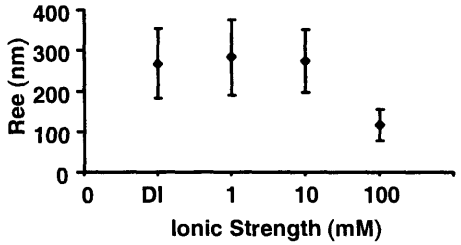

(b) A similar trend is seen in R_{ee}.

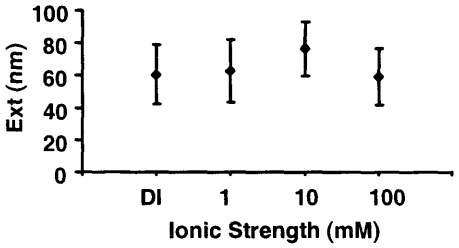

(c) A significant increase in *Ext* is seen at 0.01 M. Extension was difficult to quantify at 0.1 M due to collapse of the molecules, making the trace length difficult to measure

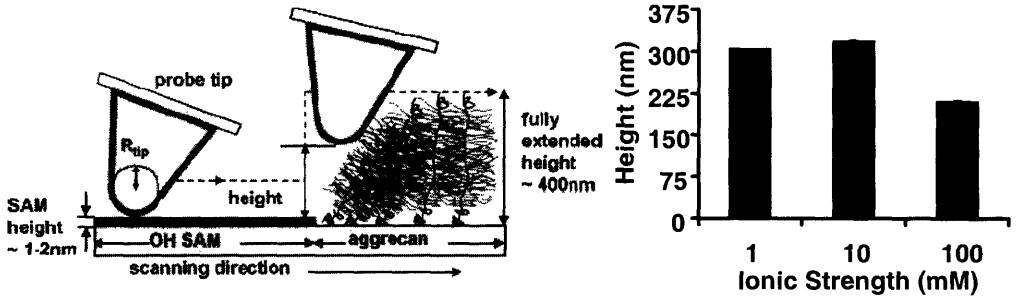

(d) Dean et al. [24] saw similar trends on AFM height measurements of patterned end-grafted aggrecan surfaces. A significant decrease in aggrecan height was not measured until 0.1 M NaCl.

Figure 3-3: Measurements (mean$\pm SD$) from AFM images of aggrecan deposited in low ionic strength bath conditions.

Ionic Strength (mM)	$L_c \pm SE$	$R_{ee} \pm SE$	$Ext \pm SE$
DI	441±9	267±9	61±2
1	451±9	283±10	62±2
10	367±13	273±12	76±3
100	197±6	116±12	59±6

Table 3.2: Summary of measurements from AFM images of various aggrecan concentrations

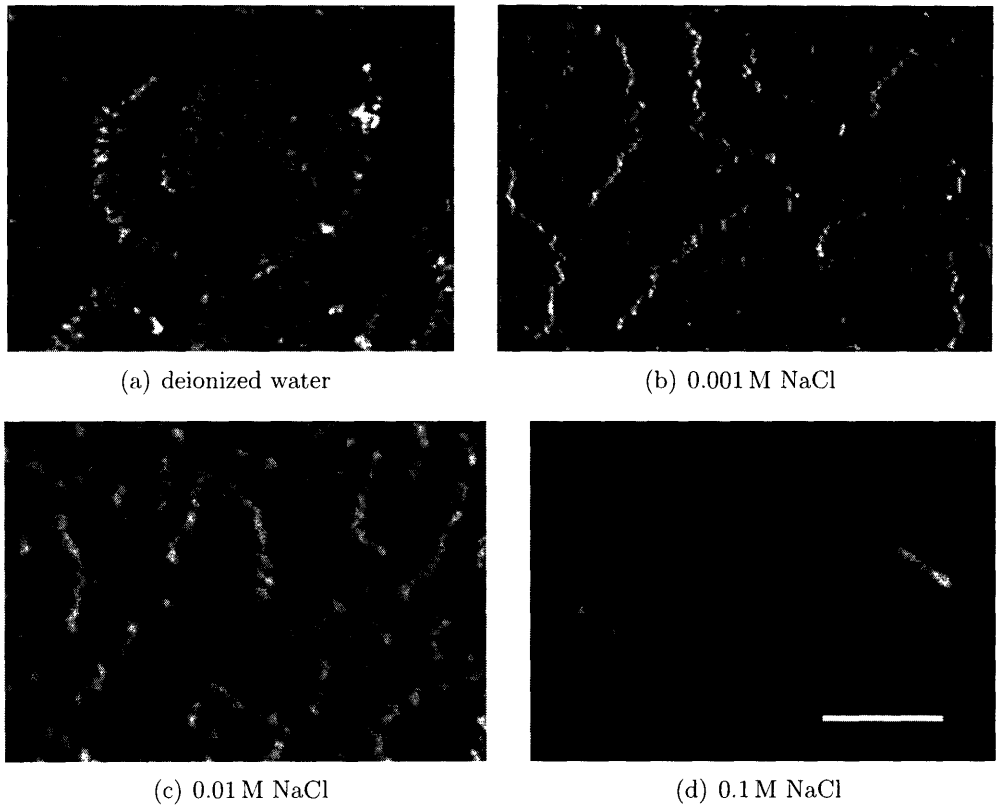

(a) deionized water (b) 0.001 M NaCl

(c) 0.01 M NaCl (d) 0.1 M NaCl

Figure 3-4: Representative tapping mode AFM images of aggrecan prepared in different conditions. While the individual GAGs are difficult to distinguish, the molecules retain a mostly extended rod-like shape in 0.01 M NaCl as seen in (a)-(c). (d) At 0.1 M NaCl, aggrecan collapses into a more ball-like structure. The scale bars equal 200 nm.

3.4 Discussion

3.4.1 Aggrecan Sample Preparation and Imaging

Highly purified aggrecan samples were used for preparation of all AFM samples, and salt solutions were filtered through a 0.200 μm filter to minimize contaminants. Aggrecan was allowed to equilibrate on the surface to ensure a relaxed conformation, which was confirmed by calculation of the kurtosis, the Gaussian distribution of angles formed by vectors projected along the aggrecan core protein (data not shown). A thin angstrom level of water exists on the mica surface even in ambient conditions [123], allowing ionization of the charged groups and thus ensuring the electrostatic

interaction between the negatively-charged GAG chains and the positively-charged APTES mica, which helps to minimize displacement of aggrecan during imaging.

3.4.2 Comparison of Aggrecan AFM Measurements on Varying Surface Densities With Conformation Measurements Assessed by Other Techniques

AFM offers additional information of direct visualization of individual molecules over usual molecular measurement techniques, which gives results on an ensemble of molecules. Light scattering has been used to measure radius of gyration of an ensemble of brush-like molecules, but conformation is difficult to measure in concentrated solutions. Arrangement of aggrecan may have a significant effect on the bulk properties of cartilage. GAG orientation, modeled as cylinders, in cartilage deformation resulted in different hydraulic permeability values, which were dependent on orientation [107]. We have been able to achieve and image effective concentrations as high as 2.3 mg/ml aggrecan. At this density, the molecules conformed and interacted with neighboring molecules more than the lower density surfaces, and a significant decrease in extension was observed. Interestingly, concentrations of aggrecan above 2 mg/ml, its overlap domain, have been found to reduce its self-diffusion coefficient, as measured by fluorescence recovery after photobleaching [41]. Eliminating the electrostatic component of aggrecan in a 4 M guanidium hydrochloride solution, Harper and Preston (1987) [117] were able to demonstrated shrinkage of aggrecan in the presence of increasing concentrations of dextran, a linear polymer, due to excluded volume effects. Changes in molecular interaction were measured in rheology experiments of aggrecan aggregate solutions. Above the overlap concentration, ~5 mg/ml, the aggregate solution exhibited physical changes from a viscoelastic liquid to a gel-like material [85, 86]. Due to limits of resolution and sample preparation, aggrecan concentrations much higher than 2.3 mg/ml were difficult to achieve for AFM imaging. The limitation of the 2D surface preparation reduces the mobility, number of interactions, and configurations that aggrecan may undergo in a 3D environment

[122, 80]. Simulation and modeling may be needed for characterization of aggrecan conformation at much higher concentrations.

3.4.3 Comparison of Aggrecan AFM Measurements in Varying Ionic Baths With Conformation Measurements Assessed by Other Techniques

The GAG structure and density along the aggrecan core protein dictates the overall conformation and stiffness of the macromolecule. Previous AFM studies on individual fetal epiphyseal and mature nasal bovine aggrecan have shown that a higher GAG packing density along with longer GAG chains can be correlated to a larger persistence length [95]. This study looks at the changes in conformation of the highly charged molecules as the ionic strength of the bath environment is varied from DI water to 0.1 M NaCl. As ionic strength is increased, charge shielding from the counterions reduces the Debye length to ~1 nm at 0.1 M NaCl. Aggrecan deposited from all conditions except for the highest ionic strength, 0.1 M NaCl, remained mostly extended. The Debye length, ~3 nm at 0.01 M, is larger than the GAG spacing along the core protein, which may explain the extended conformation at and below 0.01 M NaCl. At 0.1 M, the Debye length drops below the average GAG spacing, allowing slight collapse of the molecule exhibited in the reduction of L_c from 441 nm (DI water) to 197 nm. A significant height decrease of dense end-grafted aggrecan (Figure 3-3(d)) surfaces measured via AFM has also been seen at the bath ionic strengths 0.1 M NaCl and 1.0 M [24]. It is interesting to note the large change in conformation occurred at 0.1 M NaCl, physiologic ionic strength. Molecular simulations of an aggrecan segment with 40 short side chains (16 disaccharides long) showed a dramatic decrease in persistence length from 180 nm at 0.01 M NaCl to 40 nm at 0.1 M NaCl [91]. Light scattering of dilute aggrecan solutions showed a dependence of persistence length, L_p, to ionic bath strength where $L_p \sim (\text{ionic strength})^{-0.5}$ [76].

We have directly visualized for the first time the collapse of a highly charged macromolecule in physiologic conditions. At this condition, we are likely seeing a

diminished ability to resist compression. The physical information obtained with direct visualization of individual aggrecan at physiologic ionic strength provides more information about possible conformation of aggrecan in articular cartilage. Its interaction area and increased complexity in conformation may alter the diffusion of molecules through cartilage matrix for interaction with other extracellular molecules. Cartilage presents a very complex environment for molecular diffusion compared to other tissues or molecules that may flow through blood, which has little material or matrix to interact with before producing its intended effects.

3.5 Conclusion

These studies offer insight into the conformational changes that may occur as an increasing number of aggrecan molecules are packed into a given amount of space. With increasing aggrecan concentration, the molecules may tend to collapse or entangle to make use of all available volume. Direct visualization of the collapse of aggrecan at higher densities and at physiologic ionic strength shed light into possible conformation of aggrecan in articular cartilage. In DI water and low ionic baths $< 0.1\,\mathrm{M}$, the Debye length is greater than the GAG spacing along the core protein, causing the aggrecan to adopt a mostly extended conformation allowing for visualization of individual GAG chains. However, we obtain a more physiologic relevant view of aggrecan conformation at $0.1\,\mathrm{M}$. At this ionic strength, the Debye length reduces to about the distance between GAG chains and the aggrecan molecules appear more collapsed. Given the conformational change that occurs at physiologic condition with the additional information gathered from the density experiments, one may hypothesize that aggrecan is found in a much more compact conformation, and thereby has a reduced availability of interaction with other molecules such as collagen or enzymes.

Chapter 4

Nanomechanical Properties of Individual Chondrocytes and Their Developing Growth Factor-Stimulated Pericellular Matrix

4.1 Introduction

Chondrocytes occupy only 3-5% of the volume of adult articular cartilage, and hence, do not contribute significantly to the bulk mechanical properties of the tissue [126]. However, they are entirely responsible for the synthesis, maintenance, and turnover of the tissue's extracellular matrix (ECM). Mechanical loads and deformations applied to cartilage *in vivo* and *in vitro* are known to regulate chondrocyte synthesis and catabolic degradation of ECM macromolecules [44, 65, 133, 32]. The mechanoregulation of chondrocyte metabolism in gel scaffolds for tissue engineering depends in part on the cell's microenvironment and the stage of development of the newly synthesized, cell-associated pericellular matrix (PCM) that surrounds each cell [14].

The mechanisms underlying mechanotransduction are not completely understood.

The 2-4 μm-thick PCM contains a high percentage of type VI collagen and proteoglycans [105, 104] and is critically important to cell function from a biochemical and biomechanical perspective [100]. The PCM modulates and transfers loads from the ECM to the cell and its intracellular organelles and cytoskeleton during physiological compression. The mechanical properties of chondrocytes with and without their PCM have been measured using micropipette aspiration [42], cytoindentation [68], and in unconfined compression [74]. While Young's moduli for isolated chondrocytes have been reported in the range 0.6-4 kPa [63, 38], the PCM in adult cartilage has a higher elastic modulus (~60-70 kPa), measured via micropipette aspiration [44, 1], compression of chondrons in agarose [67], and AFM indentation [3]. The ECM has a much higher equilibrium modulus (~ 0.5 MPa) than the cell or PCM. Even newly developed PCM can alter cell deformation, as chondrocytes seeded in a 3% agarose gel deformed more and had a slower viscoelastic recovery compared to the same cells surrounded by synthesized matrix after 6 days in FBS supplemented culture [72].

The PCM may also act as a regulator of cell signaling. Scaffolds seeded with enzymatically extracted chondrons accumulated proteoglycans and type II collagen more quickly than parallel cultures of enzymatically isolated chondrocytes, which are no longer surrounded by PCM [40]. Growth factors such as insulin-like growth factor (IGF-1) and osteogenic protein 1 (OP-1) have been shown to increase PCM accumulation of cultured chondrocytes compared to chondrocytes maintained in fetal bovine serum (FBS) [84, 35, 134, 97, 77]. Chondrons in adult cartilage have a fully developed PCM architecture and morphology that is absent from the PCM of chondrocytes in young immature tissue [73]. For example, immunohistochemistry revealed a compact structure containing type VI collagen in adult chondrons but not in immature tissue in which staining for for type VI collagen is more diffuse [73]. Efforts to create tissue engineered cartilage for tissue repair thus require detailed understanding of the chondrocyte's microenvironment.

This study examines the mechanical properties of chondrocytes and their newly developing pericellular matrix using atomic force microscope (AFM)-based indenta-

tion at two length scales by probing with a nano-sized tip and a micron-sized tip. Our first objective was to characterize the mechanical properties of chondrocytes freshly isolated from immature bovine cartilage using AFM indentation with both probe tips while keeping the cells viable. To deal with the phenotypically round chondrocytes, we developed a surface to immobilize the cells in their native state, thereby extending the capabilities of AFM to measurements on non-adherent cells. The second objective was to quantify the mechanical properties of chondrocytes released from 3D alginate gel after selected periods of culture to determine the effects of the newly developing PCM on the measured cell-PCM stiffness with time in culture. Cells were maintained in medium supplemented with either FBS or the combination of IGF-1 plus OP-1 to compare the effects of these anabolic stimulants on PCM development and the resulting link between PCM structure and biochemical composition with the resulting biomechanical properties of the cell-PCM. Using Hertzian contact mechanics and finite element analyses, material properties were estimated from the AFM force-indentation curves measured with these cell preparations.

4.2 Materials and Methods

4.2.1 Cell Isolation and Culturing

Chondrocytes were isolated from femoral condyle cartilage of 2-3 week old bovine calves using sequential 0.2% pronase (Sigma) and 0.025% collagenase (Boehringer Mannheim) digestions as described [110]. Cell viability after isolation, assessed by Trypan Blue (Sigma) exclusion, was (>95%). Cells were seeded at $20{\cdot}10^6$ cells/ml in 2% w/v alginate (Kelco LVCR) in 0.9% NaCl. Beads, ~3 mm diameter, were formed through polymerization of droplets of alginate dispensed from a 22-gauge needle into 102 mM $CaCl_2$ solution. At selected times in culture, cells were released from the alginate beads by depolymerization in 55 mM NaCitrate (Fisher Scientific) as described [82]. Cell viability after release was >90% as assessed using fluorescein diacetate (FDA) (0.2 mg/ml) and ethidium bromide (EtBr) (10 μg/ml) (Sigma).

In one series of experiments, cell-seeded beads were maintained in 10% FBS hi-glucose DMEM with 20 μg/ml L-ascorbic acid (Sigma) plus 1% antibiotic-antimycotic (Sigma). In a second series, cells were cultured in 100 ng/ml recombinant human IGF-1 (PreproTech, Inc.) plus 100 ng/ml recombinant human OP-1 in hi-glucose DMEM with 1% antibiotic-antimycotic and mini-ITS (5 nM insulin (Sigma) to minimize stimulation of the IGF-1 receptor, 2 μg/ml transferrin (Sigma), 2 ng/ml selenous acid (Sigma), 420/2.1 μg/ml linoleic acid-albumin from bovine serum albumin (Sigma), and 55 μg/ml L-ascorbic acid) (Benya and Padilla 1993). Seven alginate beads were cultured in 3ml medium per well (12 well plate); medium was changed every other day.

4.2.2 Microfabrication of Silicon Wells

Chips were microfabricated on silicon wafers, each chip containing a matrix of wells made to entrap a single cell in each well (Figure 4-5). The wells were etched with a 20% KOH solution using a silicon oxide hard mask of circles with diameters of 15, 18, 20, and 22 μm. The production of inverted square pyramids from circular or square mask openings (or V-shaped trenches for rectangular mask openings) is a consequence of the etch's anisotropy. (100) and (110) crystal planes are etched much more quickly than (111) planes, so self-terminating features bound by (111) planes are produced, forming planes 55 degrees from the vertical [69].

The masking oxide was thermally grown on 100 mm diameter single crystal silicon wafers and patterned with a Buffered Oxide Etch (BOE) using a photoresist mask. The photoresist was then stripped and the wafers placed in a 80°C bath of 20% KOH for approximately 15 minutes until the etch self-terminated. The oxide mask was stripped with a second bath in BOE and the wafer was singulated with a die-saw. Microfabrication was performed at MIT's Microsystems Technology Laboratory.

4.2.3 Histology & Immunohistochemistry of Type Col VI Labeling

See Appendix E. Groups of cells released from alginate were resuspended in culture medium ($1{\cdot}10^6$ cells/ml) and fixed in 2% v/v glutaraldehyde (Polyscience, Inc.) buffered with 0.05 M sodium cacodylate (Sigma), and containing 0.7% w/v ruthenium hexammine trichloride RHT (Polyscience, Inc.) to minimize loss of PGs during fixation [60]. Fixed cells were mounted onto glass slides using a Cytospin (1400 rpm for 10 min.), air dried, and stained for sulfated PGs (Toluidine Blue O (Sigma)) and collagen (phosphomolybdic acid (Rowley Biochemical Inc.) followed by aniline blue (Rowley Biochemical Inc.)) [78]. Images were taken with a standard Nikon optical microscope. In addition, groups of cells from culture day 39 were released, mounted onto glass slides, dried for 3 hours, treated with 2 mg/ml hyaluronidase (Sigma) in 0.1 M Tris-HCl, pH 5.8, for 2.5 hours at 37°C to expose type VI collagen epitopes, then blocked with 5% donkey serum in PBS, pH 7.1, for 4 hours. The antibody for col VI (Chemicon) was incubated on the slides overnight (1:10 in 1% donkey serum in PBS), then incubated with a secondary-conjugated antibody (1:50 dilution in 1% donkey serum in PBS) for 4 hours. Slides were rinsed with PBS after each step, and the fluorescent labelled cells were viewed using a Nikon TE300 microscope.

4.2.4 Cell Appearance Pericellular Biochemical Composition

Dimethyl methylene blue dye binding (DMMB) [30] and hydroxyproline [137] assays were used as measures of sulfated GAG and collagen content, respectively. Optical micrographs of cells released at each time point were obtained to measure the diameter of the cell and to aid in estimating PCM thickness.

4.2.5 Atomic Force Microscope Imaging

Dilute solutions of chondrocytes were deposited onto freshly cleaved muscovite mica (SPI Supplies, West Chester, PA), allowed to incubate on the surface at room temperature for 5 minutes, and then rinsed gently with DI water. One edge was used to

blot dry the sample before air drying at room temperature overnight. Tapping mode AFM (TMAFM) on the Nanoscope IIIa Multimode (Digital Instruments, Santa Barbara, CA) was employed for imaging of samples in ambient conditions using Olympus AC240TS-2 rectangular Si cantilevers ($k = 2\,\mathrm{N/m}$) with a typical r_c <10 nm. The cantilever was driven just below resonant frequency (~70 kHz) and at a low scan rate of 1-3 Hz to minimize noise and sample perturbation. Data was collected on the maximum sample size of 512 x 512 pixels.

4.2.6 Atomic Force Microscope Indentation

The silicon substrates were cleaned in piranha solution (3:1 concentrated H_2S0_4/H_2O_2 (30%)) to remove all organics, then rinsed with acetone and water. The substrates were submersed in DI water for 2 days to remove all traces of piranha solution. Just before use in the AFM, culture medium was allowed to coat the silicon surface for 5 minutes. 100 μl of cell suspension was then dropped onto the surface. Using an AFM probe tip, the cells were gently pushed into the silicon wells. The wells containing cells were mapped so indentation could be repeated using a second type of probe tip. The Picoforce AFM (Veeco Instruments) was used to obtain indentation data. The ramp was varied between 3 and 6 μm to obtain full loading and unloading curves. Indentation rates of 200 nm/s, 500 nm/s, 1 μm/s, 3 μm/s, 5 μm/s, and 10 μm/s were used. Two different sized tips were used for the indentation experiments. A standard silicon nitride AFM square pyramidal tip (~50 nm nominal radius, k~0.06 N/m, Veeco) and a colloidal probe tip (2.5 μm radius, k~0.06 N/m) were used. The colloidal probe tip was prepared using the AFM to attach 2.5 μm radius silica beads (Bang Labs, #SS06N) onto tipless cantilevers (Veeco, k~0.06 N/m) with low viscosity epoxy (SPI, MBond 610) using AFM.

4.2.7 Finite Element Analysis and Tip Reconstruction

Finite element analysis (FEA) of cell indentation with a nanosized AFM pyramidal tip and micron-sized colloidal probe tips were performed using ABAQUS (ABAQUS,

Inc., Providence, RI). Because the nanosized AFM probe tip is not perfectly sharp, the blunted tip geometry was verified by two methods. Scanning electron microscopy was used to assess the overall tip geometry and end radius. To obtain a more precise estimate of the tip geometry, AFM nanoindentation on a 1% agarose slab (2.7 mm thick) was performed and simulated by FEA using the tip radius as the free fitting parameter. The bulk unconfined modulus of the 1% agarose used in the FEA model was measured by uniaxial, unconfined compression [37] to be 3.74±0.55 kPa. Four displacement controlled compression ramps of 7.5%, 10%, 12%, and 15% were applied with 200 seconds of compression followed by 600 seconds of holding to allow for complete stress relaxation.

In the FEA simulations, one quarter of the tip and cell were modelled. The well remained fixed in all directions, the cell walls were fixed to its normal direction, and the displacement of the tip occurred only in the z-direction (direction perpendicular to the cell) to ensure symmetry. The geometry of the experiment was duplicated in the FEA: a rigid inverted square pyramidal well forming walls 35° from the vertical, a spherical homogenous elastic material for the cell using the diameter measured in optical micrographs, and a rigid tip constructed as described above. Three steps occurred in the analysis: (1) gravity acted on the cell to pull it into the well, allowing the cell to deform under its own weight, (2) the tip approached and indented the cell, and (3) the tip retracted out of the cell.

4.3 Results

4.3.1 Confirmation and Characterization of Pericellular Matrix Growth

Tapping mode AFM in air was used to visualize enzymatically isolated cells and cells with associated matrix extracted from a 10% FBS culture. Newly isolated cells such as the one in Figure 4-1(a) did not have any visible signs of matrix. By day 6 a sheer halo of matrix extended a few microns away from the cell surface. Significant buildup

of a fuller matrix was seen on day 11 (Figure 4-1(b)), but individual features in higher resolution images did not reveal many details of matrix components. However by day 18 (Figure 4-1(c,d)), collagen fibrils in the matrix could easily be identified with characteristics of type II collagen having a diameter of 59±9 nm and a banding pattern of 22±2 nm (n=10).

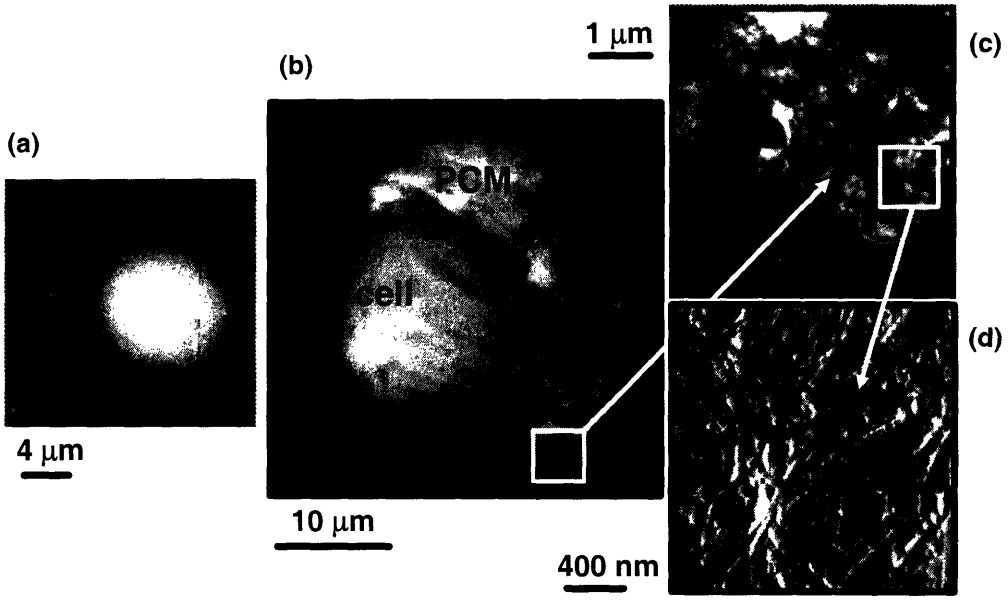

Figure 4-1: Tapping mode AFM images in air of calf chondrocytes adsorbed on mica substrates (a) enzymatically isolated (day 0), (b) chondrocyte released from alginate culture at day 11 where the PCM is clearly distinguishable from the cell body, (c) chondrocyte released from alginate culture at day 18 where a dense network of collagen fibrils is visible from a similar region on the cell in (b). (d) a higher resolution image of the selected area shown as the square in part (c) with fibrils which exhibit banding patterns and fibril diameter characteristic of type II collagen fibrils. All images are height images except (d) which is an amplitude image.

Histology images (Figure 4-2) show freshly isolated cells with no visible accumulation of proteoglycan or collagen. By day 7, proteoglycan was stained around the entire cell membrane, but collagen was not present. By day 14, the proteoglycan stain increased in size and intensity. Both cultures showed a constant but diffuse blue halo indicative of the presence of collagen. By the third and fourth weeks in culture, no significant changes in the dark PG staining were observed but collagen stain appeared to increase slightly. Small changes in shape may occur due to fixa-

tion or shrinkage from drying, so cell diameter was assessed via optical microscopy images of viable cells. A comparison of an enzymatically isolated cell (Figure 4-2) to a day 14 cell cultured with IGF-1+OP-1 showed an increase in cell size due to accumulation of cell associated matrix. Measurement of cell diameter showed a large increase from enzymatically isolated cells (7.65±0.85 μm, mean±SD) to cells released from cultures supplemented with FBS or IGF-1+OP-1. There did not appear to be an increase in the diameter of the cell with its associated matrix from day 7 to day 28 for both FBS (day 7: 13.71±2.29 μm and day 28: 14.95±2.53 μm) and IGF-1+OP-1 (day7: 13.84±2.47 μm and day 28: 13.40±1.57 μm). Hence, the PCM thickness, calculated by subtracting the total diameter measured at the time points from diameter measured from freshly isolated cells, also did not increase significantly (Fig. 3a). Instances of dividing cells sharing matrix were observed (Fig. 3b) but were not used for cell indentation analysis.

In addition, type VI collagen was visible for both types of cultured cells (Figure 4-3(c)). Cell viability remained above 80%, and chondrocytes retained their spherical phenotype but cell division was more prevalent in the IGF-1+OP-1 cultured cells (Figure 4-3(d)). GAG and collagen content increased between day 0 to day 14 in both FBS and IGF-1+OP-1 supplemented cultures (Figure 4-4). For later time points, collagen accumulation did not appear to increase in either culture. GAG continued to increase but have a lower concentration for FBS cultured cells compared to IGF-1+OP-1 cultured cells up to day 28.

4.3.2 Indentation of Freshly Isolated Cells

Indentation on chondrocytes was attempted on mica but the flat surface was not suitable as the cells tended to roll away from the tip. Because chondrocytes have a spherical morphology, a surface was created to hold the cells in place during indentation. The silicon surface was designed to be reusable and could be sterilized. A KOH etch produced inverted square pyramidal wells with diameters ranging in size from 15 to 22 μm to accommodate cells with an increasing pericellular matrix (Figure 4-5). A small drop of cell suspension was pipetted onto the surface and given a few minutes

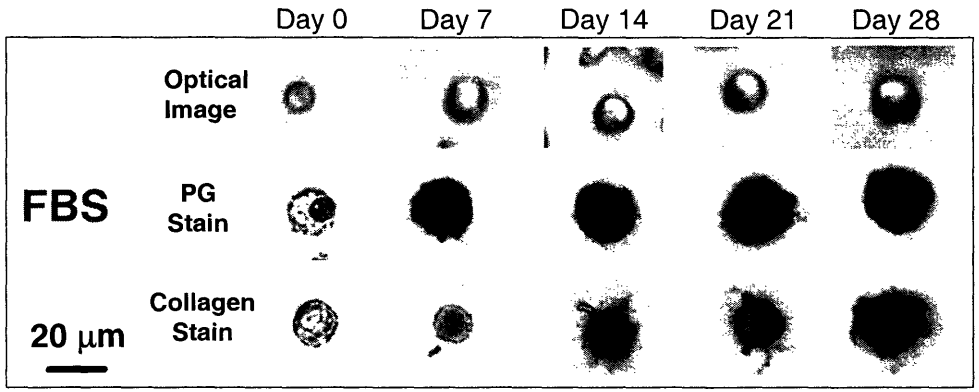

(a) Cells from FBS supplemented medium

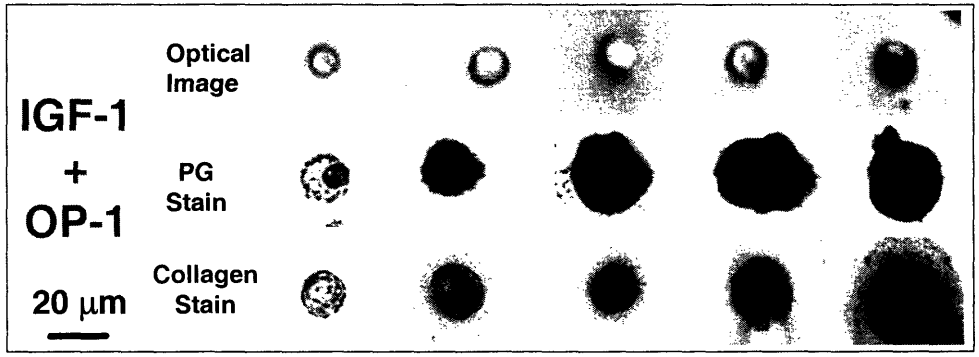

(b) IGF-1+OP-1 supplemented medium.

Figure 4-2: Optical microscopy images of individual living and histology of fixed calf chondrocytes at different culture points released from alginate beads cultured in (a) FBS supplemented medium and (b) IGF-1+OP-1 supplemented medium. The top rows of optical images in (a) and (b) were taken in culture medium. The middle rows show a dark staining for PGs (Toluidine Blue) after day 7 covering the entire cell surface. The stained cell size appears larger for the cells cultured in the IGF-1+OP-1 supplemented medium compared to the FBS supplemented medium. The bottom rows show staining for collagen (Aniline Blue), which is not as uniform and intense as the PG stain.

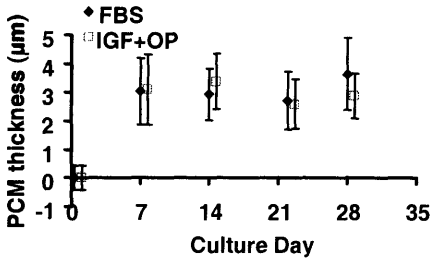

(a) PCM thickness (mean±SD) measured from optical microscope images. Cell PCM thickness was measured by subtracting the average day 0 cell diameter (n=17) from the average diameters of live cells in culture medium at days 7 (n=26), 14 (n=28), 22 (n=18), and 28 (n=18). An increase in PCM thickness is observed from day 0 (enzymatically isolated cells) up to day 7 for cultured cells after which time the PCM thickness plateaus with no significant increase (ANOVA, $p>0.1$) from day 7 to day 28 in culture.

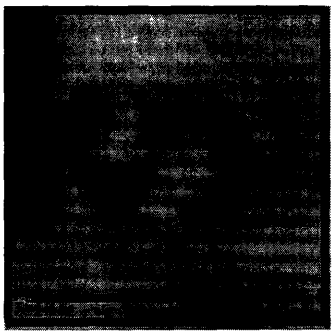

(b) Optical microscope image of cell division. Scale bar = 10 μm.

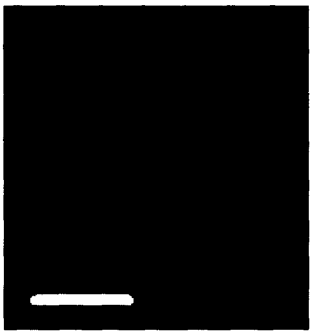

(c) Collagen VI (immunohistochemistry) was present around both FBS (shown) and IGF-1+OP-1 fed cells on day 39 cultured cells. Scale bar = 20 μm.

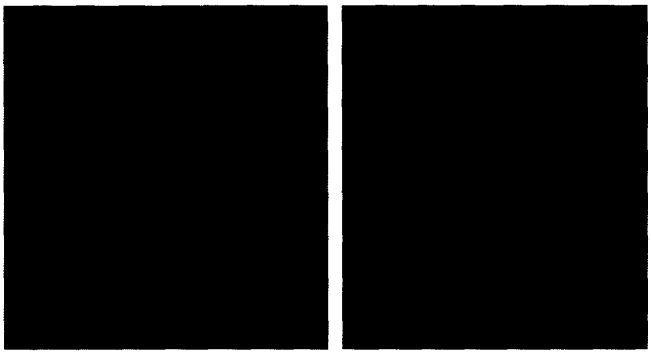

(d) Live cells shown in green (FDA dye) and dead cells in red (EtBr dye) indicate >80% viability. More cell division was seen in the IGF-1+OP-1 fed cells (right) compared to FBS fed cells.

Figure 4-3: Characterization of the PCM of calf chondrocytes cultured in alginate using either FBS or IGF-1+OP-1 supplemented medium.

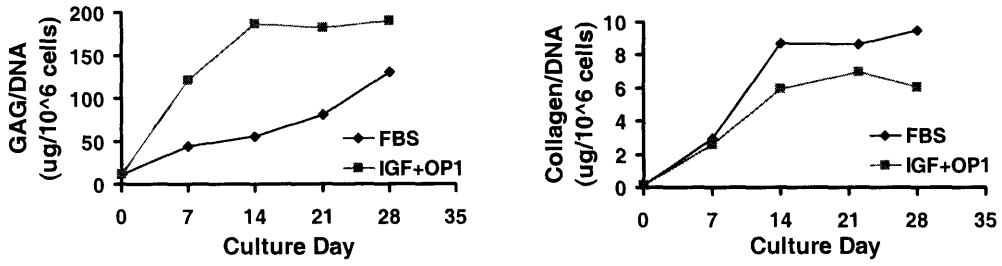

(a) (b)

Figure 4-4: Biochemical characterization of the PCM of calf chondrocytes released from alginate beads at designated time points corresponding to days that nanoindentation experiments were conducted. An increase in both GAG and collagen content is observed until day 14 for both the FBS and IGF-1+OP-1 supplemented cell cultures except for the FBS fed cells which shows increasing GAG accumulation up to day 28.

to allow the cells to settle onto the surface. The cantilever AFM probe tip was used to gently slide individual cells laterally into a selected well (Figure 4-6).

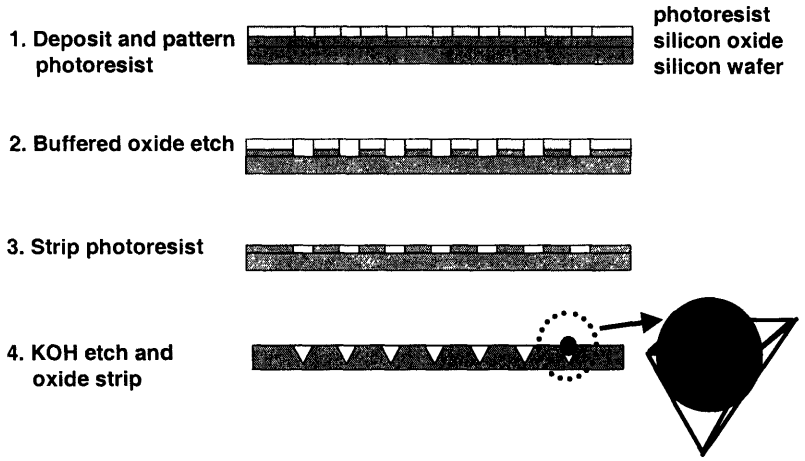

Figure 4-5: Fabrication of micron-sized square pyramidal wells in a silicon substrate for cell immobilization and nanomechanical measurements. Wells with 15, 18, 20, and 22 μm diameters were designed to hold enzymatically isolated cells and cells with associated pericellular matrix.

The indentation range was adjusted to obtain loading and unloading curves with normal displacements up to 6 μm. A series of indentation rates (200 nm/s, 500 nm/s, 1 μm/s, 3 μm/s, 5 μm/s, and 10 μm/s) were used to investigate hysteretic properties of the cells. No significant change in hysteresis was measured up to 1 μm/s. Above

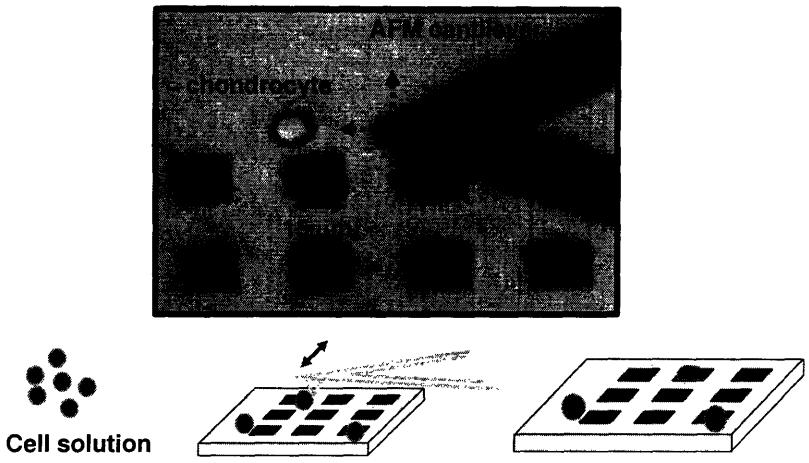

Figure 4-6: Ability to control placement of individual cells into square pyramidal Si wells using an AFM cantilever probe tip. (Above) A 10x optical microscope image of a single chondrocyte and 0.06 N/m Si_3N_4 cantilever used to maneuver an individual cell into a 15 μm diameter well.

1 μm/s, hysteresis increased in a logarithmic fashion. To limit the contribution of viscous/viscoelastic effects to the measurements, the approach curves obtained at 1 μm/s are the focus of this paper.

AFM indentation curves of enzymatically isolated cells show a nonlinear increase in repulsive force with indentation depth. For indentation of a single cell, five to six curves were averaged at one location at an indentation rate of 1 μm/s. The curves were repeatable with a relatively small standard deviation (Figure 4-7) indicating recovery and reversibility of the deformation before the start of each indentation. The micron-sized probe tip produced higher forces than the nano-sized probe tip at the same indentation distance (Figure 4-8(a)). With the nano-sized probe tip, the average maximum force obtained at 780 nm indenation was 0.76$\pm$0.27 nN. With the micron-sized probe tip, the average maximum force obtained at 780 nm indentation was 1.53$\pm$0.77 nN.

To estimate an elastic modulus from the measured force *vs.* distance curves from the nano-sized tip, the modified Hertz model of a rigid conical probe tip in contact with an elastic material was used [109]:

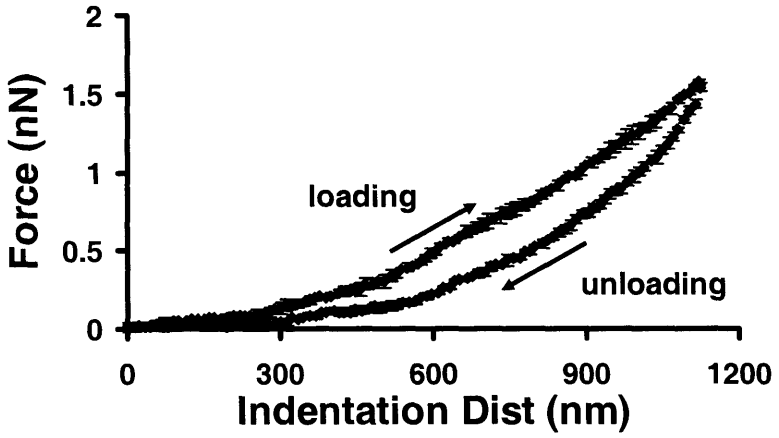

Figure 4-7: A typical AFM indentation curve (mean ± SD) on a single enzymatically isolated (day 0) calf chondrocyte immobilized in a silicon well at a z-piezo displacement rate of 1 μm/s with a nanosized square pyramidal Si_3N_4 tip (r_c~40 nm). Hysteresis was observed at all displacement rates tested (200 nm/s to 10 μm/s), but there was no change up to 1 μm/s. Therefore, the loading curves obtained at an indentation rate of 1 μm/s are used for analysis in this study.

$$F = \frac{\pi}{2} \cdot \frac{E}{1-\nu^2} \cdot \delta^2 \tan\alpha \tag{4.1}$$

where F = force (nN), δ = indentation distance (μm), E = Young's modulus (kPa), ν = Poisson's ratio = 0.4 [38], and $\alpha = 35°$ for a KOH-etched Si_3N_4 tip. This model gave an average modulus of 0.7 kPa (Figure 4-8(b)). Matching the Hertz model to the upper and lower limits of the standard deviation gave a modulus range between 0.35 kPa to 1.25 kPa.

For the micron-sized tip, the Hertz model of two contacting spheres was used assuming a rigid colloidal tip and an elastic cell [61]:

$$F = \frac{4}{3} \cdot \frac{E}{1-\nu^2} \cdot \delta^{\frac{3}{2}} \cdot \sqrt{\frac{1}{\frac{1}{R_1}+\frac{1}{R_2}}} \tag{4.2}$$

where R_1 = radius of micron-sized tip (μm) and R_2 = radius of cell (μm). The Hertz model matched the experimental data with a modulus of 1 kPa (Figure 4-8(c)).

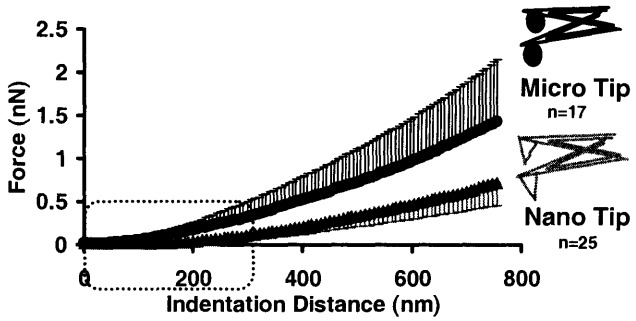

(a) Average indentation curves on loading (mean ± SD) taken with both the nano-sized (n=25 cells) and micron-sized (n=17 cells) probe tips. The force is higher for the same indentation distance using the micron-sized tip compared to the nano-sized tip.

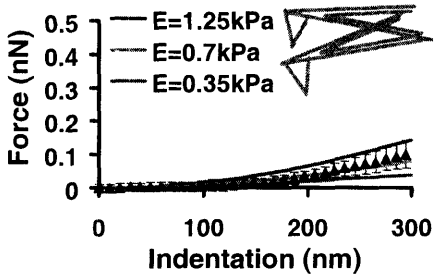

(b) Comparison with experimental data up to 300 nm indentation distance to the modified Hertz model for a conical tip.

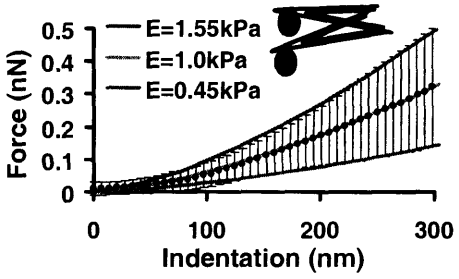

(c) Comparison with experimental data up to 300 nm indentation distance to the Hertz model for a colloidal tip and spherical cell body.

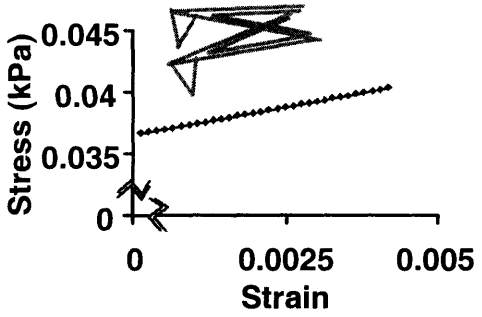

(d) Stress-strain curve. A nano-sized tip gives E=0.92 kPa up to an indentation of $\sim r_c$, 40 nm.

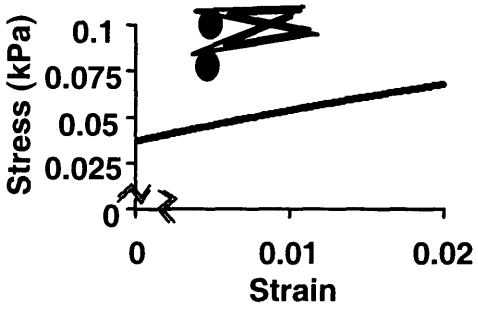

(e) Stress-strain curve. A micron-sized tip gives E=1.46 kPa up to an indentation of 200 nm.

Figure 4-8: Data on enzymatically isolated calf chondrocytes (day 0).

The upper and lower limits fit the standard deviation with moduli of 1.55 kPa and 0.45 kPa, respectively.

Moduli of 1.37 kPa and 1.46 kPa were calculated from the nano-sized and micron-sized probe tips, respectively, from the linear slope of stress-strain (σ-ϵ) graphs (Figures 4-8(d) and 4-8(e)). Over the first 40 nm and 200 nm for the nano and micron-sized tips, respectively, the σ-ϵ curve was linear. The stress was calculated by the surface integration method, i.e. dividing force by an increasing contact area with indentation depth.

$$\sigma = \frac{F}{A} \tag{4.3}$$

$$\epsilon = \frac{\delta}{2R_2} \tag{4.4}$$

$$A = 2\pi R_1 \delta \tag{4.5}$$

Using the Hertz model and a stress-strain curve, length scales at the nano and micro level gave approximately the same material properties for an enzymatically isolated chondrocyte as demonstrated by the moduli obtained from both the nano and micron-sized tips.

Given the increased complexity of the system with the cell confinement in a pyramidal well, finite element analysis was used to determine the modulus of the cell from the force *vs.* indentation distance curves. The system was first tested with frictionless and no-slip boundary conditions on the cell-well wall contact region. The no-slip boundary condition resulted in a 25% increase in the cell modulus. The moduli reported here use the frictionless boundary condition. For the nano-sized tip, the FEA predicted the cell modulus to be 0.7 kPa, as also predicted by the Hertz model (Figure 4-9(a)). For the micron-sized tip, the FEA required a slightly higher cell modulus at 3 kPa to duplicate the force *vs.* indentation distance curves (Figure 4-9(b)).

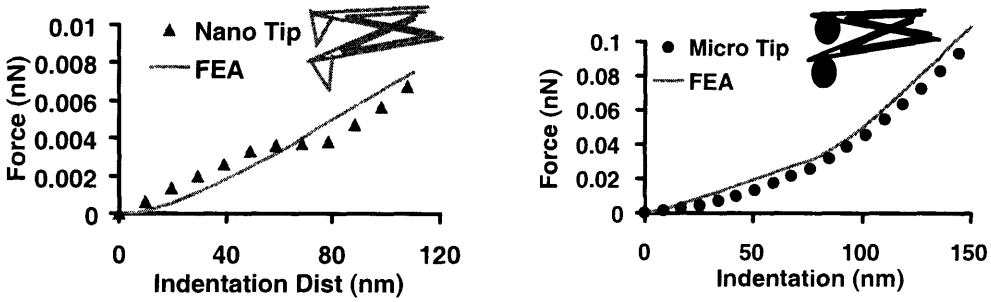

(a) With a modulus of 0.6 kPa the nano-sized probe tip (r_c~40 nm) resulted in a force *vs.* indentation distance curve best representing the experimental data.

(b) For the micron-sized tip (r_c~2.5 μm), the FEA curve matched with the experimental data when a cell modulus of 3 kPa was used.

Figure 4-9: Elastic finite element analysis predictions of indentation on loading of enzymatically isolated calf chondrocytes (day 0) with rigid nano-sized and micron-sized tips.

4.3.3 Indentation of Cells with Newly Developing Pericellular Matrix

Chondrocytes released from alginate were mechanically tested in the same fashion as the enzymatically isolated cells. For the 10% FBS fed cells, the force *vs.* indentation distance curves measured with the nano-sized and micron-sized probe tips showed a slight stiffening with each week in culture (Figures 4-10(a) and 4-10(c)). As shown by the small standard deviation bars, the measurements were repeatable over the cells tested. The force curves generally showed a very slow increase in force over the first 700 nm with the nano-sized probe tip, but the increase was less pronounced with the micron-sized tip. While there was stiffening with each week from day 7 to day 28, all measurements of cells in culture after day 0 were less stiff than the enzymatically isolated cells (Figure 4-10(b)). Comparison of the nano-sized probe tip compared to the micron-sized tip (Figure 4-10(d)) showed similar forces for the initial indentation up to 900 nm, which indicates stiffer measurements with the nano-sized tip compared to the micron-sized tip given the decreased contact area with the nano-sized tip.

Cells cultured with IGF-1 + OP-1 showed a large increase in stiffness over time with both the nano-sized tip and micron-sized tip compared to FBS cultured cells. A small increase in stiffness from day 21 to day 28 cultured cells with IGF-1+OP-1 was

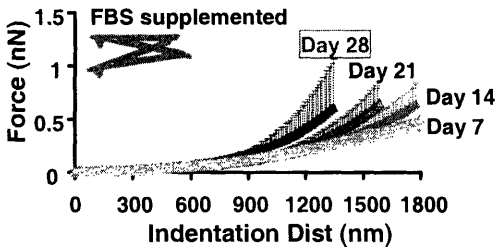

(a) On day 7 (n=5), the force increased very slowly indicative of a soft material. A slow increase was seen in stiffness in the following weeks in culture on day 14 (n=4), day 21 (n=5), and day 28 (n=6).

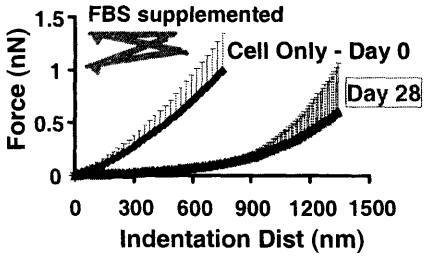

(b) Interestingly, even after 4 weeks in culture, the cells with associated matrix showed a dramatic decrease in stiffness compared to enzymatically isolated cells with the nano-sized tip.

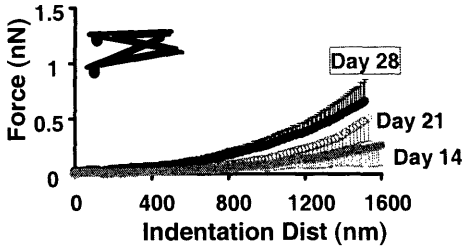

(c) Force curves obtained with a micron-sized tip exhibits stiffening with each week in culture. Day 14 (n=4), day 21 (n=5), day 28 (n=7)

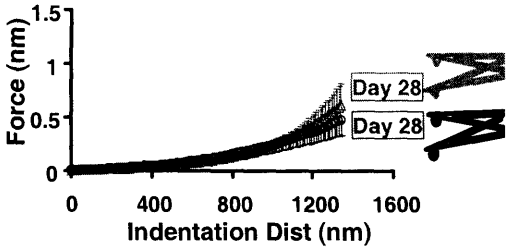

(d) The micron-sized tip generates about the same amount of force as the nano-sized tip for the first ~900 nm. Above 900 nm, the nano-sized tip (n=6) measures a higher force than the micron-sized tip (n=3).

Figure 4-10: Average AFM indentation curves (mean ± SD) on loading of individual calf chondrocytes plus cell associated matrix released from alginate at different time points from culture in 10% FBS.

seen with the nano-sized tip (Figures 4-11(a)). With the micron-sized tip, the increase in stiffness was more dramatic from day 21 to day 28 cultured cells (Figures 4-11(b)). Compared to freshly isolated cells, the day 21 cells exhibited a similar stiffness as seen in the force *vs.* indentation curves (Figures 4-11(c)). However by day 28, the cells appeared stiffer with a greater amount of force of 2.55 nN at an indentation distance of 670 nm compared to enzymatically isolated cells at a force of 1.97 nN.

A simple FEA model of a cell with an elastic shell of newly developed PCM was designed to better calculate a modulus of the more complex cell+matrix. The nano-sized tip FEA had trouble converging due to its small radius of curvature in comparison to the indentation depth so it could not be used to compare with experimental data. For the micron-sized tip FEA, the cell was modelled with a modulus of 3.0 kPa, as calculated in the FEA for the enzymatically isolated cell, and the shell modulus, with a thickness of 3.67 μm, was varied until the model output matched the experimental data. For the day 28 FBS cultured cells, the shell modulus was 0.1 kPa (Figure 4-12(a)). For the day 28 IGF-1+OP-1 cultured cells, the shell modulus was 1.5 times stiffer at 4.15 kPa (Figure 4-12(b)).

4.4 Discussion

4.4.1 Quantification of Pericellular Matrix Growth

Chondrocytes in culture were gently released from alginate to retain and minimize damage to the surrounding newly developed PCM. Developing PCM was confirmed with three methods: visualization via AFM imaging, biochemical assays of collagen and GAG content, and histology (labelling of collagen and proteoglycans with dyes and immunofluorescent antibody labelling of type IV collagen.)

The dense collagen network of the extracellular cartilage matrix has been visualized via TEM [64] and AFM [127] after enzymatic removal of proteoglycans. In this study, a dense, newly synthesized collagen network is directly seen in AFM images (Figure 4-1(d)) and is reflective of AFM images of cartilage ECM [64, 127]. The

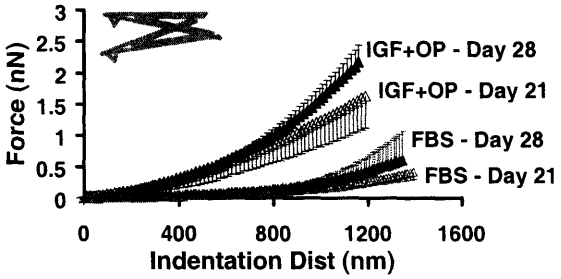

(a) The cells cultured in the combination of IGF-1 and OP-1 showed a marked increase in stiffness using the nano-sized tip compared to cells cultured in 10% FBS on day 21 (n=5) and 28 (n=5).

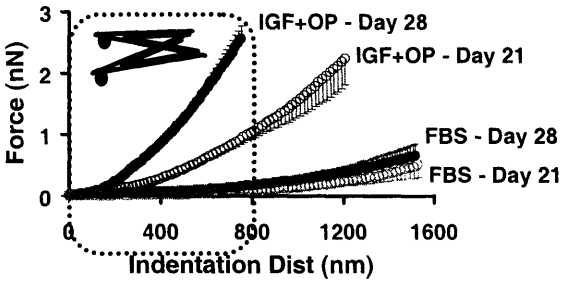

(b) Indentation with a micron-sized probe tip shows an increase in stiffness from day 21 (n=5) to day 28 (n=5)

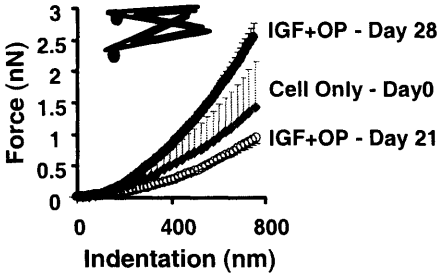

(c) Comparison of the region boxed in (b) with day 0 cells. Day 21 (n=5) and 28 (n=5) IGF-1+OP-1 cultured cells, were stiffer than enzymatically isolated cells as measured by the micron-sized tip.

Figure 4-11: Average indentation curves (mean ± SD) on loading of individual calf chondrocytes plus cell associated matrix released from alginate beads at different time points from culture in IGF-1+OP-1 supplemented medium.

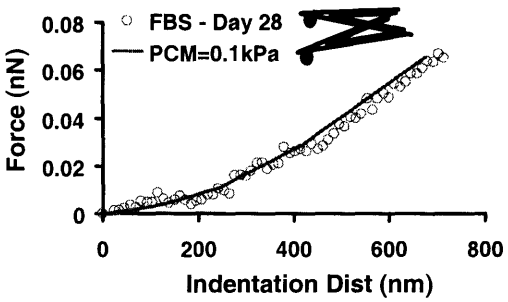

(a) The FEA shell model with a thickness of 3.7 μm and a modulus of 0.1 kPa with an underlying cell modulus of 3 kPa fit the experimental data of day 28 FBS cultured cells up to about 900 nm.

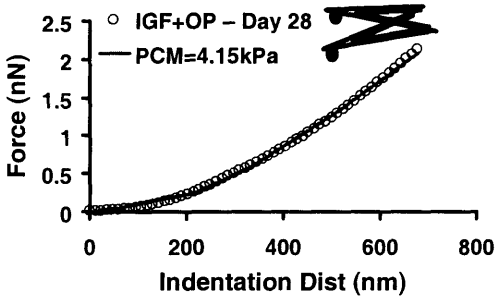

(b) The FEA shell model with a modulus of 4.15 kPa and a cell modulus of 3 kPa fit the experimental data well for day 28 IGF-1+OP-1.

Figure 4-12: Finite element analysis predictions (solid lines in plots) of indentation of individual calf chondrocytes and their cell associated matrix with the micron-sized probe tip on loading.

collagen fibril diameter and banding pattern correspond to that of type II collagen, characteristic of articular cartilage collagen. AFM images of cells released over time points (Figure 4-1) gave a secondary confirmation that PCM was growing and being retained by the cells. It is important to note that the images were taken with tapping mode in ambient conditions so some features may have been slightly altered as the cell was dried onto the mica surface.

Histology was also used to assess the accumulation of PCM with time in culture (Figure 4-2). Enzymatically isolated cells showed no proteoglycans or collagen. For later time points, both the FBS and IGF-1+OP-1 supplemented cells exhibited dark staining of proteoglycans and collagen as early as day 7. The stained region became larger on day 14 for both cultures but did not appear to increase in size with time in culture, which reflects biochemical data. GAG and collagen content levelled off at day 14 for the IGF-1+OP-1 supplemented cells. FBS showed a similar trend for the collagen but the GAG levels seemed to increase up to day 28. Optical microscopy of live cells revealed an increase in diameter from day 0 to 7 but does not increase significantly at later time points up to day 28 (Figures 4-2 and 4-3(a)). Previous studies by Loeser et al. [77] confirm the trend of GAG content being higher in IGF-1+OP-1 supplemented cells over cells maintained in either FBS, IGF-1, or OP-1 alone, indicat-

ing that the combination of IGF-1+OP-1 increased the production of proteoglycans. In addition, OP-1 has been found to help chondrocytes retain their developing PCM after release from alginate [97]. While the developing PCM appears to accumulate quickly in culture, the molecular structure and collagen architecture within the PCM may not resemble that of fully developed adult chondrons. Immunofluorescence of labelled col VI (Figure 4-3(c)), a collagen characteristic only of the PCM, showed a diffuse halo around the cell as also seen by Lee and Loeser [73], while PCM of fully developed chondrons appears compact and more uniform [103]. While these measurements quantify the composition of the PCM, it does not provide micro-structural detail such as collagen organization or cross-linking that may be occurring with time in culture.

4.4.2 Mechanical Properties of Enzymatically Isolated Cells

The repeatability of force *vs.* distance curves at $1\,\mu$m/s with both the nano-sized and micron-sized tip for a cell in one spot indicates recovery of the cellular properties between indents (Figure 4-7). Hysteresis was seen at all indentation rates from 200 nm/s up to $10\,\mu$m/s and no significant change was seen below $1\,\mu$m/s (see Appendix B). With other types of cells, a similar phenomenon was observed where hysteresis did not decrease below 500 nm/s [22]. A previous study involving cytoindentation of single adult bovine chondrocytes found a time relaxation constant of 1.32 s [68]. However in this study, an increase in hysteresis was not seen between 200 nm/s to $1\,\mu$m/s indentation rates indicating a pseudo steady state was obtained, giving an estimated relaxation time constant of $\sim$1 s. We therefore, used $1\,\mu$m/s indentation rates for data collection. Hysteresis was minimized in order to minimize viscous contributions and allow the elastic behavior to dominate in the measurements [52].

The micron-sized tip with a radius >60 times larger than the nano-sized tip resulted in a larger force for the same indentation distance (Figure 4-8(a)). To extract a modulus from the force *vs.* indentation distance curves, a number of methods were implemented. The modified Hertz model for a conical tip was used to approximate a modulus of 0.7 kPa for the nano-sized tip (Figure 4-8(b)) while the Hertz model

for a colloidal tip approximated a modulus of 1 kPa (Figure 4-8(c)). The two values fall within error of each other and indicate that the length scale of the nano-sized tip at a 40 nm radius of curvature measures the same material properties as the micron-sized tip with a radius of 2.5 μm. Without assuming a model, the modulus from the σ-ϵ curves found the nano-sized tip and micron-sized tip measured a similar modulus (0.92 and 1.46 kPa, respectively), confirming the results of the Hertz model. This data matches nicely with previous measurements of chondrocytes giving moduli ranging from 0.65 to 2.47 kPa for tensile micropipette aspiration [63] and unconfined compression [74], respectively.

The above calculations do not take into account the geometry of the system, so a more precise calculation was performed using finite element analysis. The exact geometry of the well, pyramidal tip with a 40 nm radius of curvature, and average measured cell diameter (day 0) were used. FEA predicted the same modulus as the Hertz model for the nano-sized tip. However, FEA predicted a modulus more than three times higher than the Hertz model for the cell when probed with the micron-sized tip. One reason may be that the cell appears as a semi-infinite plane to the nano-sized tip at small indentations despite the curvature of the cell while the large micron-sized tip radius is more than half radius of the cell so the curvature of the cell plays an increasingly important role in the amount of force measured. In addition for the nano-sized tip, the decreased contact area and amount of force placed on the cell reduce the displacement of the cell into the well where as the micron-sized tip induces a substantial displacement into the well. The nano-sized tip may also be probing individual structures such as the cytoskeleton filaments or organelles whereas the micron-sized tip may be giving a bulk-type of measurement.

4.4.3 Mechanical Properties of Cells with Developing Pericellular Matrix

Cell cultures supplemented with FBS or IGF-1+OP-1 produced cells with a developing PCM that increased in stiffness with each week in culture after day 7 until

day 28 in culture. With time in culture, the thickness of the PCM did not change, but GAG and collagen levels increased from day 7 to day 14, indicating accumulation of both and therefore increased concentration of ECM molecules, which may explain the increase in stiffness measured from day 7 to day 14. After day 14, the PG content continued to rise for the FBS cultured cells while the PCM thickness remained unchanged, indicating a higher PG concentration in the PCM, which may cause stiffening of the cell. PGs have been found to be the main component in resisting compression of cartilage [14]. However, IGF-1+OP-1 cultured cells showed increases in stiffness despite a leveling of PGs and collagen. One explanation may be that the PCM is undergoing molecular organization of the small PGs and collagen as well as collagen cross-liking.

For the FBS fed cells, it was surprising to see that the stiffness even after 28 days in culture was less than the stiffness measured from enzymatically isolated cells. The newly forming matrix composed of GAG, collagen, and other smaller quantities of ECM molecules may form a soft "sponge" like material where everything is loosely organized around the cell membrane. As seen previously by Lee and Loeser [73], newly developing matrix has a diffuse appearance. The rather amorphous structure, when probed via indentation, may have a softer modulus than the cell itself. Contrary to the enzymatically isolated cells, a lower stiffness is obtained with the micron-sized tip compared to the nano-sized tip. One hypothesis is that the sharpness of the nano-sized tip penetrates the developing PCM layer and may come in closer contact with the cell membrane, and thus see substrate effects from the stiffer cell, whereas the micron-sized tip with the large surface area cannot easily penetrate the PCM.

In comparison, the IGF-1+OP-1 cultured cells released on day 28 showed a significant increase in stiffness over enzymatically isolated cells (Figure 4-11(c)). IGF-1 alone has been shown to increase proteoglycan content in newly developing PCM [134]. OP-1 has also been shown to increase proteoglycan [97] as well as collagen [35] synthesis and accumulation in newly developing PCM. The combination of IGF-1+OP-1 has been shown to increase cell division as well as promote proteoglycan content in the newly developing PCM [77]. While levels of proteoglycan and collagen

from the IGF-1+OP-1 fed cells did not differ much from the FBS fed cells, there may be a difference in the microstructure such as collagen cross-linking that may be causing the measured increased stiffness. OP-1 has also been shown to increase collagen II and collagen X, a marker of chondrocyte hypertrophy in developing bones [18], which may potentially increase the stiffness of the PCM. Increase in stiffness was seen with both the sharp nano-sized tip and the larger micron-sized tip.

Because the FEA had difficulty converging at depths greater than 200 nm for the nano-sized tip due to the sharpness of the tip, we focus on FEA analysis with the micron-sized tip. The micron-sized tip converged more easily but did not yield a modulus that fit all of the experimental data for the FBS fed cells released on day 28. For the first 900 nm, the shell model fit the experimental data well and gave a PCM modulus of 0.1 kPa, which is much softer than enzymatically isolated cells. The simple shell FEA modeled the full range of experimental data for the IGF-1+OP-1 supplemented cells giving the PCM a modulus of 4.15 kPa, a slightly higher modulus than the enzymatically isolated cell of 3 kPa.

4.5 Conclusion

In this study, we developed a methodology to extend AFM capabilities to measure the mechanical properties of spherical, non-adherent cells. With the FEA model, a modulus over three times lower (0.6 kPa *vs.* 3 kPa) was obtained from the indentation of freshly isolated chondrocytes with a nano-sized tip ($r_c \sim 40\,\text{nm}$) compared to a micron-sized tip ($r_c = 2.5\,\mu\text{m}$), indicating that the underlying cytoskeletal structure may be playing a role in measuring material properties with the nano-sized tip. However, the geometry of the well used for immobilization of the cell and the curvature of the cell played less of a role in the measurement of the mechanical properties when using the nano-sized probe tip since qualitative agreement of the modulus was seen with the Hertz model and FEA. In contrast, FEA revealed a modulus three times larger than predicted by the Hertz model for indentation with the micron-sized tip. The influence of surface geometry is most likely the main source causing the difference

in predicted modulus. For the first time, we have measured the mechanical properties of newly developing PCM. It was interesting to see that a cell with newly developing PCM had a lower modulus than an enzymatically isolated chondrocyte even at day 28 for FBS fed cells but was 1.5 times higher for the IGF-1+OP-1 fed cells. An undeveloped PCM with a loose arrangement of proteoglycans and collagen may be the reason for the lower modulus. However the stiffness from day 7 to day 28 increased in both types of culture, which may be explained by increase in PG and collagen content as well as maturation of the PCM into a more organized structure.

Chapter 5

Concluding Remarks

The integrity of cartilage is dependent on the balance between collagen tensile forces and compressive resistance of aggrecan. Because more than 50% of the compressive modulus of cartilage is attributed to aggrecan, this thesis focuses on the molecular structure and properties of both single aggrecan molecules and of the aggrecan-rich pericellular matrix.

Nanometer resolution achieved via AFM of individual GAG chains attached along the core protein was seen for the first time. Direct measurement of greater GAG and core protein length as well as decreased GAG spacing along the core was correlated to an increased persistence length for the fetal epiphyseal compared to mature nasal bovine aggrecan. Two reasons may exist for the structural differences. With age, aggrecan structure has been known to vary. In addition, epiphyseal cartilage is load-bearing and thus would benefit from aggrecan with a fuller GAG brush region to resist compression whereas nasal cartilage does not need to support and is not subjected to large loads. It would be interesting to further explore other sources of aggrecan such as osteoarthritic aggrecan or aggrecan that has undergone enzymatic degradation by aggrecanase. It may reveal information as to where and how degradation occurs. Related to this, it may be interesting to image in real-time via AFM the degradation of aggrecan via recombinant aggrecanase.

As aggrecan concentration was increased from a sparse density where molecules were free to equilibrate on the surface to higher densities where aggrecan could in-

teract with neighboring aggrecan, the molecules changed conformation from an extended to a more contracted configuration. At the highest density achieved, aggrecan tended to bend around its neighbors making use of its available space while the GAG chains remained extended. In cartilage, aggrecan is found at gel-like concentrations at 20-80 mg/ml. The highest density achieved in this study was 2.3 mg/ml, but the flexibility of the molecule was becoming evident. It may be interesting to look at higher concentrations, but a modification of the sample preparation would be necessary such as use of a Langmuir-Blodgett trough. It is important to note that 2D conformation may not be representative of 3D conformation. Due to this limitation of AFM, computer simulations may be required to get an accurate picture of 3D interaction. A more dramatic collapse of aggrecan was also seen with increasing ionic strength. Not until 0.1 M NaCl did aggrecan dramatically collapse from a mostly extended structure to a ball-like arrangement. At this ionic strength, the Debye length is reduced to the distance of GAG spacing along the core protein.

Finally, the newly synthesized aggrecan-rich matrix surrounding the chondrocyte was probed via AFM nanoidentation at different point in culture. An initial decrease in stiffness occurred between an enzymatically isolated cell with a well-defined membrane boundary to a cell released at a later time point in culture that is surrounded by a loose arrangement of collagen and proteoglycans. However, from day 7 to day 28 a slow increase in stiffness was measured. Cells cultured in medium containing 100 ng/ml each of IGF-1 and OP-1 had a significantly stiffer matrix compared to cells cultured in medium containing 10% FBS. More perplexing is that the GAG and collagen content did not differ greatly between the two cultures. One hypothesis is that the microstructure of the PCM may be more developed (e.g. greater collagen cross-linking) for the cells cultured with IGF-1 and OP-1. Mechanical loading has been shown to alter biosynthesis of chondrocytes, which in turn may alter PCM structure and composition. The techniques developed in this thesis could be used to study cells seeded into alginate, mechanically stimulated, and then released for nanoindentation studies.

The micro-structure of cartilage has long been studied, but little is known about

the interplay between the molecular components that lead to tissue level properties. Understanding the basic mechanisms involved in forming complex cartilage matrix properties may lead to a treatment for damaged cartilage or improve the properties of tissue engineered cartilage. There is a lot of room for amazing discoveries at the pico- and nano-levels. This thesis has only just begun finding and started assembling a few pieces of a much larger puzzle.

Appendix A

Glossary

AFM atomic force microscopy

APTES 3-aminopropyltriethoxysilane

CS chondroitin sulfate

DMMB dimethyl methylene blue

EM electron microscopy

FACE fluorophore assisted carbohydrate gel electrophoresis

GAG glycosaminoglycan

HA hyaluronic acid

HRFS high resolution force spectroscopy

IGD interglobular domain

KS keratan sulfate

NMR nuclear magnetic resonance

QELS quasielastic light scattering

SANS small angle neutron scattering

SDSPAGE sodium dodecyl sulfatepolyacrylamide gel electrophoresis

S-GAG sulfated glycosaminoglycan

TEM transmission electron microscopy

TMAFM tapping mode atomic force microscopy

WLC worm-like chain

XPS X-ray photoelectron spectroscopy

XRD X-ray diffraction

Appendix B

More details relevant for the cell indentation measurements (See Chapter 4)

B.1 AFM Tip Reconstruction for Finite Element Analysis

An AFM probe tip does not form perfectly sharp corners but instead has a finite blunted tip radius. Tip geometry can have a significant effect on the shape of force *vs.* indentation curves, so to accurately compare experimental AFM results to FEA, the precise tip geometry must be determined.

B.1.1 Methods

The following steps were taken to determine the tip geometry:

1. A high resolution image of the tip with the scanning electron microscope (SEM) was taken to get the overall geometry of the tip. A higher resolution image was used to obtain a rough estimate for the tip radius (Figure B-1(b)).

2. Using the same tip that was used for the cell indentation, AFM indentation was performed on a 1x1 cm^2 agarose slab (1% w/v PBS). Six force vs. indentation curves/spot at 7 different spots were recorded. You want a minimum of 5 curves as there may be variation from location to location. The curves were plotted and averaged.

3. The unconfined equilibrium modulus of the agarose slab was measured by uniaxial, unconfined compression of 2.7 mm thick, 3 mm diameter agarose disks. (See Chapter 4 Methods Section for more details.)

4. A finite element model of the agarose slab indentation was created in ABAQUS (ABAQUS Inc., Providence, RI). The model used the modulus obtained from

the unconfined compression test and a Poisson's ratio of 0.45 for the agarose slab. The rigid pyramidal tip was constructed with walls 55° from the horizontal. The radius of the tip was modified until a good fit to the AFM data was obtained.

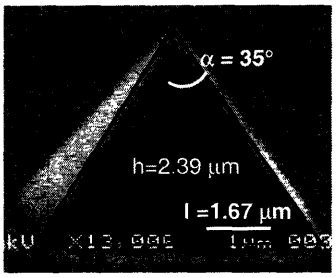

(a) SEM image of Si_3N_4 nano tip used for the indentation experiments. Measurements of whole tip agree with nominal measurements of a symmetric 35° tip opening.

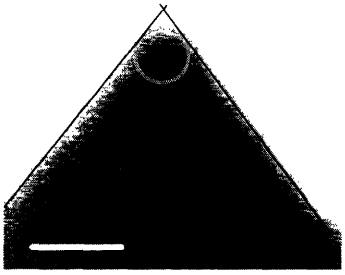

(b) Higher resolution gives a radius of curvature of 60 nm. The scale bar equals 200 nm.

Figure B-1: Tip calibration.

B.1.2 Results

1. Measurements from the SEM confirmed the walls of the AFM (nano) tip were etched 55° from the horizontal (Figure B-1(a)). The higher resolution image showed a blunted tip radius to be ~60 nm (Figure B-1(b)).
2. The AFM indentation curves with the nano tip were repeatable (Figure B-2(a)).
3. The unconfined compression tests gave a modulus of 3.74 ± 0.55 kPa for the 1% agarose slabs.
4. To create the tip, 1/4 of the tip was created by cutting a block of material to obtain the walls with the correct geometry. Tips with varying radii were created by revolving a cut of a semi-circle with a radius extending to the farthest corner from the axis. A tip with a radius ~40 nm matched best with the experimental AFM indentation data (Figure B-2(b)). This tip was used for the cell indentation FEA. (See Chapter 4)

B.2 More FEA Snapshots Comparing the Effects of Tip Geometry and PCM Properties

The graphs can be located in Chapter 4, Figures 4-9 and 4-12. These snapshots give you a physical idea about the deformation the cell is undergoing due to the nano and

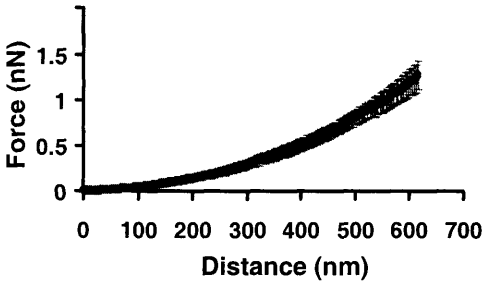

(a) AFM indentation with nano tip on a 1% agarose slab were repeatable. Individual curves shown as thin lines. Average shown as a thick line. (n=7, mean± SD)

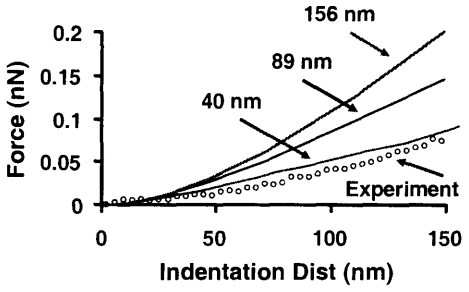

(b) A series of FEA indentations with varying tip radii on a slab of agarose. FEA of indentation with the R_c ~40 nm nano tip fit the experimental data well. A picture of one quarter of the tip is shown in the inset.

Figure B-2: AFM tip calibration using indentation on 1% agarose and FEA.

micro tips as well as varying PCM properties. A shell model was created to model the newly synthesized PCM surrounding the cell.

B.2.1 Results

Figures B-3(a) and B-3(b) are also in Chapter 4 as Figures 4-9(a) and 4-9(b). The FEA with a ~40 nm nano tip radius of curvature fit the experimental data well. Figures 3b,d are snapshots of the indentation simulation with the von Mises stresses plotted; red indicating the largest stress and blue indicating very low stress. Greater stresses and more deformation are seen in the cell when indented with the micro tip compared to the nano tip.

Figures B-4(c) and B-4(d) are also in Chapter 4 as Figures 4-12(a) and 4-12(b). The cell, 7.6 μm diameter, was modeled with a modulus of 3 kPa. The PCM was modeled as being 3.55 μm thick with a modulus of 0.1 kPa for the day 28 cells cultured in FBS (Fig. 4a). Because the IGF-1+OP-1 (Figure B-4(b)) produced much stiffer cells for day 28, a PCM modulus of 4.15 kPa was used to match the experimental data. At an indentation distance of 860 nm, the cell was more deformed (0.155 μm *vs.* 0.014 μm) when surrounded by the stiffer PCM. The softer PCM absorbed the indentation force and did not transmit the load as readily as the stiffer PCM to the underlying cell. Interestingly, the deformation of the PCM by the tip was approximately the same for both the 0.1 kPa and 4.15 kPa PCM stiffness (0.63 μm *vs.* 0.59 μm, respectively.)

B.3 Effect of Mesh Density and Boundary Conditions

The choice of mesh density can have a significant effect on the accuracy of FEA results. To verify that the mesh was dense enough to obtain accurate results, two different densities of meshes were implemented. Boundary conditions may also influence the

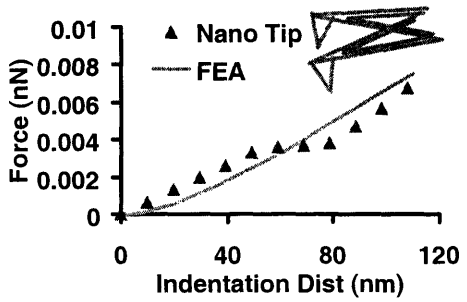

(a) Comparison of experimental data with FEA for the nano-tip

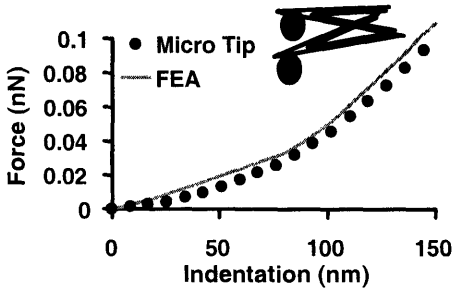

(b) Comparison of experimental data with FEA for the micro-tip

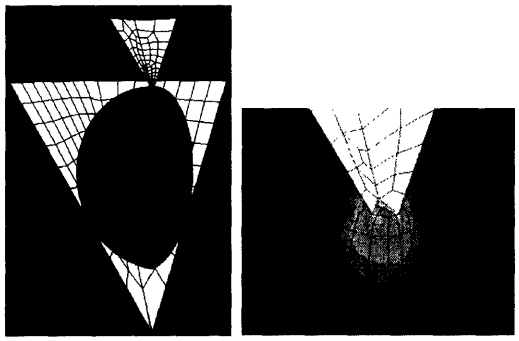

(c) FEA corresponding to Figure B-3(a)

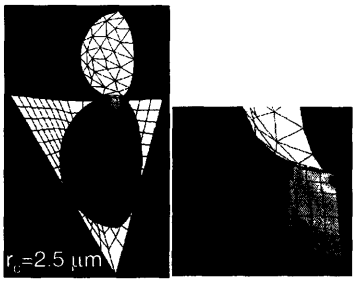

(d) FEA corresponding to Figure B-3(b)

Figure B-3: Nano *vs.* micro-tips in the FEA model. Note that deformation and resulting stresses (pictured) were much larger for the micro tip compared to the nano tip.

(a) The shell model with a modulus of 0.1 kPa for the PCM fit the experimental data well for day 28 FBS cultured cells. Note that the color scale of (a) and (b) are not the same.

(b) The shell model with a modulus of 4.15 kPa for the PCM fit the experimental data well for day 28 IGF-1 + OP-1 cultured cells.

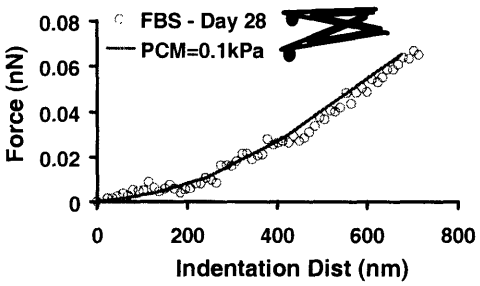

(c) Experimental indentation results using the micro tip on day 28 FBS cultured cells.

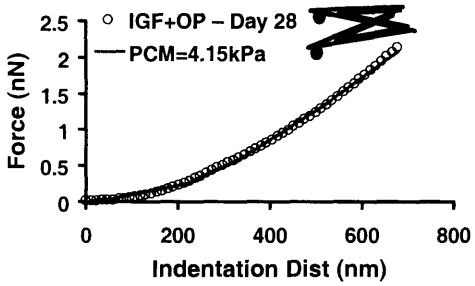

(d) Experimental indentation results using the micro tip on day 28 IGF-1+OP-1 cultured cells.

Figure B-4: Comparison of shell models. The PCM for the FBS and IGF-1+OP-1 deformed by approximately the same amount at 630 nm and 590 nm, respectively. However, the cell did not experience most of the loading when surrounded by the softer PCM and deformed only 14 nm compared to 155 nm for the stiffer PCM.

FEA results. The exact interaction between the cell and well wall are unknown, so the two extremes of no-slip and frictionless boundary conditions were implemented.

B.3.1 Results

A FEA pictorial representation of the micro tip indentation of a chondrocyte immobilized in a well is shown in Figure B-5(a). Agreement of the resultant force *vs.* indentation curves for the two mesh sizes confirms the accuracy of the FEA model results (Figure B-5(b))

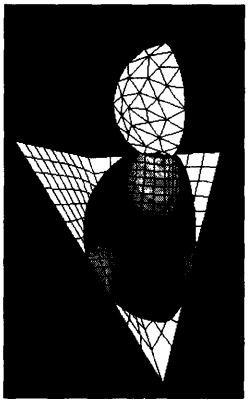

(a) Taking advantage of the symmetry of the system, one quarter of the experimental geometry was duplicated for FEA to minimize computational time. A snapshot of a well immobilizing an elastic cell during indentation with a rigid micro tip.

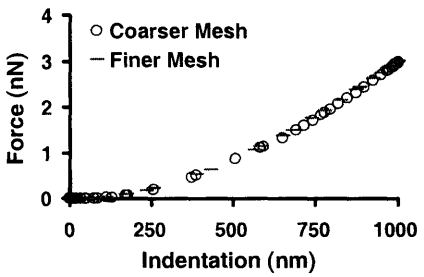

(b) The agreement of force vs. indentation FEA results using two different sized meshes verified that both meshes were dense enough to obtain accurate results

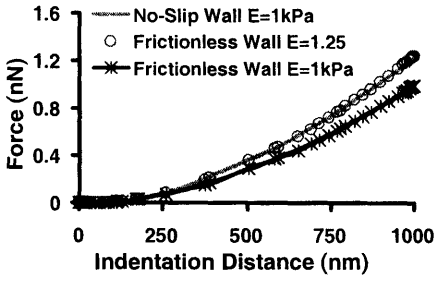

(c) A no-slip boundary condition between the cell and well wall resulted in a decreased cell modulus.

Figure B-5: Validating the accuracy of FEA mesh and effect of cell-well boundary condition.

Interestingly, a no-slip boundary condition between the cell and wall resulted in a lower modulus compared to the frictionless boundary condition (Figure B-5(c)). This implies that if the wall is frictionless, then the tip has to indent more of the cell to

obtain an equally large resultant force to that of the no-slip wall, which may be due to the cell "slipping" more into the well.

B.4 Effect of Indentation Rate on AFM Measurements

Chondrocytes exhibit viscoelastic and poroelastic behavior [68, 74]. In order to minimize the viscous effects, a series of measurements at indentation rates of 0.2, 0.5, 1, 3, 5, and 10 μm/s were recorded on enzymatically isolated chondrocytes. (See Chapter 4 for details.) The hysteresis was normalized to the hysteresis measured at 1 μm/s.

B.4.1 Results

As seen in Figure B-6, there is little change in hysteresis between 0.2 - 1 μm/s. This indicates that the viscous effects are minimized and that the elastic properties dominate. An indentation rate of 0.2 - 1 μm/s with a maximum indentation depth of 1 μm/s gives the cell a relaxation time between 1-5 seconds. This agrees with previous results in which the relaxation time constant for chondrocytes had been measured at 1-3 seconds [74]. For these reasons, all indentations in the experiment were recorded at 1 μm/s.

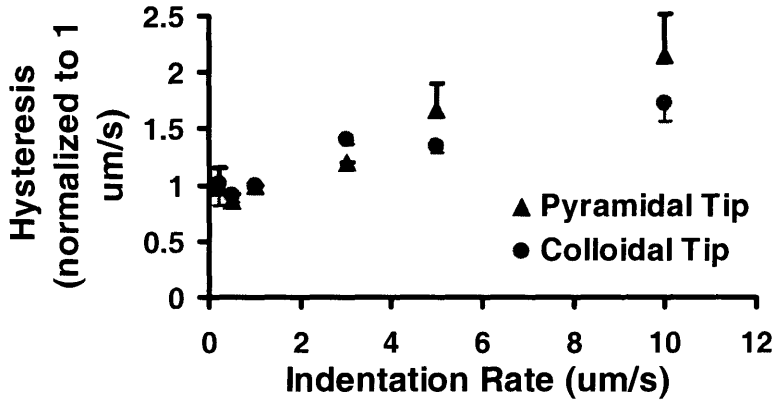

Figure B-6: Averaged hysteresis (mean ± sem) exhibited at 0.2, 0.5, 1, 3, 5, and 10 μm/s. Between 0.2-1 μm/s, little change in hysteresis was seen, indicating that the viscous effects were minimized and elastic properties dominating. Therefore, all indentations in the experiment were recorded at 1 μm/s.

Appendix C

Cell Histology Staining Protocol

C.1 Fixing Cells

SafefixII Use a 1:1 ratio of cell suspension to fixative (SafefixII, Cat No. 042-600, Fisher Scientific; note; this is much safer than paraformaldehyde). You can use the fixed cells immediately. See Appendix D.

RHT See Appendix E. RHT has been shown to preserve proteoglycans for histological staining. See Chapter 3 for results.

C.2 Mounting Cells onto a Slide

Cytospin (Cyto-Tek Miles, Diagnostic Division, Mishawaka, IN; Massachusetts General Hospital, contact: Han-Hwa Hung)

- Can use blotting paper for the insert gasket between the fluid chamber and the slide
- 3 ml of hetastarch 6% (in lactated electrolyte injection) + two drops of cell solution ($1{\cdot}10^6$ cells/ml)
- spin cells (14x100 rpm) for 10 min.
- wipe away excess fluid around the cell mounted area
- air dry

C.3 Toluidine Blue

Tol Blue is used for staining negatively charged molecules and is typically used to stain for proteoglycans.

0.1% Tol Blue Stain (1 g per 1000 g DI water) [Sigma-Aldrich Toluidine Blue O, Cat No. 198161, FW 305.83] To make this solution, dissolve the Tol blue powder into DI water. Filter through filter paper to remove larger particles.

Gently pipette ~100 μl of Tol Blue onto the mounted cells on glass slide. Incubate for 5 minutes. For RHT fixed samples, incubate for 2 minutes or less. The stain may be very dark. Shake off excess dye. Gently dip the slide a few times (3-4) in DI water. You don't want to rinse too well or the stain will wash away.

C.4 Aniline Blue

Aniline blue is typically used to stain for collagen. The phosphomolybdic acid is taken up by connective tissue (e.g. collagen I and II). A substitution reaction occurs for phosphomolybdic with aniline blue.

- Phosphomolybdic Acid (PMA), 1% ag [Rowley Biochemical Inc., Danver, MA; CatNo. F-362-7]
- Aniline Blue Solution [Rowley Biochemical Inc., Danver, MA; CatNo. F-362-4]

Gently pipette ~150 μl of PMA onto the mounted cells on glass slide. Incubate for 2 minutes. Shake off excess PMA. Pipette ~150 μl of Aniline Blue. Incubate 5-8 minutes. Shake off excess dye. Gently dip the slide 2-3 times in DI water (can also try 95% ethanol.) This dye rinses off easily, so do not dip the slide too many times.

C.5 Mounting Coverslips

Once the slides are dry, you can protect the samples with coverslips. Using a blunted glass probe, drip one drop (You only need one! It will spread.) of Toluene [Permount, Fischer Scientific, Cat No. UN1294] onto the cell area. Quickly place a coverslip over the drop. Allow to dry in hood overnight. Use xylene to remove any toluene adhered to the glass probe.

C.6 Taking Pictures

Division of Comparative Medicine (16-849) has a nice microscope that can capture the images on a computer. Contact Arlin in Pathology (617-253-9442).

Appendix D

Results from Fixation with SafeFix II

Safefix II offers a safe alternative to the usual fixatives including gluteraldehyde, and formalin. The main ingredient is glyoxal, which produces aldehyde-type fixation.

Cells, released from alginate beads at different points in culture, were suspended at $1{\cdot}10^6$ cells/ml medium. For fixation, the cell suspension was mixed with a 1:1 ratio of SafeFix II. The cells were mounted onto glass slides using a Cytospin (1400 rpm for 10 minutes). The slides were allowed to air dry before staining.

Results: Unlike the RHT fixed cells, the proteoglycan stain is not as dark, presumably due to loss of PGs during fixation. However, the PCM could be clearly identified apart from the cell. Freshly isolated cells showed no visible accumulation of proteoglycan or collagen (Figure D.1) By day 7, a ring of proteoglycan was stained and seen as a light purple dye ring around the cell membrane, but no collagen ring was visible. However by day 14, the halo of proteoglycan remained constant but a diffuse blue halo indicative of collagen was also present. By the third and fourth weeks in culture, the cell membrane displayed a more prominent and darkly stained halo of collagen and proteoglycan.

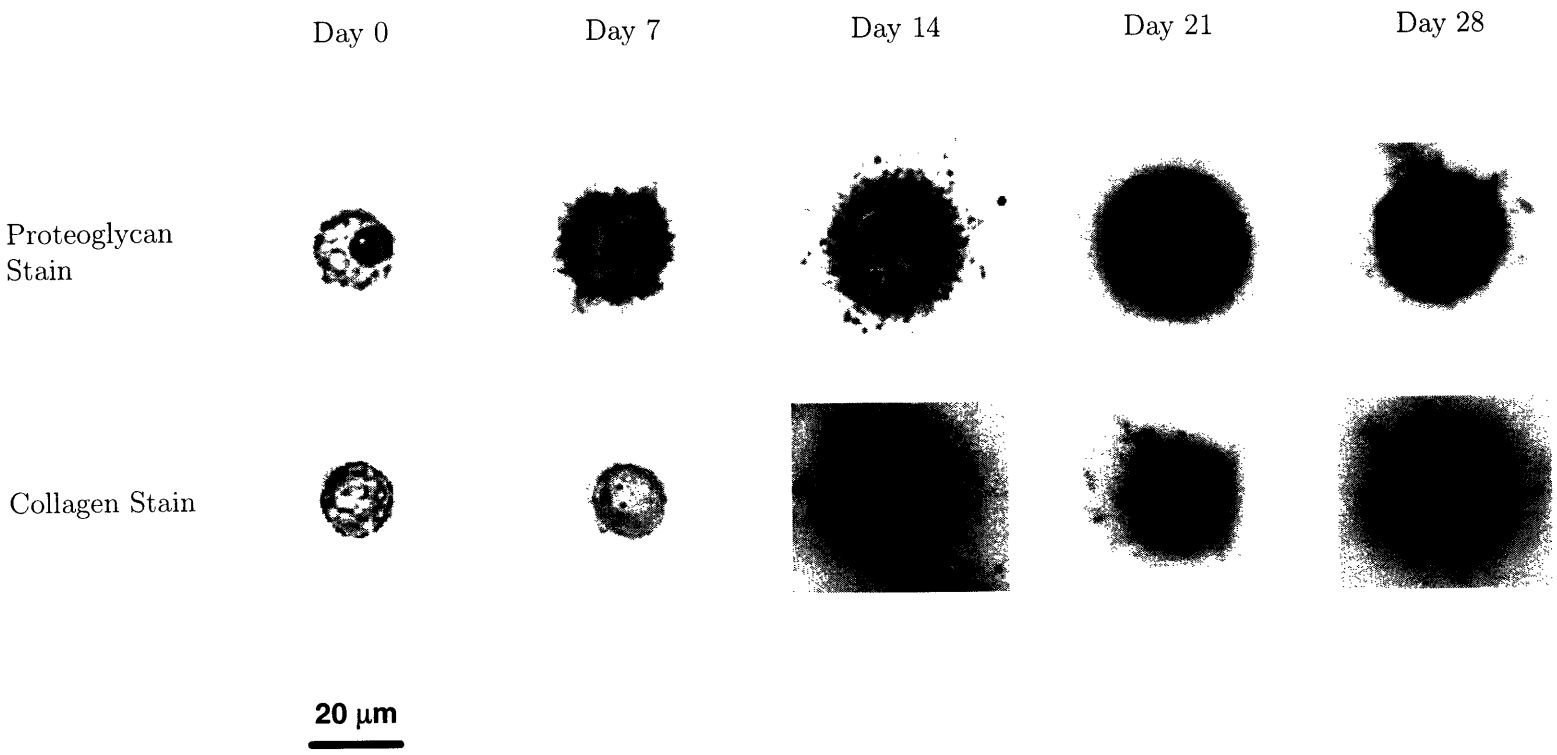

Table D.1: Histology of chondrocytes and their associated matrix released from alginate at different time points. Cells were fed 10% FBS. No staining for proteoglycans or collagen was seen on enzymatically isolated cells. After 7 days in culture, a clear halo of proteoglycans but not collagen is visible. In the following weeks up to day 28, proteoglycan and collagen buildup are visible.

Appendix E

RHT Fixation for Light Microscopy

E.1 Introduction

Objective: Fix cartilage for histology using Ruthenium Hexammine Trichloride (RHT), a cationic dye which binds to and precipitates negatively-charged GAG chains, and gluteraldehyde as a protein crosslinker. This combination retains more GAG in the tissue, allowing for a more-native GAG state for subsequent toluidine blue staining.

Background for this technique can be found in [60, 57, 58, 14].

Warning: Sodium cacodylate is a dangerous reagent, containing arsenic. Use only in the hood, and dispose of as toxic waste.

E.2 Procedure

1. Make the following solutions (reagent information in Section D)

   Solution A. 0.1 M sodium cacodylate stock, 40 mL

   - 0.86 g sodium cacodylate (MW 214)
   - Water
   - Dissolve sodium cacodylate powder in 30 mL water. pH to 7.4 w/pH paper. Bring volume to 40 mL.

   Final concentration: 0.1 M sodium cacodylate.

   Solution B. Prefix solution, 3 mL

   - 1.5 mL **Solution A**
   - 1.26 mL water
   - 240 μL 25% gluteraldehyde

   Mix these reagents in the fume hood.
   Final concentrations: 0.05 M sodium cacodylate, 2% gluteraldehyde

   Solution C. Wash solution, 25 mL

- 25 mL **Solution A**
- 95 mg NaCl (MW 59)

Add **Solution A**, NaCl. pH to 7.4
Final concentrations: 0.1 M sodium cacodylate, 65 mM NaCl, osmolality 330 mOsm.

2. 10 minutes before fixation, make **Solution D** by adding 21 mg RHT to 3 mL **Solution B**. The solution will first turn yellow, then dark brown/black. Final concentration of fixative: 0.05 M sodium cacodylate, 2% (v/v) gluteraldehyde, 0.7% (w/v) RHT.

3. Add an equal volume of RHT solution to the cell suspension.

4. Cytospin cells onto glass slides. Rinse the slides gently with **Solution C**.

E.3 Solution Storage

Solution A: Store indefinitely at room temperature

Solution B: Store at 4°C for up to one week. Parafilm cap of bottle to prevent evaporation.

Solution C: Store indefinitely at room temperature

E.4 Reagent Information

Reagent	**Cat number / Location**
sodium cacodylate trihydrate, MW 214	Sigma C-0250
25% gluteraldehyde	chemical fridge. If none in 15 mL conical tube, open another ampule in the hood
sodium chloride (NaCl, MW 58.4)	chemical cabinet
Ruthenium (III) hexamine trichloride (RHT), MW 308.7	chemical cabinet, in small cardboard boxes

Table E.1: Reagent Information

Appendix F

Casting Alginate Beads with Cells

F.1 Autoclave

- 50 ml beaker
- Three 500 ml bottles (for solutions below)
- One spatula (to move beads)

F.2 Solutions

- 2% alginate in 0.9% NaCl
- 0.9% NaCl: 9 g in 1000 ml DI water
- 150 mM NaCl (FW 58.44): 4.38 g in 500 ml DI water
- 102 mM CaCl2 (FW 111) in 0.9% NaCl: 5.66 g in 500 ml of 150 mM NaCl
- 55 mM Na Citrate (FW 294.10) in 150 mM NaCl: 8.09 g in 500 ml of 150 mM NaCl

Filter all solutions through a 200 μm filter and into the sterile bottles.

F.3 Making the beads

1. Fill the sterile 50 ml beaker with 30 ml of 102 mM $CaCl_2$ solution.
2. Get a count of cells using the hemacytometer. Spin cells down (if needed). 1800 rpm, 10 minutes Suction off supernatant (being careful not to suck up any cells). Gently tap bottom of vial to break up cells. May need to add a 1 ml sterile PBS (no Mg++ and Ca++, pH 7) to help break up the cells.
3. Add appropriate amount of alginate. [conc: $20{\cdot}10^6$ cells/ml; *can be 10-15*$\cdot 10^6$ *cells/ml*]

4. Use a 16 G needle and 3 ml syringe to suction up the alginate-chondrocyte solution. Remove as many air bubbles as possible from the syringe.

5. Remove 16 G needle and replace with 22 G needle. Hold the syringe at a 45° angle with the hole facing downward.

6. With steady pressure, drop even-sized droplets into the $CaCl_2$ solution. Halfway through you may want to exchange the $CaCl_2$ solution with fresh solution so the Ca++ does not get depleted.

7. After 10 minutes, suction off the $CaCl_2$ and rinse twice with 20 ml sterile PBS (no Mg++ and Ca++). Let each rinse go for 1 minute.

8. Replace PBS with culture medium.

9. Fill a 12-well plate with 2 ml culture medium in each well. Using a sterile spatula, transfer 6-8 beads per well.

10. Do a cell viability assay on one of the beads.

11. Keep alginate-cell beads in an incubator.

F.4 Dissolving the beads

1. Put 4 beads into a 1.5 ml Eppendorf tube. Add 1.2 ml NaCitrate. Place in a 37°C water bath or incubator for 10 minutes. Shake gently to mix. Do not vortex.

2. Spin 3000-4000 rpm (~1000 RCF) in Eppendorf centrifuge 5415C for 5 minutes.

3. Remove supernatant. Add 1 ml 0.9% NaCl. Centrifuge 3000-4000 rpm, 5 minutes. Repeat.

4. Re-suspend final pellet in PBS (if doing a cell viability assay) or culture medium at desired concentration (~0.5 ml).

5. Do a cell viability assay.

OR

1. Put 15 beads into a 15 ml conical tube. Add 5 ml NaCitrate. Place in 37°C water bath for 10 minutes. Shake gently to mix. Five more minutes with frequent shaking if the beads are not dissolved. Do not vortex.

2. Spin <1000 rpm (with CBE centrifuge) for 6 minutes.

3. Remove supernatant. Add 3 ml of 0.9% NaCl to rinse. Spin <1000 rpm. Re-suspend in medium.

Appendix G

AFM Imaging of Chondrocytes Cultured in Alginate

G.1 Dissolving the beads

1. Put four beads into a 1.5 ml Eppendorf tube. Add 1.3 ml of 55 mM NaCitrate (in 150 mM NaCl). Place in a 37°C water bath or incubator for 15 minutes. Mix slightly with 200 μl pipette.

2. Spin 3000 rpm (735 RCF) in Eppendorf centrifuge 5415C for 5 minutes.

3. Remove supernatant. Add 1 ml PBS (no Mg^{+2}, Ca^{+2}). Centrifuge 3000-4000 rpm, 5 minutes. Repeat.

4. Re-suspend final pellet in PBS (if doing a cell viability assay) or culture medium at desired concentration (~0.5 ml).

G.2 Preparing the AFM sample

1. Cut mica into 1x1 cm^2 pieces.

2. Pipette 30 μl of cells suspension onto cleaved mica. Keep sample enclosed in a Petri dish to minimize contamination.

3. Allow cells to attach for 30-60 minutes onto the mica at room temperature.

4. Rinse gently with a few drops of DI water. Blot edge dry with filter paper. Mount using double sided adhesive to sample disc. Allow to air dry until all signs of moisture are gone. Image the same day of prep.

G.3 AFM tapping mode imaging in air

1. Align laser and tune an Olympus 2 N/m Si cantilever (Veeco Inc.). (~70-80 kHz)

2. Shift the drive frequency to slightly below the resonance peak.

3. Using the optical microscope, position the cantilever tip over the cell. Image at a large scans (20-35 μm) at a slow scan rate (1-1.5 Hz) to minimize the tip velocity and increase resolution.

Appendix H

Protocol for AFM Aggrecan Sample

H.1 0.01% AP Mica v/v MilliQ

1. Make dilution in MilliQ water: 2 μl of APTES (3-aminopropyltriethoxysilane) with 20 ml MilliQ water. Shake by inverting the vial a few times.
2. Cleave mica with tape. Make sure the cleaved plane comes off cleanly in one piece.
3. Incubate 60 μl (or enough to cover the entire surface but not spill off) of the 0.01% AP solution on the cleaved mica. Keep in a humidity controlled environment (i.e. a sealed box with water to minimize evaporation of the solution) at room temperature. Incubate for 20 minutes.
4. Rinse gently in a stream of MilliQ water for ~10 seconds. Blot one edge of the mica to dry. (Nitrogen drying optional.)
5. Use prepared mica in the same day.

H.2 Diluted Aggrecan

1. Thaw frozen aggrecan from ~80°C freezer. The concentration is 2 mg/ml (GAG).
2. Use 0.25 ml of the concentrated aggrecan plus 0.75 ml water to obtain a final amount of 500 μg per vial. A more dilute solution will result in a sparser aggrecan surface if a dilution of 250 μg/ml (GAG) aggrecan is made.

H.3 Samples

1. Incubate 50 μl of aggrecan dilution onto the dry AP mica for times ranging from 20-30 min. Keep the samples in a humidity controlled (i.e. in an air tight container) environment at room temperature.

2. Rinse gently in a stream of MilliQ water for ~10 seconds. Blot one edge of the mica to dry. Air dry.

3. Image the sample the same day or next day.

Appendix I

List of Supplies for Chondrocyte Indentation Experiments

I.1 Cell Isolation and Culture

Name	Vendor	Catalog Number
pronase	Sigma	P-5147
collagenase-P	Boehringer Mannheim	12-49-002
DMEM	Invitrogen	11965-092
trypan blue	Sigma	T-8154
alginate	Kelco	LVCR
L-ascorbic acid	Sigma	A-4544
antibiotic-antimycotic	Sigma	A-5955
rIGF-1	PreproTech	100-11
insulin	Sigma	I0516
transferrin	Sigma	T8158
selenous acid	Sigma	S9133
linoleic acid-albumin	Sigma	L9530

Table I.1: Chemicals for Cell Isolation and Culture

I.2 Histology

Name	Vendor	Catalog Number
SafefixII	Fischer Scientific	23-011116
RHT	Polysciences	17253
sodium cacodylate	Sigma	C-0250
gluteraldehyde	Polysciences	1909
toluidine blue o	Sigma	198161
phosphomolybdic acid	Rowley Biochemical	F-362-7
aniline Rowley	Biochemical	F-367-5
hyaluronidase	Sigma	H-3506
col VI antibody	Chemicon	AB782
2 rhodamine-conjugated AB	Jackson Immunoresearch	705-225-003
muscovite mica	SPI Supplies	1804 V-5

Table I.2: Chemicals for Histology

I.3 AFM

Name	Vendor	Catalog Number
APTES (aminopropyltriethoxysilane)	Pierce Chemical	80370
muscovite mica	SPI Supplies	1804 V-5
silica beads	Bang Labs	SS06N
tipless cantilevers	Veeco	NP-020
tapping mode cantilevers	Asylum Research	AC240-TS
contact mode cantilevers	Veeco	MLCT

Table I.3: Chemicals for AFM sample preparation

Bibliography

[1] L.G. Alexopoulos, M.A. Haider, T.P. Vail, and F. Guilak. Alterations in the mechanical properties of the human chondrocyte pericellular matrix with osteoarthritis. *J Biomech Eng*, 125:323–333, 2003.

[2] L.G. Alexopoulos, G.M. Williams, M.L. Upton, L.A. Setton, and F. Guilak. Osteoarthritic changes in the biphasic mechanical properties of the chondrocyte pericellular matrix in articular cartilage. *J Biomech*, 38(3):509–517, 2005.

[3] D.M. Allen and J.J. Mao. Heterogeneous nanostructural and nanoelastic properties of pericellular and interterritorial matrices of chondrocytes by atomic force microscopy. *J Struct Biol*, 145:196204, 2004.

[4] M.B. Aydelotte and K.E. Kuettner. Differences between sub-populations of cultured bovine articular chondrocytes. i. morphology and cartilage matrix production. *Connect. Tissue Res.*, 18(3):205–222, 1988.

[5] E. Balnois, S. Stoll, K. J. Wilkinson, J. Buffle, M. Rinaudo, and M. Milas. Conformation of succinoglycan as observed by atomic force microscopy. *Macromolecules*, 33:7440–7447, 2000.

[6] M. Bathe, G.C. Rutledge, A.J. Grodzinsky, and B. Tidor. A coarse-grained molecular model for glycosaminoglycans: Application to chondroitin, chondroitin sulfate, and hyaluronic acid. *Biophys J*, 88:3870–3887, 2005.

[7] M.T. Bayliss and S.Y. Ali. Age-related changes in the composition and structure of human articular-cartilage proteoglycans. *Biochem. J.*, 176:683–693, 1978.

[8] G. Binnig, C.F. Quate, and C. Gerber. Atomic force microscope. *Phys. Rev. Lett.*, 56(9):930–933, 1986.

[9] J. Bonaventure, N. Kadhom, L. Cohen-Solal, K.H. Ng, J. Bourguignon, C. Lasselin, and P. Freisinger. Reexpression of cartilage-specific genes by dedifferentiated human articular chondrocytes cultured in alginate beads. *Exp. Cell. Res.*, 212(1):97–104, 1994.

[10] J. Buckwalter, L. Rosenberg, and L-H Tang. The effect of link protein on proteoglycan aggregate structure. *J. Biol. Chem.*, 259(9):5361–5363, 1984.

[11] J. A. Buckwalter and L. C. Rosenberg. Electron microscopic studies of cartilage proteoglycans. direct evidence for the variable length of the chondroitin sulfate-rich region of proteoglycan subunit core protein. *J. Biol. Chem.*, 257:9830–9839, 1982.

[12] J. A. Buckwalter and L. C. Rosenberg. Structural changes during development in bovine fetal epiphyseal cartilage. *Collagen Rel. Res.*, 3:489–504, 1983.

[13] J. A. Buckwalter and L. C. Rosenberg. Electron microscopic studies of cartilage proteoglycans. *Electron Microscopy Review*, 1:87–112, 1988.

[14] M. D. Buschmann and A. J. Grodzinsky. A molecular model of proteoglycan-associated electrostatic forces in cartilage mechanics. *Journal Biomechanical Engineering*, 117(2):179–92, 1995.

[15] A. Calabro, R.J. Midura, A. Wang, L.A. West, A. H. K. Plaas, and V. C. Hascall. Fluorophore-assisted carbohydrate electrophoresis (face) of glycosaminoglycans. *Osteoart. and Cart.*, 9(SA):S16–S22, 2001.

[16] T. A. Camesano and K. J. Wilkinson. Single molecule study of xanthan conformation using atomic force microscopy. *Biomacromolecules*, 2:1184–1191, 2001.

[17] J. Chang and C.A. Poole. Confocal analysis of the molecular heterogeneity in the pericellular microenvironment produced by adult canine chondrocytes cultured in agarose gel. *Histochem J*, 29(7):515–528, 1997.

[18] P. Chen, S. Vukicevic, T.K. Sampath, and F.P. Luyten. Osteogenic protein-1 promotes growth and maturation of chick sternal chondrocytes in serum-free cultures. *J. Cell Sci.*, 108:105–114, 1995.

[19] S. Chubinskaya, K. Huch, M. Schulze, L. Otten, M.B. Aydelotte, and A.A. Cole. Gene expression by human articular chondrocytes cultured in alginate beads. *J. Histochem. Cytochem.*, 49(10):1211–1220, 2001.

[20] R. L. Cleland. Persistence length of hyaluronic acid: an estimate from small-angle x-ray scattering and intrinsic viscosity. *Arch. Biochem. Biophys.*, 180:57–68, 1977.

[21] R. L. Cleland and J. L. Wang. Ionic polysaccharides. iii. dilute solution properties of hyaluronic acid fractions. *Biopolymers*, 9:799–810, 1970.

[22] A.M. Collinsworth, S. Zhang, W.E. Kraus, and G.A. Truskey. Apparent elastic modulus and hysteresis of skeletal muscle cells throughout differentiation. *Am. J. Phys: Cell Phys.*, 283:1219–1227, 2002.

[23] M.K. Cowman, M. Lin, and E. A. Balazs. Tapping mode atomic force microscopy of hyaluronan : Extended and intramolecularly interacting chains. *Biophys. J.*, 75:2030–2037, 1998.

[24] D. Dean, L. Han, C. Ortiz, and A.J. Grodzinsky. Nanoscale conformation and compressibility of cartilage aggrecan using microcontact printing and atomic force microscopy. *Macromolecules*, 38(10):4047–4049, 2005.

[25] D. Dean, J. Seog, C. Ortiz, and A. J. Grodzinsky. A new molecular-level theoretical model for the electrostatic interactions between polyelectrolyte macromolecules using glycosaminoglycans as a model system. *Langmuir*, 19(13):5526–5539, 2003.

[26] A. J. Deutsch, R. J. Midura, and A. H. Plaas. Structure of chondroitin sulfate on aggrecan isolated from bovine tibial and costochondral growth plates. *J. Orthop. Res.*, 13(2):230–9, 1995.

[27] Peter Diggle, Kung-Yee Liang, and Scott L. Zeger. *Analysis of longitudinal data.* Oxford statistical science series; 13. Clarendon Press; Oxford University Press, Oxford; New York, 1994.

[28] K.J. Doege, M. Sasaki, T. Kimura, and Y. Yamada. Complete coding sequence and deduced primary structure of the human cartilage large aggregating proteoglycan, aggrecan. human-specific repeats, and additional alternatively spliced forms. *J. Biol. Chem.*, 266(2):894–902, 1991.

[29] J. Dudhia, C.M. Davidson, T.M. Wells, D.H. Vynios, T.E. Hardingham, and M.T. Bayliss. Age-related changes inthe content of the c-terminal region of aggrecan in human articular cartilage. *Biochem. J.*, 313:933–940, 1996.

[30] R. W. Farndale, D. J. Buttle, and A. J. Barrett. Improved quantitation and discrimination of sulphated glycosaminoglycans by use of dimethylmethylene blue. *Biochim Biophys Acta*, 883(2):173–7, 1986.

[31] J.B. FitzGerald, A.J. Grodzinsky, M. Jin, M. Zheng, and D.J. Wood. Low-amplitude dynamic compression regulates expression of anabolic and catabolic genes in cartilage explants. In *50th Annual Meeting of the Orthopaedic Research Society*, volume 29, page 830, San Francisco, California, 2004.

[32] J.B. FitzGerald, M. Jin, D. Dean, D.J. Wood, M.H. Zheng, and A.J. Grodzinsky. Mechanical compression of cartilage explants induces multiple time-dependent gene expression patterns and involves intracellular calcium and cyclic amp. *J. Biol. Chem.*, 279(19):19502–11, 2004.

[33] J.B. Fitzgerald, M. Jin, and A. Grodzinsky. Shear and compression duration, rate, and magnitude differentially regulate the temporal transcription profiles of functionally-related genes in cartilage explants. *J. Biol. Chem.*, in submission.

[34] C. R. Flannery, M. W. Lark, and J. D. Sandy. Identification of a stromelysin cleavage site within the interglobular domain of human aggrecan. evidence for proteolysis at this site in vivo in human articular cartilage. *J Biol Chem*, 267(2):1008–14, 1992.

[35] J. Flechtenmacher, K. Huch, E.J. Thonar, J.A. Mollenhauer, S.R. Davies, T.M. Schmid, W. Puhl, T.K. Sampath, M.B. Aydelotte, and K.E. Kuettner. Recombinant human osteogenic protein 1 is a potent stimulator of the synthesis of cartilage proteoglycans and collagens by human articular chondrocytes. *Arthritis Rheum*, 39(11):1896–1904, 1996.

[36] E. Flikkema and G. ten Brinke. Influence of rigid side chain attraction on stiffness and conformations of comb copolymer brushes strongly adsorbed on a flat surface. *Macromol. Theory Simul.*, 11:777–784, 2002.

[37] E.H. Frank, M. Jin, A.M. Loening, M.E. Levenston, and A.J. Grodzinsky. A versatile shear and compression apparatus for mechanical stimulation of tissue culture explants. *J. Biomech.*, 33:1523–1527, 2000.

[38] P.M. Freeman, R.N. Natarajan, J.H. Kimura, and T.P. Andriacchi. Chondrocyte cells respond mechanically to compressive loads. *J. Orthop. Res.*, 12:311–320, 1994.

[39] T.T. Glant, C. Hadhazy, K. Mikecz, and A. Sipos. Appearance and persistence of fibronectin in cartilage. specific interaction of fibronectin with collagen type ii. *Histochem.*, 82:149–158, 1987.

[40] R.D. Graff, S.S. Kelley, and G.M. Lee. Role of pericellular matrix in development of a mechanically functional neocartilage. *Biotech. Bioeng.*, 82(4):457–464, 2003.

[41] P. Gribbon and T.E. Hardingham. Macromolecular diffusion of biological polymers measured by confocal fluorescence recovery after photobleaching. *Biophys J*, 75:10321039, 1998.

[42] F. Guilak. The deformation behavior and viscoelastic properties of chondrocytes in articular cartilage. *Biorheology*, 37(1-2):27–44, 2000.

[43] F. Guilak, W. R. Jones, H. P. Ting-Beall, and G. M. Lee. The deformation behavior and mechanical properties of chondrocytes in articular cartilage. *Osteoarthritis Cartilage*, 7(1):59–70., 1999.

[44] F. Guilak, B.C. Meyer, A. Ratcliffe, and V.C. Mow. The effects of matrix compression on proteoglycan metabolism in articular cartilage explants. *Osteoarthr. Cart.*, 2(2):91–101, 1994.

[45] F. Guilak and V. C. Mow. The mechanical environment of the chondrocyte: a biphasic finite element model of cell-matrix interactions in articular cartilage. *J Biomech*, 33(12):1663–73., 2000.

[46] F. Guilak, A. Ratcliffe, and V. C. Mow. Chondrocyte deformation and local tissue strain in articular cartilage: a confocal microscopy study. *J Orthop Res*, 13:410–421, 1995.

[47] H. Haga, S. Sasaki, K. Kawabata, E. Ito, T. Ushiki, and T. Sambongi. Elasticity mapping of living fibroblasts by afm and immunofluorescence observation of the cytoskeleton. *Ultramicroscopy*, 82(1-4):253–8., 2000.

[48] T. Hardingham. Proteoglycans: Their structure, interactions and molecular organizatioin in cartilage. *Biochem. Soc. Trans.*, 9:489–497, 1981.

[49] T. E. Hardingham and A. J. Fosang. Proteoglycans: many forms and many functions. *FASEB J.*, 6:861–870, 1992.

[50] V. C. Hascall and S.W. Sajdera. Proteinpolysaccharide complex from bovine nasal cartilage: The function of glycoprotein in the formation of aggregates. *J. Bio. Chem.*, 224:2384–2396, 1969.

[51] V.C. Hascall, C.J. Handley, D.J. McQuillan, G.K. Hascall, H.C. Robinson, and D.A. Lowther. The effect of serum on biosynthesis of proteoglycans by bovine articular cartilage in culture. *Arch. Biochem. Biophys.*, 224(1):206–223, 1983.

[52] E. Hassan, W. Heinz, M. Antonik, N. Costa, S. Nageswaran, C. Schoenenberger, and J. Hoh. Relative microelastic mapping of living cells by atomic force microscopy. *Biophysical Journal*, 74:1564–1578, 1998.

[53] H.J. Hauselmann, M.B. Aydelotte, B.L. Schumacher, K.E. Kuettner, S.H. Gitelis, and E.J.-M.A. Thonar. Synthesis and turnover of proteglycans by human and bovine adult articular chondrocytes cultured in alginate beads. *Matrix*, 12:116–129, 1992.

[54] H.J. Hauselmann, R.J. Fernandes, S.S. Mok, T.M. Schmid, J.A. Block, M.B. Aydelotte, K.E. Kuettner, and E.J. Thonar. Phenotypic stability of bovine articular chondrocytes after long-term culture in alginate beads. *J. Cell Sci.*, 107(1):17–27, 1994.

[55] T.M. Hering, J. Kollar, and T.D. Huynh. Complete coding sequence of bovine aggrecan: comparative structural analysis. *Archives of Biochemistry and Biophysics (ABB)*, 345(2):259–270, 1997.

[56] O. Horikawa, H. Nakajima, T. Kikuchi, S. Ichimura, H. Yamada, K. Fujikawa, and Y. Toyama. Distribution of type vi collagen in chondrocyte microenvironment: study of chondrons isolated from human normal and degenerative articular cartilage and cultured chondrocytes. *J. Orthop. Sci.*, 9(1):29–36, 2004.

[57] E. B. Hunziker, W. Herrmann, and R. K. Schenk. Ruthenium hexammine trichloride (RHT)-mediated interaction between plasmalemmal components and pericellular matrix proteoglycans is responsible for the preservation of chondrocytic plasma membranes in situ during cartilage fixation. *J Histochem Cytochem*, 31:717–727, 1983.

[58] E. B. Hunziker, A. Ludi, and W. Herrmann. Preservation of cartilage matrix proteoglycans using cationic dyes chemically related to ruthenium hexaammine trichloride. *J Histochem Cytochem*, 40:909–917, 1992.

[59] E. B. Hunziker, M. Stolz, and U. Aebi. Nanotechnology in medicine: moving from the bench to the bedside. *Chimia*, 56:520–526, 2002.

[60] E.B. Hunziker, W. Herrmann, and R.K. Schenk. Improved cartilage fixation by ruthenium hexammine trichloride (rht). a prerequisite for morphometry in growth cartilage. *J Ultrastruct Res*, 81:1–12, 1982.

[61] K.L. Johnson and J.A. Greenwood. An adhesion map for the contact of elastic spheres. *J Colloid Interface Sci*, 192:326–333, 1997.

[62] I.L. Jones, S.E. Larsson, and R. Lemperg. The glycosaminoglycans of human articular cartilage: concentration and distribution in different layers in the adult individual. *Clin. Orthop. Relat. Res.*, 127:257–264, 1977.

[63] W. R. Jones, H. P. Ting-Beall, G. M. Lee, S.S. Kelley, R.M. Hochmuth, and F. Guilak. Alterations in the young's modulus and volumetric properties of chondrocytes isolated from normal and osteoarthritic human cartilage. *J Biomech*, 32:119–127, 1999.

[64] J. S. Jurevlin, D. J. Muller, M. Wong, D. Studer, A. Engel, and E. B. Hunziker. Surface and suburface morphology of bovine humeral articular cartilage as assessed by atomic force and tranmission electron microscopy. *J. Struc. Bio.*, 117:45–54, 1996.

[65] Y.J. Kim, R.L. Sah, A.J. Grodzinsky, A.H. Plaas, and J.D. Sandy. Mechanical regulation of cartilage biosynthetic behavior: physical stimuli. *Arch. Biochem. Biophys.*, 311(1):1–12, 1994.

[66] J. Kisiday, M. Jin, B. Kurz, H. Hung, C. Semino, S. Zhang, and A.J. Grodzinsky. Self-assembling peptide hydrogel fosters chondrocyte extracellular matrix production and cell division: implications for cartilage tissue repair. *Proc. Natl. Acad. Sci. U.S.A.*, 99(15):9996–10001, 2002.

[67] M.M. Knight, J.M. Ross, A.F. Sherwin, D.A. Lee, D.L. Bader, and C.A. Poole. Chondrocyte deformation within mechanically and enzymatically extracted chondrons compressed in agarose. *Biochim. Biophys. Acta*, 1526:141–146, 2001.

[68] E.J. Koay, A.C. Shieh, and K.A. Athanasiou. Creep indentation of single cells. *J Biomech Eng*, 125:334–341, 2003.

[69] G. T. A. Kovacs, N. I. Maluf, and K. E. Petersen. Bulk micromachining of silicon. *Proceedings of the IEEE*, 86(8):1536–1551, August 1998.

[70] O. Kratky and G. Porod. *Recl. Trav. Chim. Pays-Bas.*, 68:1106, 1949.

[71] S. Lecommandoux, F. Checot, R. Borsali, M. Schappacher, A. Deffieux, A. Brulet, and J.P. Cotton. Effect of dense grafting on the backbone conformation of bottlebrush polymers: Determination of the persistence length in solution. *Macromolecules*, 35:8878–8881, 2002.

[72] D.A. Lee and D.L. Bader. Development and characterization of an in vitro system to study strain-induced cell deformation in isolated chondrocytes. *In Vitro Cell Devel. Biol.*, 31:828–835, 1995.

[73] G.M. Lee and R.F. Loeser. Interactions of the chondrocyte with its pericellular matrix. *Cells Mats*, 8:135–149, 1998.

[74] N.D. Leipzig and K.A. Athanasiou. Unconfined creep compression of chondrocytes. *J Biomech*, 38(1):77–85, 2005.

[75] F. Lemare, N. Steimberg, C. Le Griel, S. Demignot, and M. Adolphe. Dedifferentiated chondrocytes cultured in alginate beads: restoration of the differentiated phenotype and of the metabolic responses to interleukin-1beta. *J. Cell Physiol.*, 176(2):303–313, 1998.

[76] X. Li and W.F. Reed. Polyelectrolyte properties of proteoglycan monomers. *J. Chem. Phys.*, 94:4568–4580, 1991.

[77] R.F. Loeser, C.A. Pacione, and S. Chubinskaya. The combination of insulin-like growth factor 1 and osteogenic protein 1 promotes increased survival of and matrix synthesis by normal and osteoarthritic human articular chondrocytes. *Arthritis Rheum*, 48(8):2188–2196, 2003.

[78] E.G. Luna. *Manual of Histological Staining Methods.* McGraw-Hill Publication, New York, 3rd edition, 1968.

[79] F.P. Luyten, V.C. Hascall, S.P. Nissley, T.I. Morales, and A.H. Reddi. Insulin-like growth factors maintain steady-state metabolism of proteoglycans in bovine articular cartilage explants. *Arch Biochem Biophys*, 267(2):416–425, 1988.

[80] B. Maier and J.O. Radler. Conformation and self-diffusion of single dna molecules confined to two dimensions. *Phys. Rev. Lett.*, 82(9):1911–1914, 1999.

[81] A. Maroudas. Physicochemical properties of articular cartilage. In M. A. R. Freeman, editor, *Adult Articular Cartilage*, pages 215–290. Pitman Medical, Kent, England, 1979.

[82] K. Masuda, R.L. Sah, M.J. Hejna, and E. Thonar. A novel two-step method for the formation of tissue-engineered cartilage by mature bovine chondrocytes: the alginate-recovered chondrocyte (arc) method. *J. Orthop. Res.*, 21:139–148, 2003.

[83] M. B. Mathews and L. Decker. *Biochim. Biophys. Acta*, 498:259–263, 1977.

[84] D.J. McQuillan, C.J. Handley, M.A. Campbell, S. Bolis, V.E. Milway, and A.C. Herington. Stimulation of proteoglycan biosynthesis by serum and insulin-like growth factor-i in cultured bovine articular cartilage. *Biochem. J.*, 240:423–430, 1986.

[85] N. Meechai, A.M. Jamieson, J. Blackwell, and D.A. Carrino. Nonlinear viscoelasticity of concentrated solutions of aggrecan aggregate. *Biomacromolecules*, 2:780–787, 2001.

[86] N. Meechai, A.M. Jamieson, J. Blackwell, D.A. Carrino, D.A. Carrino, and R. Bansal. Viscoelastic properties of aggrecan aggregate solutions: Dependence on aggrecan concentration and ionic strength. *J Rheology*, 46(3):685–707, 2002.

[87] M. Morgelin, M. Paulsson, T. E. Hardingham, D. Heinegard, and J. Engel. Cartilage proteoglycans. assembly with hyaluronate and link protein as studied by electron microscopy. *Biochem. J.*, 253:175–185, 1988.

[88] M. Morgelin, M. Paulsson, A. Malmstrom, and D. Heinegard. Shared and distinct features of interstitial proteoglycans from different bovine tissues revealed by electron microscopy. *J. Bio. Chem.*, 264(20):12080–12090, 1989.

[89] V.C. Mow and A. Ratcliffe. Structure and function of articular cartilage and meniscus. In V.C. Mow and W.C. Hayes, editors, *Basic Orthopaedic Biomechanics*, page 113177. Lippincott-Raven, Philadelphia, 2nd edition, 1997.

[90] N. Nemoto, M. Nagai, A. Koike, and S. Okada. Diffusion and sedimentation studies on poly(macromonomer) in dilute solution. *Macromolecules*, 28:3854–3859, 1995.

[91] L. Ng, M. Bathe, C. Ortiz, and A. Grodzinsky. Aggrecan conformation depends on gag-gag interactions: the effects of aggrecan concentration, gag molecular weight, and bath ionic strength. In *Annual Meeting of the Orthopaedic Research Society*, Washington D.C., 2005.

[92] L. Ng, A.H.K. Plaas, A.J. Grodzinsky, and C Ortiz. Atomic force microscopy studies of the conformation of cartilage aggrecan and related constituents.

[93] L. Ng, A.H.K. Plaas, C. Ortiz, and A.J. Grodzinsky. Afm imaging of othe conformation and interactions of aggrecan, hyaluronan, and their constituents, Feb. 2002.

[94] L. Ng, K. Taik, A.H.K. Plaas, A.J. Grodzinsky, and C. Ortiz. Ultrastructure and nanomechanics of biological tissues : Cartilage and bone, 2002.

[95] L. J. Ng, A. H. K. Plaas, J. D. Sandy, A. J. Grodzinsky, and C. Ortiz. Individual cartilage aggrecan macromolecules and their constituent glycosaminoglycans visualized via atomic force microscopy. *Journal Structural Biology*, 143(3):242–257, 2003.

[96] NIAMS. Handout on health: Osteoarthritis, 2000. National Institute of Arthritis and Musculoskeletal and Skin Diseases.

[97] Y. Nishida, C.B. Knudson, K.E. Kuettner, and W. Knudson. Osteogenic protein-1 promotes the synthesis and retention of extracellular matrix within bovine articular cartilage and chondrocyte cultures. *Osteoarthr Cart*, 8(2):27–136, 2000.

[98] M. Paulsson, M. Morgelin, H. Wiedemann, N. Beardmore-Gray, D. Dunham, T. Hardingham, D. Heingard, R. Timpl, and J. Engel. Extended and globular protein domains in cartilage proteoglycans. *Biochem. J.*, 245:763–772, 1987.

[99] S. J. Perkins, A. Miller, T. E. Hardingham, and R. Muir. Physical properties of the hyaluronate binding region of proteoglycan from pig laryngeal cartilage : Densitometric and small angle neutron scattering studies of carbohydrates and carbohydrate-protein macromolecules. *J. Mol. Bio.*, 1981.

[100] B. Petit, K. Masuda, A.L. DSouza, L. Otten, D. Pietryla, D.J. Hartmann, N.P. Morris, D. Uebelhart, T.M. Schmid, and E. J-M. A. Thonar. Characterization of crosslinked collagens synthesized by mature articular chondrocytes cultured in alginate beads: comparison of two distinct matrix compartments. *Exper Cell Res*, 225:151–161, 1996.

[101] A. H. K. Plaas, L.A. West, and R.J. Midura. Keratan sulfate disaccharide composition determined by face analysis of keratanase ii and endo-beta-galactosidase digestion products. *Glycobiology*, 11(10):779–790, 2001.

[102] A. H. K. Plaas, S. Wong-Palms, P.J. Roughley, R.J. Midura, and V. C. Hascall. Chemical and immunological assay of the nonreducing terminal residues of chondroitin sulfate from human aggrecan. *J. Biol. Chem.*, 272(33):20603–20610, 1997.

[103] C. A. Poole. Articular cartilage chondrons: form, function and failure. *J Anat*, 191(Pt 1):1–13., 1997.

[104] C. A. Poole, S. Ayad, and R.T. Gilbert. Chondrons from articular cartilage: Immunohistochemical evaluation of type vi collagen organisation in isolated chondrons by light, confocal and electron microscopy. *J Cell Sci*, 103:1101–1110, 1992.

[105] C.A. Poole, S. Ayad, and J.R. Schofield. Chondrons from articular cartilage: (i). immunolocalization of type vi collagen in the pericellular capsule of isolated canine tibial chondrons. *J. Cell Sci.*, 90:635–643, 1988.

[106] C.A. Poole, M.H. Flint, and B.W. Beaumont. Chondrons in cartilage: ultrastructural analysis of the pericellular microenvironment in adult human articular cartilages. *J. Orthop. Res.*, 5(4):509–522, 1987.

[107] T.M. Quinn, P. Dierickx, and A.J. Grodzinsky. Glycosaminoglycan network geometry may contribute to anisotropic hydraulic permeability in cartilage under compression. *J Biomech*, 34(11):1483–90, 2001.

[108] T.M. Quinn, V. Morel, and J.J. Meister. Static compression of articular cartilage can reduce solute diffusivity and partitioning: implications for the chondrocyte biological response. *J Biomech*, 34(11):1463–9, 2001.

[109] M. Radmacher. Measuring the elastic properties of biological samples with the afm. *IEEE Eng Med Biol*, 16(2):47–57, 1997.

[110] P.M. Ragan, V.I. Chin, H.H. Hung, K. Masuda, E.J. Thonar, E.C. Arner, A.J. Grodzinsky, and J.D. Sandy. Chondrocyte extracellular matrix synthesis and turnover are influenced by static compression in a new alginate disk culture system. *Arch. Biochem. Biophys.*, 383(2):256–264, 2000.

[111] M. Raspanti, T. Congiu, and S. Guizzardi. Tapping-mode atomic force microscopy in fluid of hydrated extracellular matrix. *Matrix Biol.*, 20:601–604, 2001.

[112] C. Rivetti, M. Guthold, and C. Bustamante. Scanning force microscopy of dna deposited onto mica: equilibration versus kinetic trapping studied by statistical polymer chain analysis. *J Mol Biol*, 264(5):919–32, 1996.

[113] L. Rosenberg, W. Hellmann, and A. K. Kleinschmidt. Macromolecular models of proteinpolysaccharides from bovine nasal cartilage based on electron microscope studies. *J. Bio. Chem.*, 245(16):4123–4130, 1970.

[114] N. Rotter, G. Tobias, M. Lebl, A.K. Roy, M.C. Hansen, C.A. Vacanti, and L.J. Bonassar. Age-related changes in the composition and mechanical properties of human nasal cartilage. *Arch. Biochem. Biophys.*, 403:132–140, 2000.

[115] A. Round, M. Berry, T.J. McMaster, A.P. Corfield, and M. J. Miles. Glycopolymer charge density determines conformation in human ocular mucin gene products: an atomic force microscope study. *J. Struct. Biol.*, 145(3):246–253, 2004.

[116] A. N. Round, M. Berry, T. J. McMaster, S. Stoll, D. Gowers, A. P. Corfield, and M. J. Miles. Heterogeneity and persistence length in human ocular mucins. *Biophys. J.*, 83:16611670, 2002.

[117] Harper G. S. and Preston B. N. Molecular shrinkage of proteoglycans. *J Biol Chem*, 262(17):8088–8095, June 15, 1987.

[118] J. D. Sandy and C. Verscharen. Analysis of aggrecan in human knee cartilage and synovial fluid indicates that aggrecanase (adamts) activity is responsible for the catabolic turnover and loss of whole aggrecan whereas other protease activity is required for c-terminal processing in vivo. *Biochem J*, 358(Pt 3):615–26, 2001.

[119] J. Seog, D. Dean, A. H. K. Plaas, S. Wong-Palms, A. J. Grodzinsky, and C. Ortiz. Direct measurement of glycosaminoglycan intermolecular interactions via high-resolution force spectroscopy. *Macromolecules*, 35(14):5601–5615, 2002.

[120] Z. Shao, J. Mou, D.M. Czajkowsky, J. Yang, and J.Y. Yuan. Biological atomic force microscopy: What is achieved and what is needed. *Advances in Physics*, 45:1–86, 1996.

[121] S. S. Sheiko. Imaging of polymers using scanning force microscopy: From superstructures to individual molecules. *Advances in Polymer Science*, 151:62–174, 2000.

[122] S. S. Sheiko, M. Gerle, K. Fischer, M. Schmidt, and M. Moller. Wormlike polystyrene brushes in thin films. *Langmuir*, 13:5368–5372, 1997.

[123] S. S. Sheiko and M. Moller. Visualization of macromolecules : A first step to manipulation and controlled response. *Chem. Rev.*, 101:4099–4123, 2001.

[124] R. Shogren, T.A. Gerken, and N. Jentoft. Role of glycosylation on the conformation and chain dimensions of o-linked glycoproteins: light-scattering studies of ovine submaxillary mucin. *Biochem.*, 28(13):5525–5536, 1989.

[125] D.P. Speer and L. Dahners. The collagenous architecture of articular cartilage. correlation of scanning electron microscopy and polarized light microscopy observations. *Clin. Orthop. Relat. Res.*, 139:267–275, 1979.

[126] R.A. Stockwell and G. Meachim. *The chondrocytes.* Adult Articular Cartilage. Pitman Medical Publishing Co Ltd, Kent, 1979.

[127] M. Stolz, R. Raiteri, A. U. Daniels, M. R. VanLandingham, W. Baschong, and U. Aebi. Dynamic elastic modulus of porcine articular cartilage determined at two different levels of tissue organization by indentation-type atomic force microscopy. *Biophysical Journal*, 86(5):3269–3283, 2004.

[128] J. Tamayo and R. Garcia. Deformation, contact time, and phase contrast in tapping mode scanning force microscopy. *Langmuir*, 12(18):4430–4435, 1996.

[129] K. Tanaka. Physiochemical properties of chondroitin sulfate: Ion binding and secondary structure. *J. Biochem. (Japan)*, 83:647–653, 1978.

[130] B.A. Todd, J. Rammohan, and S.J. Eppell. Connecting nanoscale images of proteins with their genetic sequences. *Biophysical Journal*, 84:3982–91, 2003.

[131] S. Treppo, H. Koepp, E.C. Quan, A.A. Cole, K.E. Kuettner, and A.J. Grodzinsky. Comparison of biomechanical and biochemical properties of cartilage from human knee and ankle. *J. Orthop. Res.*, 18:739–748, 2000.

[132] W.R. Trickey, G.M. Lee, and F. Guilak. Viscoelastic properties of chondrocytes from normal and osteoarthritic human cartilage. *J. Orthop. Res.*, 18(6):891–898, 2000.

[133] W.B. Valhmu, E.J. Stazzone, N.M. Bachrach, F. Saed-Nejad, S.G. Fischer, V.C. Mow, and A. Ratcliffe. Load-controlled compression of articular cartilage induces a transient stimulation of aggrecan gene expression. *Arch. Biochem. Biophys.*, 353(1):29–36, 1998.

[134] G.J.V.M. van Osch, W.B. van den Berg, E.B. Hunziker, and H.J. Hauselmann. Differential effects of igf-1 and tgfbeta-2 on the assembly of proteoglycans in pericellular and territorial matrix by cultured bovine articular chondrocytes. *Osteoarthr. Cart.*, 6:187–195, 1998.

[135] I. Wataoka, K. Kobayashi, and K. Kajiwara. Effect of the carbohydrate side-chain on the conformation of a glycoconjugate polystyrene in aqueous solution. *Carb. Res.*, 340:989–995, 2005.

[136] M. Wintermantel, M. Gerle, K. Fischer, M. Schmidt, I. Wataoka, H. Urakawa, K. Kajiwara, and Y. Tsukahara. Molecular bottlebrushes. *Macromolecules*, 29:978–983, 1996.

[137] J.F. Woessner. Determination of hydroxyproline in tissue and protein samples containing small amounts of this amino acid. *Arch. Biochem. Biophys.*, 93(2):440–447, 1961.

[138] S. Yamamoto, J. Hitomi, M. Shigeno, S. Sawaguchi, H. Abe, and T. Ushiki. Atomic force microscopic studies of isolated collagen fibrils of the bovine cornea and sclera. *Arch. Histol. Cytol.*, 60:371–378., 1997.